Roll stability control of autonomous truck combinations

Daniel Trombitas

Master of Science Thesis

TU Delft Delft University of Technology

Delft Center for Systems and Control

Roll stability control of autonomous truck combinations

Master of Science Thesis

For the degree of Master of Science in Systems and Control at Delft University of Technology

Daniel Trombitas

July 2, 2019

Faculty of Mechanical, Maritime and Materials Engineering (3mE) · Delft University of Technology

The work in this thesis was supported by Volvo Group Trucks Technology. Their cooperation is hereby gratefully acknowledged.

Delft University of Technology
Department of

The undersigned hereby certify that they have read and recommend to the Faculty of Mechanical, Maritime and Materials Engineering (3mE) for acceptance a thesis entitled

Roll stability control of autonomous truck combinations

by

Daniel Trombitas

in partial fulfillment of the requirements for the degree of

Master of Science Systems and Control

Dated: July 2, 2019

Supervisor(s):

Dr.ir. Tamas Keviczky

Dr.ir. Thorsten Helfrich

Dr.ir. Leo Laine

Reader(s):

Dr.ir. Max Mendel

Ir. Giannis Delimpaltadakis

Dr.ir. Barys Shyrokau

Abstract

Commercial heavy vehicles are especially prone to rolling over due to their inherent properties, such as the high centre of gravity - track width ratio and compliant chassis frame. Autonomous trucks cannot become widespread without eliminating this danger by guaranteeing rollover-free vehicle motion. Currently existing Roll Stability Control implementations rely on the assumption of having a responsible driver behind the steering wheel – therefore, unsupervised driving will need a higher level of roll safety than what the currently used methods can provide. Fortunately, there are two main attributes of self-driving vehicles that can be utilized to achieve this goal: Information about the reference path ahead of the truck will be available and the used algorithms may have a full control authority over the available actuators.

This thesis project developed two, redundant rollover mitigation techniques to be run in parallel, for a tractor-trailer combination: The proactive and reactive Roll Stability Control methods. These vehicle motion controllers are separate, independent functional entities.

The proactive approach functions as a module between the reference trajectory generation and tracking algorithms. It analyzes the given reference and utilizes a roll motion prediction model to make projections about a Rollover Index defined as the load transfer between left and right side wheels, during reference tracking. Based on the predicted rollover propensity, it poses a safe speed limitation to the tracking algorithm. In this project, the prediction horizon is fixed to 35 metres.

The reactive Roll Stability Control is designed to mitigate imminent rollovers that could not be anticipated based on motion reference information. This controller is placed within the motion control paradigm of Control Allocation. The objective of Control Allocation is to coordinate different actuators to achieve both longitudinal and yaw accelerations as desired by the higher-level tracking controller. Roll stability is achieved by extending the set of functionalities of this framework, using both brakes and steering to realize the needed interventions. Emphasis is put an accurate wheel lift-off detection, using lateral acceleration, steering angle and accurately estimated roll angle signals.

Design choices during syntheses of both controllers were made based on the conclusions of a thorough analysis of roll dynamics, carried out using a high-fidelity vehicle model, provided

and validated by Volvo Group Truck Technologies. Subsequently, both controllers were implemented within Volvo's real-time framework. While the proactive method's performance was only assessed using simulations, the reactive controller was tested on Volvo's proving grounds.

The thesis concludes that achieving a higher level of roll stability of (autonomous) heavy vehicles is possible, whilst having a less conservative overall behaviour compared to traditional approaches. This research contributes to making a step towards the next generation of rollover prevention for automated trucks.

Table of Contents

List of Figures

List of Tables

Acknowledgements

First and foremost, I want to thank my day-to-day supervisor, Thorsten Helfrich for his assistance during this project and his friendliness outside work. The dedication with which he supervised the thesis has set an example for my future career. I would like to thank the members of the Vehicle Motion Management team for making me feel welcome and at home; Leo Laine for the continuous supply of fresh ideas, trust and never-ending smile. From the first day until the last, I was treated like a true colleague.

I would like to thank my supervisor in Delft, Tamas Keviczky, who made this project possible for me. There was never a lack of patient but critical review and valuable advice.

Lastly, I would like to thank Sara for her love and support, especially during the last ten months.

Delft, University of Technology
July 2, 2019

Daniel Trombitas

Chapter 1

Introduction

The development of autonomous vehicles (AV) is accelerating, which could profoundly affect a variety of sectors. While it is unlikely that any on-road vehicles will become "fully autonomous" in the short term, AV's are already a reality in some confined applications that feature controlled environments, such as mining and farming. In the medium term however, on-highway trucks will likely be the first vehicles to feature a level-4 automation technology on public roads [10]. Issued by the Society of Automotive Engineers (SAE) International in 2014 [11], standard level-4 automation allows the driver to disengage from active roadway monitoring, with different preconditions for the environment. This will help to optimize supply chains and logistics operations, as players employ self-driving to increase efficiency and flexibility. Current growth in the usage of vehicle automation technologies (e.g. driver-assistance systems) is causing incremental shifts in the responsibility of driving, with the primary motivation of reducing the frequency of road accidents [10]. This thesis is concerned with roll stability of level-4 automated heavy vehicles, which is one of the crucial and indispensable safety features of the future's self-driving trucks.

1-1 Roll safety of heavy vehicles

Ever since automotive transportation exists, the risk of vehicle rollover has been present. A rollover can be defined as an event that involves at least one vehicle quarter turning about the longitudinal axis [12]. Rollover risk is especially high for commercial road vehicles, due to their inherent construction: They typically possess (from a rollover perspective) disadvantageous centre of gravity - track width ratio (see Figure 1-1) and relatively low chassis- and suspension stiffness. In addition, dynamic behaviour of articulated vehicle combinations increase the rollover propensity. In general, one way of dividing rollovers into two categories is distinguishing between tripped and untripped ones. *Tripped rollover* occurs when the vehicle is exposed to forces from an external object, eg. tyres hitting the curb, digging into soft ground or collision. On the other hand, an *untripped rollover* results from excessive cornering forces, as a collective consequence of steering, vehicle speed and sufficiently large friction

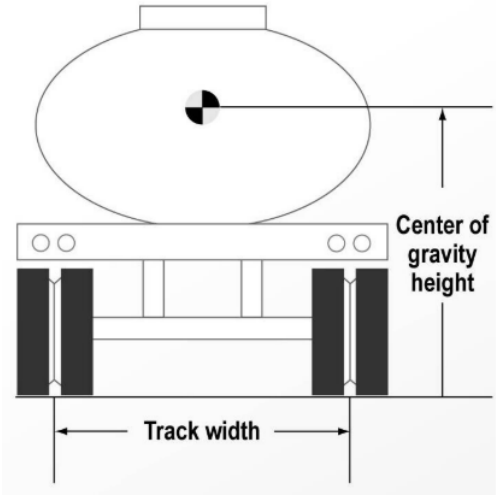

Figure 1-1: Fundamental parameters of the roll stability of a heavy vehicle [1]

between the tyres and road surface. Untripped rollovers are usually relatively uncommon amongst passenger cars, due to their inherently lower rollover propensity: Rolling over would most likely be caused by external factors, as cars are - under usual conditions - more prone to sliding than rolling over. This is not the case with trucks however, as a typical heavy vehicle can easily roll over within its possible manoeuvring envelope, tyre-limits and comfortable accelerations [8]. Within untripped rollovers, one can differentiate between [13]:

- Steady-state rollover: Happens during slowly increased lateral acceleration, eg. driving into hairpin curve or highway exit.
- Transient rollover: Complex manoeuvres executed at high speeds can trigger roll eigenmodes, which can be amplified by subsequent turns (see e.g. Figure 1-2). Modelling such an event shall involve wheel lifts, suspension end-stops and bump stops.

Despite the fact that modern rollover prevention systems are already commercialized, they generally assume a driver being in-the-loop. Therefore, eliminating human factors and developing a reliable rollover controller for autonomous heavy vehicles would be a great added value and a step towards the ideal, accident-free roads. For more details and statistical data about typical scenarios and circumstances causing rollovers, as well as the state-of-the-art, the reader is referred to the literature study work preceding this thesis [14].

1-2 Research goals and motivation

Currently available Roll Stability Control (RSC) methods do not provide sufficient roll safety for autonomous trucking. This means that the driver is still bears the responsibility in case of an accident. Consequently, self-driving trucks will have to take advantage of the full control authority over the vehicle to ensure rollover-free operation. Luckily, in the self-driving case, interference with driver commands cannot happen – this opens up new actuation possibilities. The functionalities realized by these actuations shall be implemented within the premises of

the present autonomous vehicle motion control architecture of Volvo, introduced in Chapter 3. Doing so, the proposed RSC could supply at least an equivalent set of features as a commercially available mechanism, and possibly more.

In addition, AV's generally utilize trajectory planning, offering predictions of vehicle states in time. Incorporating roll dynamics into these projections is a novel approach, which shall be conceptually examined within the thesis project. Given the promising real-life results, the research project could potentially make the first step towards the next generation of Roll Stability Control for heavy vehicles, showing higher efficiency compared to today's production ESC systems – with the broader goal of guaranteeing absolute roll safety of level-4 automated Volvo trucks.

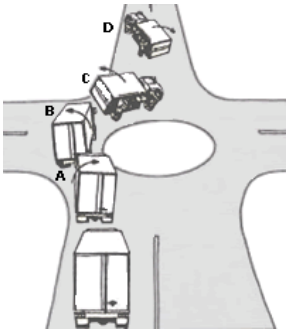

Figure 1-2: Rollover in roundabout, a transient scenario [2]

1-3 Requirements and scope

The aim is to find a general solution that entails a rollover preventing control mechanism capable of covering all traffic scenarios involving extensive cornering or dynamic manoeuvres, ensuring their roll safety. Satisfactory RSC performance in all of the used test cases shall ensure the required generality. These cases shall be set up and parameterized in simulations in such a way that they remain reconstructible in real-life, at Volvo's proving grounds.

Maximizing roll safety is achieved by constructing multiple, redundant "layers" of rollover protection. Ideally, each layer should be able to prevent rollovers at all times, using inherently different approaches. The plan of approach is to consider Roll Stability Control already at the trajectory planning phase (proactive or preventive design), not merely at the imminent occurrence of the rollover event (reactive design).

According to Figure 1-3, the first two layers constitute the **proactive RSC**. The highest-level layer ensures that the vehicle's reference trajectory does not impose a motion that could lead to extreme lateral accelerations and therefore to a potential rollover. This in done by using mere kinematic calculations – it is assumed that the trajectory generator takes care of this. Subsequently, during reference trajectory tracking, the truck combination's closed-loop trajectory is analyzed. This is to acknowledge that the vehicle will never perform perfect reference tracking, ie. the vehicle's states can deviate from their references. The dynamics of this deviation are dependent on the used tracking algorithm. The second level of roll safety shall involve a predictive method, which can grasp the dynamic behaviour of the vehicle during trajectory following, but is general enough so that it is not dependent on the actual choice of tracking controller.

To account for prediction uncertainties, unexpected events and edge cases, a last safety layer is to be implemented as **reactive RSC**. This has to supply inherent rollover safety of vehicle motion regardless of the tracking controller's demands. Both approaches rely heavily on system model parameters, out of which the Centre of Gravity (CoG) height is of utmost importance (as shown in Chapter 2). Unfortunately, there is no straight forward way of measuring this parameter. Hence, CoG height uncertainty has to be accounted for.

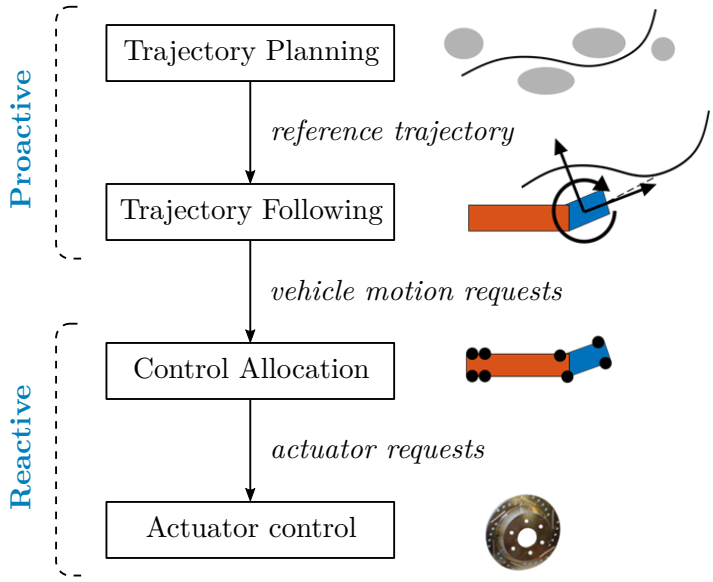

Figure 1-3: Layered control structure to perform Roll Stability Control of an autonomous truck

The control architecture has to preserve its real-time calculation capabilities, even after extending its domains' abilities during the thesis project. This implies an appropriate choice of plant model complexity for the particular applications, which are presented in Chapter 2. Furthermore, these new functionalities shall co-operate with the existing framework outlined in Chapter 3 so that testing in Volvo's high-fidelity simulator, as well as in real-life become possible.

As Chapter 4 will point out, rollovers of articulated vehicles are mostly related to trailer dynamics – for more details, see [14]. The scope of the thesis project will only cover one particular type of heavy vehicle combinations, defined by the European Council Directive 96/53 EC, European vehicle combinations for international traffic (the configuration is depicted in Figure 1-4). Standard technical details, such as unit masses, allowed payload and dimensions can be found in [3]. In addition, only passive suspension elements will be assumed during controller design.

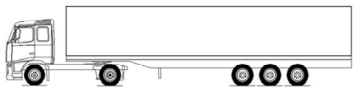

Figure 1-4: The most commonly used vehicle combination: Tractor-semitrailer – represented with the chosen configuration [3]

1-4 Thesis outline

The following **Chapter 2**, models of vehicle tyres and chassis will be presented. These consist of mathematical representations on which the different layers of the proposed Roll Stability Control will rely. In **Chapter 3** will introduce Volvo's current framework and vehicle motion control architecture. Different functionality domains will be described along with the corresponding relevant control algorithms. Subsequently, mathematical problem formulations of the thesis project will be given. **Chapter 4** will detail mechanical phenomena that are

essential to understand rollovers. Afterwards, comprehensive test cases will be shown and reflected upon. **Chapters 5** and **6** will deal with controller synthesis. Derivation, performance and limitations of each approach will be discussed in detail. Real-life tests at Volvo's proving grounds will be given by **Chapter 7**. The test cases will be reproduced in simulations, highlighting differences. Drawing the main conclusions and summarizing the thesis outputs will be dealt with in **Chapter 8**, along with recommendations for future work.

Chapter 2

Modelling heavy vehicles

Rotation around axes x_i, y_i and z_i presented on Figure 2-1 are called roll, pitch and yaw, respectively. As one will see in Chapter 4, the roll motion of articulated heavy vehicle has certain different aspects and scenarios. These need to be approached accordingly, which involves choosing appropriate system models. Firstly, tyre models will be given, describing the connection between the road surface and the vehicle chassis. Furthermore, as vehicle yaw and roll motions are coupled during transient manoeuvres [15] and because the chosen truck configuration's roll motion cannot be directly actuated (i.e. no Active Roll Control (ARC) is installed), models for yaw motion are also presented. Despite the coupled three dimensional movement of the vehicle chassis, only planar models will be covered. For coupled and more detailed models, as well as for additional factors effecting roll motion, see [14]. The previously

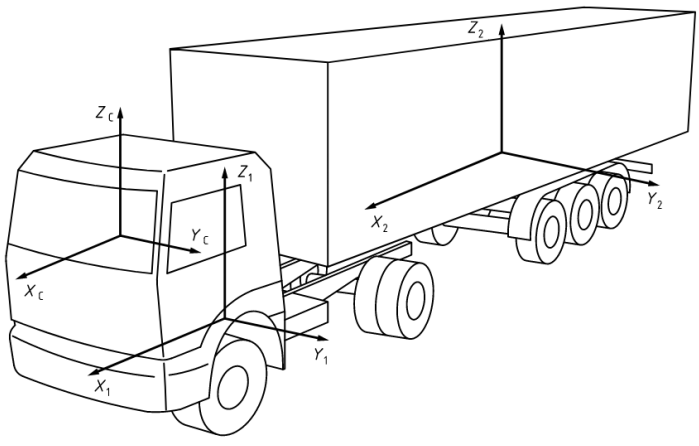

Figure 2-1: Vehicle coordinate frames of the chosen configuration, according to (and taken from) ISO 8855:2011(E) – indices $1, 2, c$ correspond to tractor, trailer and cab coordinate systems

written literature review [14] introduced a broad variety of vehicle models – in this work, only the ones utilized will be presented.

2-1 Tyre dynamics

Tyre modelling is of great importance, after all it provides the only possibility to transfer forces between the vehicle and the road. The symbols used in this section are valid for an individual wheel and tire forces are defined in the coordinate frame of the respective wheel, according to Figure 2-2. Tyre dynamics is a well-researched area, with several models of

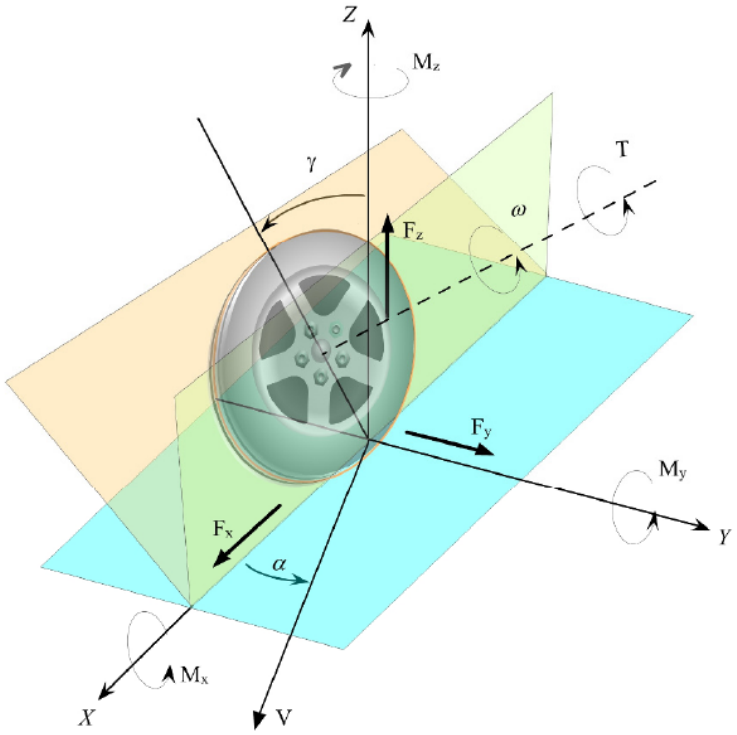

Figure 2-2: Tyre forces and moments in a general case, wheel coordinates [4]

varying complexity having been developed, both from physical and empirical perspectives – the reader is referred to [16]. Generally, it is assumed that tyre forces F_{friction} result from friction:

$$F_{\text{friction}} = \mu F_z \tag{2-1}$$

where μ is the friction coefficient and F_z is the normal load. Popular tyre models describe changes of friction in terms of the relative motion between a tyre and the road surface called slip. Slip is easier to understand, if it is broken down into two categories corresponding to longitudinal and lateral directions.

2-1-1 Longitudinal slip

When torque is applied on a wheel, longitudinal slip σ_x develops. It is defined as the normalized relative velocity of the tyre contact patch with respect to the ground:

$$\sigma_x = \frac{R_e\omega - v_x}{R_e\omega} \quad \text{if } R_e\omega \geq v_x \tag{2-2a}$$

$$\sigma_x = \frac{R_e\omega - v_x}{v_x} \quad \text{if } R_e\omega < v_x \tag{2-2b}$$

where ω is the angular velocity of the tyre, v_x is the longitudinal velocity of wheel centre and R_e is the effective rolling radius. The two cases correspond to accelerating and braking, respectively [4].

2-1-2 Lateral slip

The lateral slip describes ratio of the wheel's velocities in the x and y directions. It is expressed using the slip angle α:

$$\alpha = -\arctan\left(\frac{v_y}{v_x}\right) \tag{2-3}$$

where v_y is the lateral velocity of wheel centre, such that a positive lateral force will correspond to a positive slip angle. Alternatively, one can define the lateral slip σ_y as:

$$\sigma_y = \frac{v_y}{R_e\omega} \tag{2-4}$$

Steering and sliding motion develop lateral slip.

Remarks: The rotation of the wheel about the x-axis can be described using the camber angle γ_c according to Figure 2-2. The total slip can be written as $\sigma = \sqrt{\sigma_x^2 + \sigma_y^2}$.

2-1-3 Force generation

In [16], the tyre is regarded as a system, described by the above-mentioned variables as inputs, and the generated forces F_x, F_y and aligning moment M_z as output:

$$F_x = F_x(\sigma_x, \alpha, \gamma_c, F_z) \tag{2-5}$$

$$F_y = F_y(\sigma_x, \alpha, \gamma_c, F_z) \tag{2-6}$$

$$M_z = M_z(\sigma_x, \alpha, \gamma_c, F_z) \tag{2-7}$$

In the following, relatively simpler models will be discussed, which utilize the same philosophy but are more applicable in real-life scenarios.

Linear models

By examining the gradient of the tyre force-slip characteristics, it is reasonable to assume linear dynamics between small slip values and the resulting force:

$$F_x = C_x \sigma_x \tag{2-8a}$$
$$F_y = C_\alpha \alpha \tag{2-8b}$$
$$M_z = -C_M \alpha \tag{2-8c}$$

where C_x is the longitudinal (or braking) stiffness, C_α is the lateral (or cornering) stiffness and C_M is known as the aligning stiffness.

Lateral Dugoff tyre model

The used empirical lateral Dugoff tyre model is a simple way of capturing tyre nonlinearities at moderate slip rates – in our case until $\sigma_y \approx 0.15$ (or $\alpha \approx 8°$), see Figure 2-3. The formulation is used to obtain normalized lateral tyre forces $F_y^* = F_y/F_z$, therefore the corresponding cornering stiffnesses are defined in the dimension [1/rad]. For a deeper insight, see [17]. The friction coefficient is set to $\mu = 1$, which is a reasonable approximation of the friction between the heavy vehicle's tyres and dry asphalt. In addition, a low-μ scenario is typically not dangerous from a rollover perspective.

$$F_y^* = C_\alpha \alpha \qquad \text{if } C_\alpha \alpha < \frac{\mu}{2} \tag{2-9a}$$
$$F_y^* = \mu - \frac{\mu^2/4}{C_\alpha \alpha} \qquad \text{if } C_\alpha \alpha \geq \frac{\mu}{2} \tag{2-9b}$$

Table 2-1: Used parameters in the tyre model 2-9 – $C_{\alpha,\mathsf{F/R/T}}$ stand for cornering stiffness values of the front/read/trailer tyres

Parameter	Value
$C_{\alpha,F}$	6.85 [1/rad]
$C_{\alpha,R}$	16.177 [1/rad]
$C_{\alpha,T}$	16.177 [1/rad]
μ	1 [-]

The magic formula

Although not explicitly used, for general understanding of tyre dynamics, the so-called magic formula is hereby briefly mentioned. This model gives a more accurate representation of the slip-force curve. It is the product of a collaboration between H. B. Pacejka at Delft University of Technology and Volvo in the mid 1980's and became popular world-wide since then [16]. The main expression of the formula is as follows:

$$F(x) = D \sin(C \arctan(Bx - E(Bx - \arctan(Bx)))) \tag{2-10}$$

where x stands for either σ_x or α, $B = C_\alpha/(CD)$ is the stiffness factor, with $C_\alpha = c_1 \sin\left(2\arctan\left(\frac{F_z}{c_2}\right)\right)$, c_1 being the maximum cornering stiffness and c_2 the load at maximum cornering stiffness, D is the peak factor (often defined as μF_z), C, E are shape factors, which can also have various definitions. Nonetheless, there are other versions of the formula. Although the added complexity of the Magic formula allows to capture the reduced capability of the tyre at high slip levels, the Dugoff model has sufficient performance for moderate slip levels, as show in Figure 2-3 – more comprehensive comparison in [18]. In our application, the conservative assumption of tyre saturation above $\alpha = 5°$ is made.

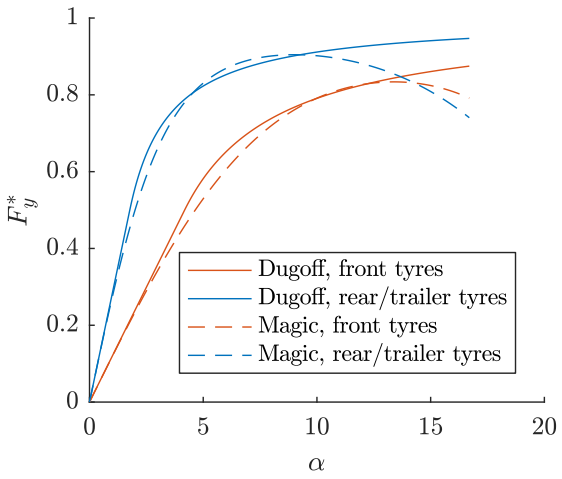

Figure 2-3: Comparison of Dugoff model and Magic formula with the used parameters according to Table 2-1 – the shape factors C, E of (2-10) where intuitively selected to emphasize the difference between the approaches

Remark: A particular analysis of lateral tyre forces at especially large slip angles is given in [4], derived by modelling the tyre contact patch. It is also important to note that (contrary to passenger cars) heavy truck handling nonlinearities are vastly influenced by the slip angle/lateral force relationship being sensitive to vertical load F_z.

2-1-4 Combined slip

So far, the survey has assumed slip to appear in directional isolation, which is called pure slip. However, in rollover situations, next to lateral forces acting on the tyres, the typical reaction generally involves usage of braking forces. This is a so-called combined slip scenario, when friction forces in the x and y directions are coupled (see Figure 2-4). This makes modelling harder, since the maximal resultant force available from the tyre is inherently limited.

It is a standard approach to combine empirical and physical models to suit an application – such an example is given in [19].

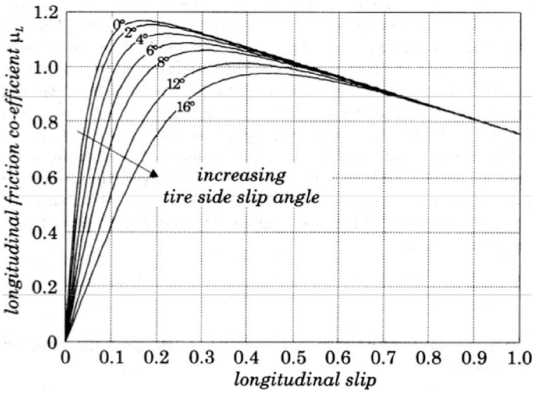

(a) Longitudinal friction coefficient in terms of longitudinal slip

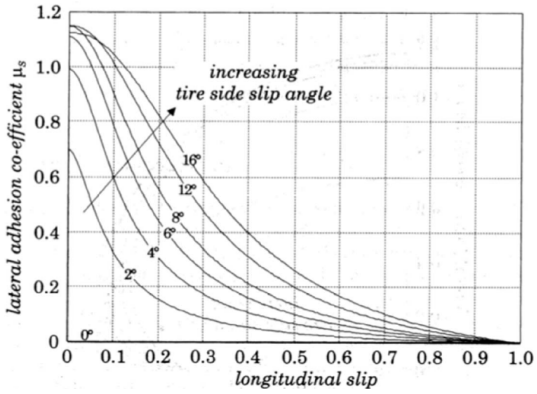

(b) Lateral friction coefficient in terms longitudinal slip

Figure 2-4: Longitudinal and lateral slip figures [5]

Friction ellipse

The friction ellipse is widely used model for combined slip. It is based on the assumption that longitudinal and lateral frictional forces cannot exceed their individual maximum value, modelled by the functions $\bar{F}_x(\mu, F_z)$ and $\bar{F}_y(\alpha, \mu, F_z)$, respectively. This implies an ellipse bounding the possible resultant frictional force on the tyre. This ellipse is given by:

$$\left(\frac{F_x}{\bar{F}_x}\right)^2 + \left(\frac{F_y}{\bar{F}_y}\right)^2 = 1 \tag{2-11}$$

This model has been validated empirically [20]. Using the simplification $\bar{F}_x = \bar{F}_y = \mu F_z$, one arrives to the formulation called *friction circle*:

$$F_x^2 + F_y^2 = (\mu F_z)^2 \tag{2-12}$$

Mapping between tyre and chassis coordinate frames

Once steering with steering angle δ is considered, tyre forces can be expressed in the frame of reference of the vehicle by applying the rotation matrix $R(\delta)$

$$R(\delta) = \begin{bmatrix} \cos\delta & -\sin\delta \\ \sin\delta & \cos\delta \end{bmatrix} \tag{2-13}$$

to the individual wheel force vectors. Then, definition of the body side-slip angle β yields, see Figure 2-5:

$$\beta = \delta - \alpha \tag{2-14}$$

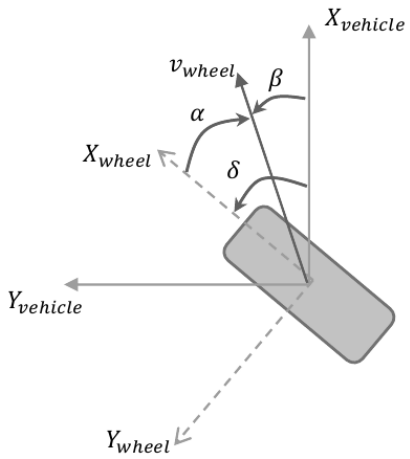

Figure 2-5: Illustration of the slip angle α, the body side-slip angle β and the wheel angle (steer) δ [6]

Relation to rollover control

The discussed combined slip phenomenon has a big role to play in rollover mitigation. Lateral tyre forces are obviously a significant factor in roll stability, being the direct consequence of lateral acceleration and lateral load transfer. According to the friction ellipse (2-11), vast longitudinal tyre forces can saturate the tyres and thus reduce the lateral capacity of the vehicle. In some applications, this so-called *deep-slip* scenario is exploited to mitigate rollovers: Intense lateral accelerations are reduced, but the vehicle motion will be less controllable due to skidding. In addition, lateral corridors have to be taken into account.

Conversely, the friction ellipse (or circle) formulation 2-12 can also be used to relate lateral utilization of a tyre to its longitudinal (braking) capacity. Determining braking torque constraints is crucial, as it might affect the RSC's potential.

2-2 Roll motion model

Heavy vehicles are complex systems from a mechanical perspective. There is a high number of phenomena that affect roll motion, which are not explicitly described by the models in this section. Factors such as anti-roll bars, dynamic load, lateral tyre shift, roll steer and effect of yaw motion are described by the previously written literature survey [14].

Roll motion of rigid body

Firstly, assume that the axles and tires have negligible mass compared to the vehicle chassis. In addition, assume a flat road surface with zero bank angle. A completely rigid vehicle body without suspension and with stiff tyres will also be presumed. The only Degree of Freedom (DoF) will be the roll angle ϕ. In this case, roll motion only happens when the

lateral acceleration reaches the level [7]

$$a_y = \frac{l_t g}{2h_{cg}} \tag{2-15}$$

Then, one of the model's wheels starts lifting off, where l_t is the vehicle track width, h_{cg} is the CoG height and g the gravitational constant, see Figure 2-6. For this reason, (2-15) is called the Static or Steady-State Rollover Threshold (SRT).

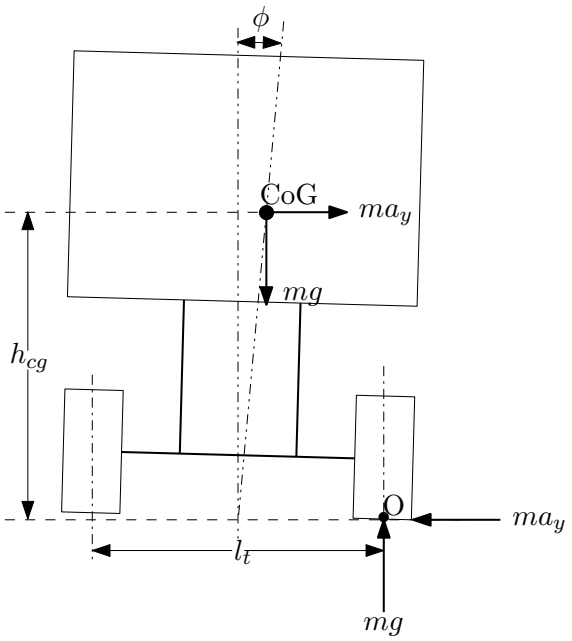

Figure 2-6: Rigid vehicle model with one roll Degree of Freedom ϕ, track width l_t and the total vehicle unit mass m, based on [7] – O is the assumed roll centre

Dynamic roll motion model

More dynamics can be incorporated into the model if one regards the two main compliances allowing a dynamic roll motion: Tyre compliance and chassis suspension. The mechanical moments causing roll, according to [4] are the following:

- *Restoring moment*, resulting from the lateral load transfer between left and right side tires, as shown by Figure 2-7,
- *overturning moment*, originating from the lateral acceleration of the CoG,
- *lateral displacement moment*, due to the lateral shift of the CoG.

These moments result in two, clearly distinguishable Degrees of Freedom: ϕ_t ("unsprung" roll angle due to tyre compliance) and ϕ_s ("sprung" roll angle of the chassis suspension), which are depicted by Figure 2-7. However, since our goal is model-based prediction and control synthesis, it is essential that the choice of roll DoF leads to measurable – or accurately

estimated – system state(s). Hardware solutions are available for particular applications that make it possible to measure the overall roll motion of a heavy vehicle, which can be used to validate the related estimation techniques (see Chapter 7). However, the axle-level roll motion related to ϕ_t and is especially hard to measure, not to mention its complex relation to the suspension roll ϕ_s. In addition, Volvo's high-fidelity simulator does not regard roll motion in such detail that it would motivate a higher DoF model description. For these reasons, a "global" roll angle ϕ is assumed with roll centre O being on ground level, as shown by Figure 2-7. This leads to a single DoF model, which is fairly easy to describe mathematically. Taking the above-mentioned restoring, overturning and lateral displacement moments into

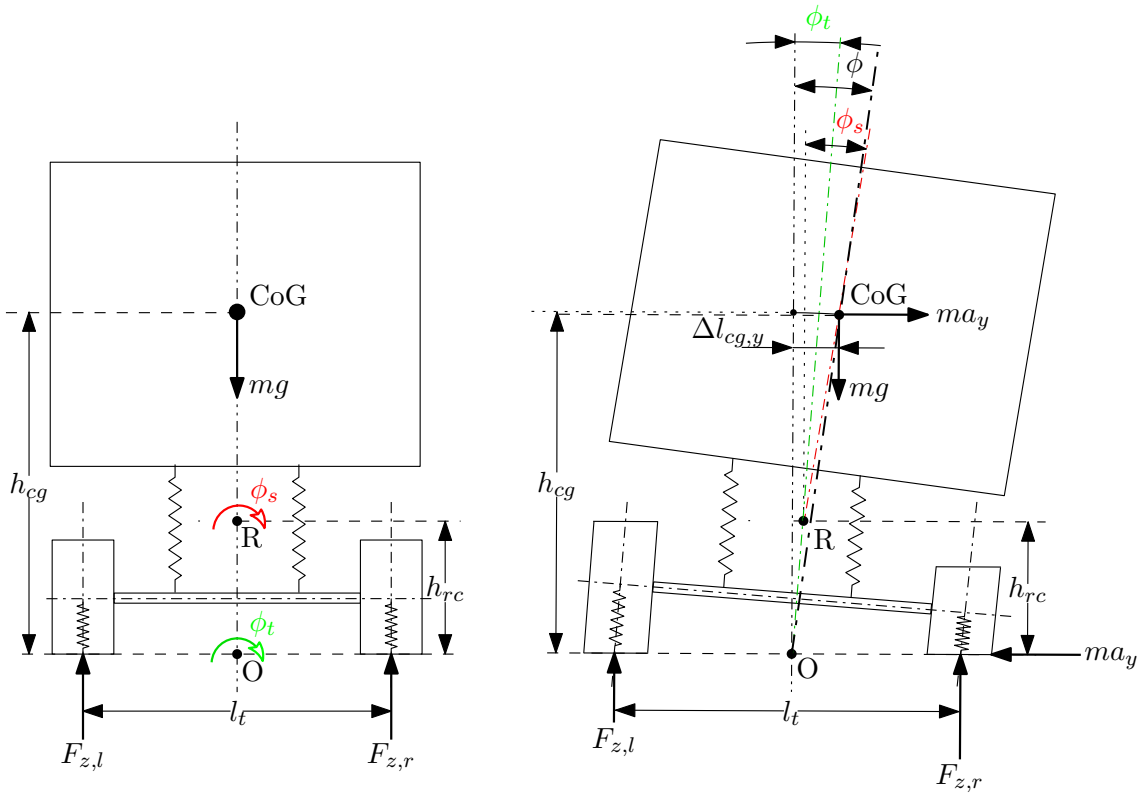

Figure 2-7: Vehicle model with two roll DoF, based on [7] – with roll angle ϕ_t about the axle roll centre O, roll angle ϕ_s about the suspension roll centre R, height of suspension roll centre from ground h_{rc}, CoG height h_{cg} and lateral shift of CoG $\Delta l_{cg,y}$; behaviour can be approximated by the total roll angle ϕ as *single DoF*

account, the dynamics of the total roll angle ϕ becomes:

$$(I_{xx} + mh_{cg}^2)\ddot{\phi} = F_y h_{cg} \cos\phi + mgh_{cg} \sin\phi + \frac{l_t}{2}(F_{z,l} - F_{z,r}) \tag{2-16}$$

where I_{xx} is the roll moment of inertia about the CoG, m the total mass of the vehicle unit, l_t the vehicle track width (assumed to be the same as the distance between left and right suspensions), with the CoG height assumed to be known. The spring deflection caused by the roll angle ϕ (see Figure 2-8) will produce a difference in the left and right suspension forces $F_{z,l}$ and $F_{z,r}$:

$$F_{z,l} - F_{z,r} = -k_\phi l_t \sin\phi \tag{2-17}$$

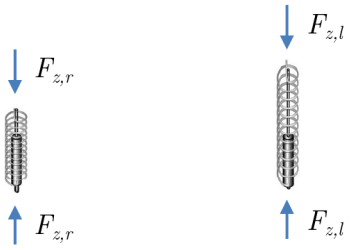

Figure 2-8: Suspension forces of the one DoF roll model [4]

with lumped suspension roll stiffness k_ϕ. Plugging (2-17) into (2-16) and adding roll damping to the model (following the same line of argumentation as with the stiffness) yields:

$$(I_{xx} + mh_{cg}^2)\ddot{\phi} = ma_y h_{cg} \cos\phi + mgh_{cg} \sin\phi - \frac{1}{2}k_\phi l_t^2 \sin\phi - \frac{1}{2}b_\phi l_t^2 \dot{\phi} \cos\phi \tag{2-18}$$

where b_ϕ is the linear suspension roll damping coefficient.

It turns out (as it will be seen in Chapters 5 and 6) that this, one DoF model is sufficient to capture the dominant mode of roll motion and makes it possible analyze manoeuvres in our tests cases. What is more, it works with a low amount of parameters, which beneficial for the system identification method used in Chapter 5. This model assumes a pendulum-like behaviour and applies at each axle. This means that it does not account for the twisting motion of the flexible truck frame structure. This frame flexibility is mostly problematic with long trailers. However, even single trucks suffer from a weak structure (in contrast to

Figure 2-9: Rollover of a torsionally compliant flat-bed trailer – rear axle can lift-off virtually independently of the front end [8]

passenger cars), which in an extreme case can lead to the rear of the truck rolling over while the front wheels remain in contact with the ground (see Figure 2-9). This "twisting" motion of the vehicle is called warp. For more details and related modelling, the reader is referred to [14].

The model (2-18) can take warp into account without modelling the torsionally compliant frame between axles, if a_y and ϕ are interpreted as the lateral acceleration and roll angle at each individual axle. Then, warp motion of the trailer can be approximated as

$$\Delta\phi_w = \phi_R - \phi_T \tag{2-19}$$

where $\Delta\phi_w$ is the warp of the trailer and $\phi_{R/T}$ are the total roll angles of the chassis at the rear tractor axle and at the trailer axles, respectively. This idea will be exploited in Chapter 5 during parameter identification of (2-18).

Effect of road bank angle

When trucking becomes autonomous, knowledge of the road properties lying ahead will be a prerequisite. This could involve the bank angle ϕ_{bank}, which means two things: Road bank angle should be regarded when planning with roll motion, furthermore, the otherwise unreliable and sensitive bank angle estimation [21] would be a merely complementary safety function. Figure 2-10 shows a situation on with road bank angle worsening the rollover propensity: Additional bank angle causes larger overturning moment.

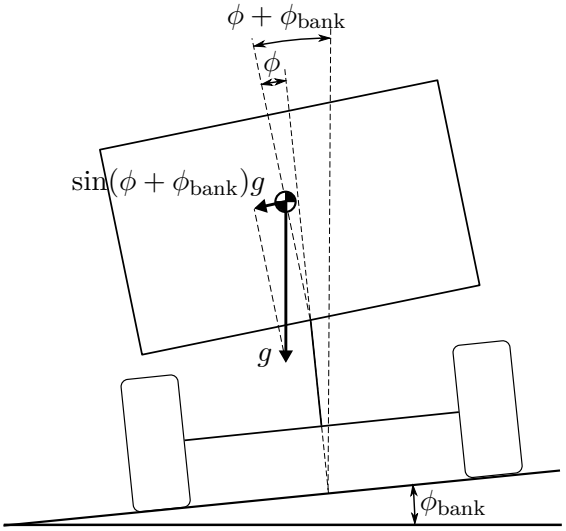

Figure 2-10: Effect of road bank ϕ_{bank}

2-3 Horizontal motion models

According to the model (2-18), the sole excitation input of roll motion is the lateral acceleration a_y, since our chosen vehicle configuration does not possess Active Roll Control hardware. Lateral acceleration yields either due to environmental factors (road bank – see Figure 2-10, cross-wind and sudden, asymmetrical changes in vertical tyre forces caused by e.g. potholes) or cornering. In this section, models that describe the evolution of a_y during cornering manoeuvres will be discussed.

2-3-1 Steering geometry

To acquire more accurate models, vehicle dimensions have to be modelled, which also implies that steering geometry can be incorporated into the vehicle model. An intuitive description called Ackermann geometry is based on the requirement that the rotation axes of all wheels

should intersect in one point. This is defined for the whole vehicle, as shown on Figure 2-11. An alternative approach is the so-called parallel steering geometry, with $\delta_i = \delta_o$, defined for

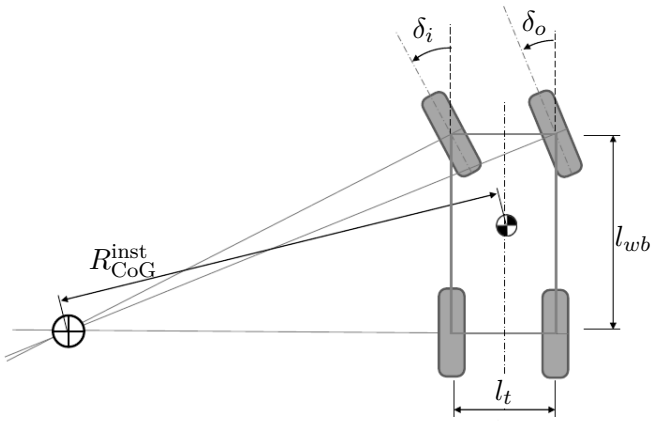

Figure 2-11: Ackermann steering geometry, using the example of a passenger car with front axle steering – the condition of Ackermann steering is that $1/\tan(\delta_o) = 1/\tan(\delta_i) + l_t/l_{wb}$ is satisfied, where $\delta_{i/o}$ are the steering angles of the inner/outer front wheels and l_{wb} is the wheel base; $R_{\mathsf{CoG}}^{\mathsf{inst}}$ is the radius from the centre of instantaneous rotation to CoG – based on a figure from [13]

an axle. For low-speed scenarios, such as parking, Ackermann steering gives better manoeuvrability and lower tyre wear, whereas for high-speed cases, where the vehicle slightly drifts outside of the curve, the instantaneous centre is closer to the one assumed by parallel steering.

2-3-2 Single-track models

The linear bicycle – or single-track – model is obtained by lumping the front and rear wheel pairs to single wheels, approximating multi-axles as single ones and linearizing the equations. This is done by equivalent wheel base l_{wb} calculations to arrive to the simplified form as shown on Figure 2-12. In general, these single-track models fail to capture the following phenomena, according to [13],[22]:

- Large deviations from Ackerman geometry,
- varying axle cornering stiffness due to dynamic effects,
- additional yaw moment due to ESC interventions,
- 3D effects, such as roll motion,
- units are merely rigid body masses,
- no suspension, chassis or cabin dynamics.

Bicycle models can be extended with sub-models of e.g. axles or roll motion. This way, some additional effects can be approximately grasped and propagated to the superior one-track vehicle model. In our case, the model (2-18) will be applied at each axle of the given

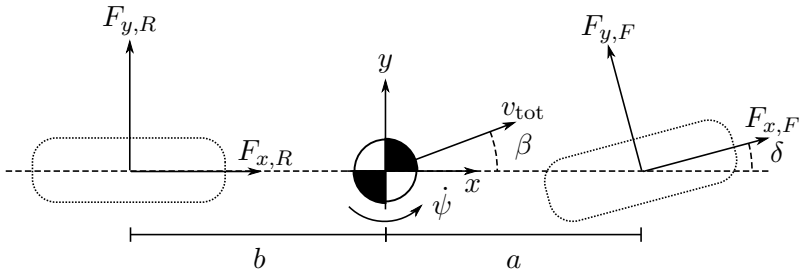

Figure 2-12: Single-track model, showing the combined front and rear tire forces $F_{x/y,F/R}$, total velocity of the CoG v_{tot}, the side-slip angle β at the CoG and the steering angle δ – based on [9]

bicycle model. Multiple types of this approach exist, which should be used according to the application (different control objectives, speeds etc.):

- Kinematic vehicle model,
- Dynamic vehicle model in terms of road-error variables,
- Dynamic vehicle model in terms of yaw rate and vehicle slip angle,
- Dynamic vehicle model in terms of inertial lateral position (or velocity) and yaw angle (or rate).

Kinematic bicycle model

Firstly, the kinematic bicycle model will be given. Zero longitudinal and lateral slip on the front and rear bicycle tyres will be assumed. The motion reference point will be the centre of the rear axle. The yaw rate will become:

$$\dot{\psi} = \frac{v_x}{R_R^{\text{inst}}} \tag{2-20}$$

where $R_R^{\text{inst}} = 1/\rho_R$ is the radius from the centre of instantaneous rotation to the rear axle with ρ_R being the corresponding path curvature. One should also regard the geometrical relation:

$$\tan(\delta) = \frac{l_{wb}}{R_R^{\text{inst}}} = l_{wb}\rho_R \tag{2-21}$$

Using (2-20) and (2-21), one can write:

$$\dot{x}_R = v_x \cos(\psi) \tag{2-22a}$$
$$\dot{y}_R = v_x \sin(\psi) \tag{2-22b}$$
$$\dot{\psi} = v_x \frac{\tan(\delta)}{l_{wb}} \tag{2-22c}$$

where x_R, y_R are the position of the rear axle. Due to the zero tyre slip assumption, the rear (unsteered) axle has no side-slip. Therefore, using (2-22c), one can write:

$$a_{y,R}^{\text{kin}} = v_x\dot{\psi} = v_x^2 \frac{\tan(\delta)}{l_{wb}} \tag{2-23}$$

where $a_{y,R}^{\text{kin}}$ is the lateral acceleration of the rear tractor axle, resulting from the kinematic bicycle model.

Dynamic bicycle model

Assuming that the steering angle δ is small and the speed v_x is constant, the effect of lateral tyre forces acting on a general single-track model is described by the following system of equations:

$$m\left(\dot{v}_y + v_x\dot{\psi}\right) = F_{y,F} + F_{y,R} \tag{2-24a}$$

$$I_{zz}\ddot{\psi} = aF_{y,F} - bF_{y,R} \tag{2-24b}$$

where I_{zz} is the yaw moment of inertia about the CoG, v_x and v_y are the longitudinal and lateral velocities of the CoG, $\dot{\psi}$ the yaw rate, a and b geometrical parameters according to Figure 2-12. As mentioned earlier, there are multiple ways of approaching the dynamic bicycle model. Our choice of system states is motivated based on its relevance for roll motion modelling, i.e. directly expressed lateral acceleration. Generally, one can substitute any tyre model into (2-24), but for simplicity, the linear model (2-8b) will be used for now, namely $F_{y,i} = C_{\alpha,i}\alpha_i$ (i marking either of the tyres). If the corresponding tyre slip angle values α_i are approximated as follows:

$$\alpha_F \approx \delta - \frac{v_y + a\dot{\psi}}{v_x} \tag{2-25}$$

$$\alpha_R \approx -\frac{v_y - b\dot{\psi}}{v_x} \tag{2-26}$$

then, a substitution into (2-24) yields a linearized, 2 DoF system that is described by the following state-space equation:

$$\begin{bmatrix}\dot{v}_y\\ \ddot{\psi}\end{bmatrix} = \begin{bmatrix}-\frac{C_{\alpha,F}+C_{\alpha,R}}{mv_x} & \frac{bC_{\alpha,R}-aC_{\alpha,F}}{mv_x} - v_x\\ \frac{bC_{\alpha,R}-aC_{\alpha,F}}{I_{zz}v_x} & -\frac{a^2C_{\alpha,F}+b^2C_{\alpha,R}}{I_{zz}v_x}\end{bmatrix}\begin{bmatrix}v_y\\ \dot{\psi}\end{bmatrix} + \begin{bmatrix}\frac{C_{\alpha,F}}{m}\\ \frac{aC_{\alpha,F}}{I_{zz}}\end{bmatrix}\delta \tag{2-27}$$

where $C_{\alpha,F}$ and $C_{\alpha,R}$ are the cornering stiffnesses of the front and rear axles.

The above model can be extended with a semitrailer model, as shown by Figure 2-13. Again, the linearized version is hereby presented, although nonlinear versions exist, as well. The extended state-space model has been derived by [23], defining the following abbreviations according to [16]:

$$C_1 = C_{\alpha,F} + C_{\alpha,R} \tag{2-28a}$$

$$Cs_1 = a_1C_{\alpha,F} - b_1C_{\alpha,R} \tag{2-28b}$$

$$Cq_1^2 = a_1^2C_{\alpha,F} + b_1^2C_{\alpha,R} \tag{2-28c}$$

with the indices 1 and 2 corresponding to the tractor and the trailer, respectively, q_1 being the length of an average moment arm and s_1 the distance of the neutral steer point from the

CoG. The model becomes:

$$\begin{bmatrix} m_1+m_2 & -m_2(h_1+a_2) & -m_2a_2 & 0 \\ -m_2h_1 & I_{1,zz}+m_2h_1(h_1+a_2) & m_2h_1a_2 & 0 \\ -m_2a_2 & I_{2,zz}+m_2a_2(h_1+a_2) & I_{2,zz}+m_2a_2^2 & 0 \\ 0 & 0 & 0 & 1 \end{bmatrix} \begin{bmatrix} \dot{v}_{y,1} \\ \dot{\psi}_1 \\ \ddot{\gamma} \\ \dot{\gamma} \end{bmatrix} = -\frac{1}{v_{x,1}} \cdot$$
$$\cdot \begin{bmatrix} C_1+C_{\alpha,T} & C_1s_1-C_{\alpha,T}(h_1+l_2)+(m_1+m_2)v_{x,1}^2 & -C_{\alpha,T}l_2 & -C_{\alpha,T}v_{x,1} \\ C_1s_1-C_{\alpha,T}h_1 & C_1q_1^2+C_{\alpha,T}h_1(h_1+l_2)-m_2h_1v_{x,1}^2 & C_{\alpha,T}h_1l_2 & C_{\alpha,T}h_1v_{x,1} \\ -C_{\alpha,T}l_2 & C_{\alpha,T}l_2(h_1+l_2)-m_2a_2v_{x,1}^2 & C_{\alpha,T}l_2^2 & C_{\alpha,T}l_2v_{x,1} \\ 0 & 0 & -v_{x,1} & 0 \end{bmatrix} \cdot$$
$$\cdot \begin{bmatrix} v_{y,1} \\ \dot{\psi}_1 \\ \dot{\gamma} \\ \gamma \end{bmatrix} + \begin{bmatrix} C_{\alpha,F} \\ a_1C_{\alpha,F} \\ 0 \\ 0 \end{bmatrix} \delta \quad (2\text{-}29)$$

where $C_{\alpha,F}$, $C_{\alpha,R}$ and $C_{\alpha,T}$ are the cornering stiffnesses of the tractor front/rear and semi-trailer axles, a_i, b_i, h_1 are geometric parameters according to Figure 2-13, $l_i = a_i + b_i$, γ is the articulation angle. In this convention, $\psi_2 = \psi_1 + \gamma$ applies, therefore $\dot{\psi}_2 = \dot{\psi}_1 + \dot{\gamma}$. Introduction of multiple single-track axes is also possible, see [23]. The current thesis project

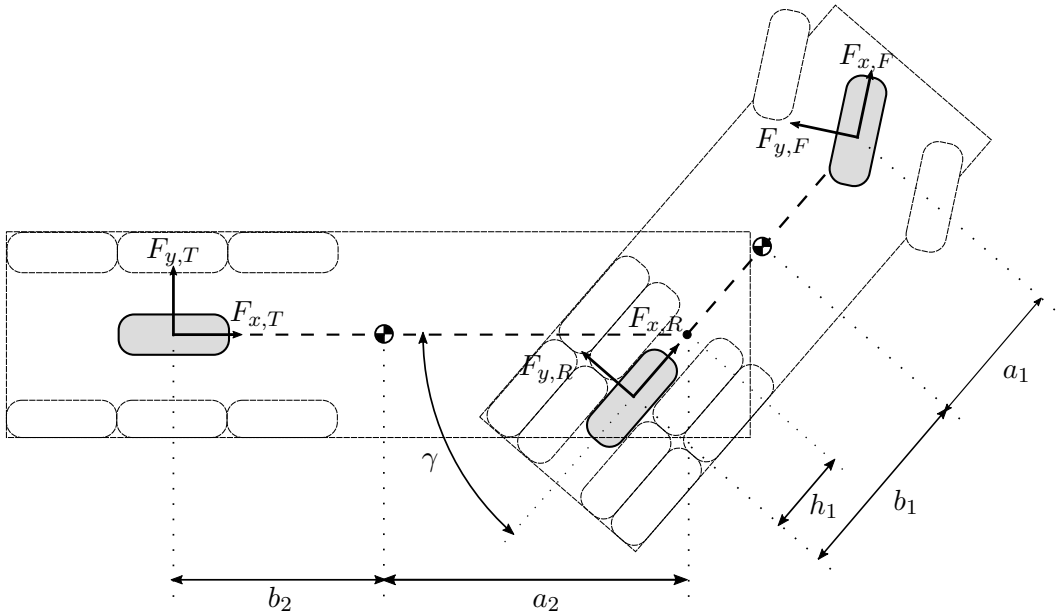

Figure 2-13: Single-track model of a tractor-semitrailer combination, with lumped axles

will not make use of two-track horizontal planar models, therefore a more detailed discussion of yaw, lateral and longitudinal motions is omitted.

For models in more detail (including tractor-trailer coupling and interaction) the reader is referred to the previously written literature survey [14].

2-4 Summary

This chapter introduced mathematical models that will be needed to analyze roll performance of heavy vehicles. Most importantly, it defined the paradigm and mathematical symbols that will be used to throughout the project. The given model equations will be referred to in the upcoming chapters. Firstly, the standard ISO 8855:2011(E) coordinate system was given, which will serve as basis for future signal charts. Then, tyre models were presented, as the sole connection between vehicle chassis and road surface. Emphasis was put on force generation and the combined slip phenomenon. The used Dugoff tyre model was compared to the more detailed Magic tyre model, to point our its limitations with our tyre parameters. Subsequently, standard roll and yaw planar chassis motion models were presented and argumentation for the chosen simplifications was given. Roll motion models will have a big importance in analyzing rollover events and predicting them, and horizontal motion models will help to understand the needed actuations for rollover mitigation.

Chapter 3

System Overview and Problem Formulation

Before starting with modelling and controller synthesis, it is important that one is familiar with Volvo's vehicle motion reference architecture. This chapter provides insight into this framework. Subsequently, problem formulations are given for both the proactive and reactive Roll Stability Control methods. The solutions of the proposed problem formulations shall fit into the described paradigm and work together with the existing functionalities.

3-1 Full vehicle motion reference architecture

Firstly, the whole control architecture is briefly presented. This consists of different levels of functional entities, namely, as described in eg. [22]:

- Functionality Domain (FD): Representing the highest order domains. These unite the lower-level controller implementations and gather sensor data, which is then made available throughout the software.
- Functionality Area (FA): These are the second level entities in the architecture and make a division between eg. traffic situation predictions and the corresponding ego vehicle behavioural decisions.
- Functionality Unit (FU): These stand for the concrete software functions that represent the control systems, having a clear functionality.

The main Functionality Domains and their interaction is illustrated by Figure 3-1, focusing on the domains used in the scope of this thesis project. A short description of the FD's is given by [24]: The **FD-Transport Mission Management** is responsible for fleet management and route assignment. Examples could be weekly or daily plans for each vehicle managed by a fleet owner or fleet optimisation with respect to energy consumption and cost. The **FD-Route**

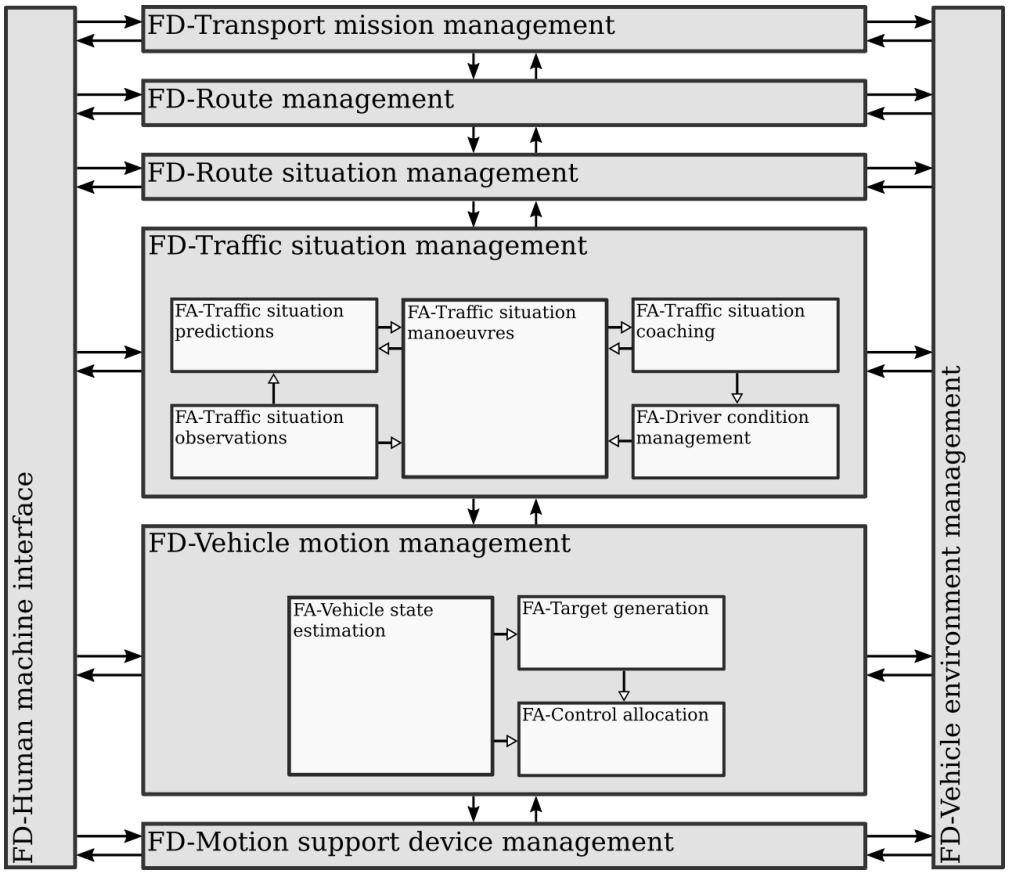

Figure 3-1: Overview of envisaged vehicle motion reference architecture – arrows represent data flow.

Management treats vehicle performance for an actual designated route within the spatial horizon of 100 km. **FD-Route situation management** functionalities are usually related to road segments between 1-5 km. Examples are fuel saving strategies, exiting a highway.

The **FD-Traffic Situation Management (TSM)** operates with a temporal horizon of up to 10 s. Safety-critical functionalities are regarded, with the consideration of obstacles and surrounding traffic, as well as subject vehicle stability limits. Controllers based on motion prediction are implemented within this Functionality Domain. **FD-Vehicle Motion Management (VMM)** coordinates actuators usage on a temporal horizon up to 1 s. **FD-Motion Support Device Management** runs at 1 kHz frequency, measuring sensors and controlling actuators.

The **FD-Vehicle environment management** encapsulates functionalities related to external surroundings, for instance lane and road sign detection. **FD-Human machine interface** handles driver intentions, in case there is one.

In the following, details of FD-TSM and FD-VMM will be given, introducing relevant parts of the used tool chain. Subsequently, the interaction between the two domains will be outlined.

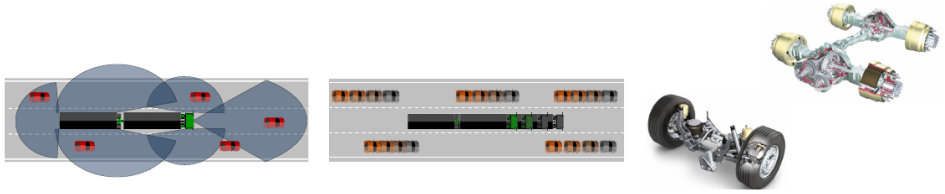

Figure 3-2: Most important FD's from a Roll Stability Control design perspective, from left to right: FD-Vehicle Environment Management, FD-Traffic Situation Management and FD-Vehicle Motion Management [24]

3-2 Interaction between Functionality Domains

Figure 3-3 depicts communication between FD-TSM and FD-VMM, strictly from the perspective of communicated signals that are directly needed for vehicle motion control and are relevant to Roll Stability Control. In other words, miscellaneous functionalities of the domains are not plotted.

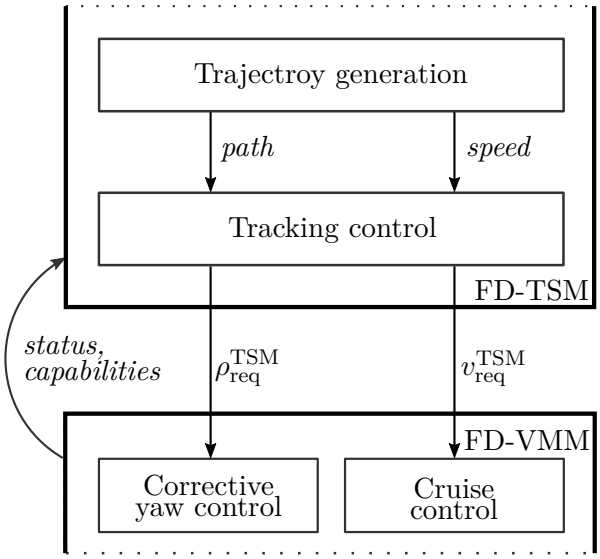

Figure 3-3: Communication between FD-TSM and FD-VMM (domains are only partially represented) – $\rho_{\text{req}}^{\text{TSM}} \in \mathbb{R}$ is the TSM's curvature request and $v_{x,\text{req}}^{\text{TSM}} \in \mathbb{R}$ is its speed request

Firstly, the FD-TSM layer processes the received environmental information, using it to generate a reference trajectory. This will consist of a reference path and speed profile on a horizon. A tracking algorithm (see e.g. [25]) translates the path-relative position, orientation and speed of the vehicle to a curvature reference request. This, along with the trajectory's speed reference will be sent to FD-VMM. Here, a cruise controller takes care of the appropriate speed reference tracking, taking into account various safety factors, as well. Furthermore, the yaw controller ensures a stable path following. Based on current physical states, vehicle status and capabilities are communicated towards FD-TSM, which will take these into account during trajectory generation. The sampling frequency of both domains is 100 Hz.

3-3 Traffic Situation Management

As mentioned before, FD-TSM is responsible for safe vehicle motion with a temporal horizon of up to 10 s, considering obstacles, surrounding traffic and vehicle stability. This implies a large set of functions realizing – amongst others – trajectory planning and tracking in complex environments. In this thesis, the environmental factors are significantly reduced in order to have an exclusive focus on vehicle stability. The sole purpose of FD-TSM in our case is handling ego vehicle motion: Trajectory planning and tracking in simple, pre-defined environments, supplying references to FD-VMM. It is this *reduced-functionality FD-TSM's* task to manage vehicle trajectory generation on a certain prediction horizon and to ensure that the vehicle tracks it and stays within a satisfactory vicinity of the reference.

The pre-defined surroundings are manifested as a horizontal reference path and an associated speed profile. The path is defined as a curvature function $f_\rho : \mathbb{R} \to \mathbb{R}$ in terms of path length, see (3-1).

$$\rho_{\text{ref}}(s) = f_\rho(s) \tag{3-1a}$$

$$v_{x,\text{ref}}(s) = f_v(s), \quad s \in [0, s_l] \tag{3-1b}$$

where $\rho_{\text{ref}}(s)$ is the pre-defined curvature at curve length s, $v_{x,\text{ref}}(s)$ the corresponding speed reference according to the function $f_v : \mathbb{R} \to \mathbb{R}$. The natural parameter s is defined on the interval $[0, s_l]$, with s_l being the path length. Using a mapping $\zeta : \mathbb{R} \to \mathbb{R}^3$, the curvature profile is transformed as follows:

$$\begin{bmatrix} x_{\text{ref}}(s) \\ y_{\text{ref}}(s) \\ \psi_{\text{ref}}(s) \end{bmatrix} = \zeta\left(\rho_{\text{ref}}(s)\right), \quad s \in [0, s_l] \tag{3-2}$$

where $(x_{\text{ref}}(s) = f_x(s), y_{\text{ref}}(s) = f_y(s))$ is the path description in global coordinates, and $\psi_{\text{ref}}(s) = f_\psi(s)$ is the corresponding path heading information, with $f_x, f_y, f_\psi : \mathbb{R} \to \mathbb{R}$. Hence, the total reference trajectory can be described by the function $f_r : \mathbb{R} \to \mathbb{R}^4$

$$\begin{bmatrix} x_{\text{ref}}(s) \\ y_{\text{ref}}(s) \\ \psi_{\text{ref}}(s) \\ v_{x,\text{ref}}(s) \end{bmatrix} = f_r(s) = \begin{bmatrix} f_x(s) \\ f_y(s) \\ f_\psi(s) \\ f_v(s) \end{bmatrix}, \quad s \in [0, s_l] \tag{3-3}$$

This trajectory can be visualized, see for instance Figure 3-4. In the current thesis project, FD-TSM's *trajectory generation* functionality means taking the next s_H metres of the pre-defined reference $\{f_r(s)|s \in [s_0, s_0 + s_H]\}$, with $s_H \in \mathbb{R}^+$ being the horizon length, s_0 the path length at the starting point of the trajectory horizon (which is by definition the closest point of the path to the rear axle of the tractor) and $0 \leq s_0,\ s_0 + s_H \leq s_l$, therefore $\{f_r(s)|s \in [s_0, s_0 + s_H]\} \subseteq \{f_r(s)|s \in [0, s_l]\}$ applies. The "generated" (cut) trajectory can be described by the same function $f_r : \mathbb{R} \to \mathbb{R}^4$, defined over the interval $[s_0, s_0 + s_H]$:

$$f_r(s), \quad s \in [s_0, s_0 + s_H] \tag{3-4}$$

or

$$f_r(s'), \quad s' \in [0, s_H] \tag{3-5}$$

where $s' = s - s_0$.

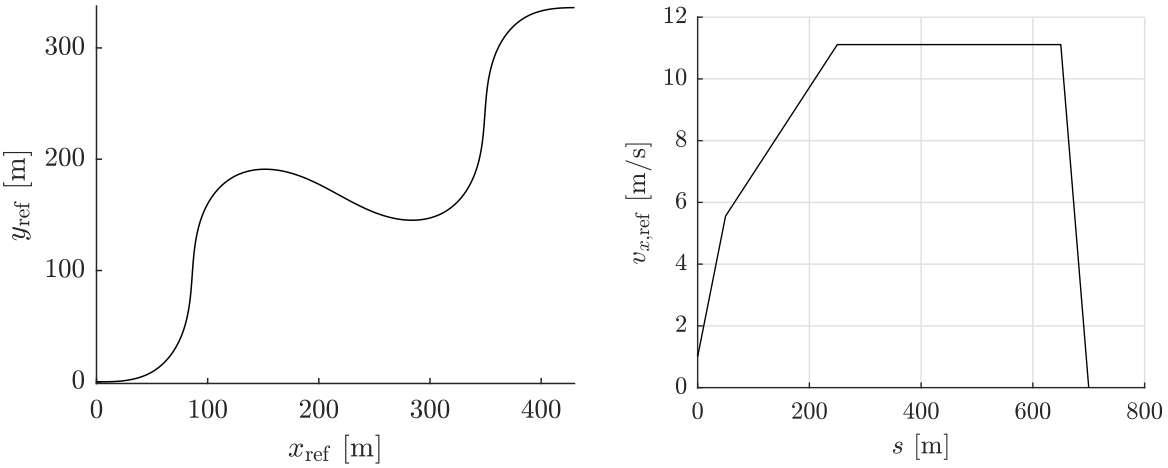

(a) Path information, top down view

(b) Speed reference information

Figure 3-4: A slalom manoeuvre – reference path and speed profile, as a pre-defined environment for the reduced-functionality FD-TSM

Remark: As shown, the default parametrization of the used prediction horizon is spatial – this formulation is a straight forward parametrization of the road, and can have advantages in case of obstacles being present. Due to toolchain limitations and real-time implementability, the horizon length is fixed to $s_H = 35$ m.

Trajectory tracking is achieved by means of a Pure-Pursuit[1] control algorithm, along the following steps:

1. Find the current location of the tractor's rear axle in the global coordinate system (x_R, y_R)
2. Find the closest point on the path to (x_R, y_R), denoted $(x_{\text{closest}} = x_{\text{ref}}(s_0), y_{\text{closest}} = y_{\text{ref}}(s_0))$
3. Choose a constant look-ahead distance based on vehicle speed, $d_{la}(v_x)$ – this will determine tracking characteristics and define the goal point (x_{la}, y_{la}) on the path, having d_{la} distance from $(x_{\text{closest}}, y_{\text{closest}})$
4. Transform the goal point to vehicle-local coordinates
5. Calculate the required steering $\delta_{\text{req}}^{\text{TSM}}$ and subsequently the curvature $\rho_{\text{req}}^{\text{TSM}}$ to the goal point
6. Set the required speed $v_{x,\text{req}}^{\text{TSM}} = v_{x,\text{ref}}(s_0) = f_{r,4}(s_0)$

Nevertheless, it is important to note that the fully functional FD-TSM might apply more advanced methods, such as Model Predictive Control (MPC), Rapidly-Expanding Random Trees (RRT) or neural network-based algorithms. In addition, much more complex environments with traffic involvement will be considered. As mentioned before, the Roll Stability Control to be designed has to meet its performance goals regardless of the tracking controller

[1]For a general overview of Pure-Pursuit, including its history and different implementations, see e.g. [25]

utilized by FD-TSM. Because of this, the used tracking controller will not be discussed in more detail. Instead, focus will be put on analyzing the reference trajectory $\{f_r(s)|s \in [s_0, s_0 + s_H]\}$ generated with horizon length of s_H, according to (3-5), from a rollover danger perspective.

3-4 Vehicle Motion Management

As previously mentioned, FD-VMM coordinates actuator usage on a temporal horizon up to 1 s. This happens by firstly processing FD-TSM's curvature and speed requests: The decoupled yaw and cruise controllers of the *Target Generator (TG)* can modify these requests based on measured and estimated vehicle states, then apply closed-loop control to obtain the global forces/moments needed to achieve them. These forces/moments will be realized by the available actuation possibilities of the given vehicle configuration. Coordinating actuators is the task of *Control Allocation (CA)*. An overview of this control structure is depicted by Figure 3-5.

In the following, the utilized Control Allocation paradigm will be described – for a broader overview on CA, as well as alternative formulations, see [14]. Subsequently, the Target Generator and its components will be presented, which adjust the requests from FD-TSM and translate them as virtual inputs for the Control Allocator. It will be presumed that the state estimation techniques of FD-VMM work out-of-the-box.

3-4-1 The Control Allocation paradigm

Firstly, let us consider an over-actuated dynamic system in discrete state-space form:

$$x(k+1) = f(x(k), v(k)) \tag{3-6a}$$
$$v(k) = h(x(k), u(k)) \tag{3-6b}$$

where $k \in \mathbb{Z}$ is the time step with sampling time T_s and $t = k \cdot T_s$, the state vector is $x \in \mathbb{R}^n$, the control input vector $u \in \mathbb{R}^m$ and the virtual input vector $v \in \mathbb{R}^p$. This hierarchical distinction is made so that the high-level dynamics f can be grasped and a primary controller can be designed using v. The control law can be any general algorithm capable of driving the truck. The lower-level actuator model is represented by h. The problem is to find a unique mapping from the demanded virtual input v to the actual system inputs u, such that it leads to the same dynamics as in (3-6b). A commonly used approach is the distribution of v according to the following linear relation:

$$v = Bu \tag{3-7}$$

where $B \in \mathbb{R}^{p \times m}$ is called the control efficiency matrix. The inverse problem of calculating u is ill-posed if $m > p$, since the mapping is not unique, which applies if the system (3-6) is over-actuated. In addition, one can consider the actuator (rate) constraints

$$\underline{u} \leq u \leq \bar{u} \tag{3-8a}$$
$$\underline{\dot{u}} \leq \dot{u} \leq \bar{\dot{u}} \tag{3-8b}$$

where (3-8b) can be incorporated into (3-8a) in discrete time, for example for $\bar{\dot{u}}$:

$$\bar{\dot{u}}(t) \approx \frac{\overline{\Delta u}(k)}{T_s} = \frac{\bar{u}(k) - u(k-1)}{T_s} \quad \rightarrow \quad \bar{u}(k) \approx \bar{\dot{u}} T_s + u(k-1) \quad \forall k \in \mathbb{Z} \tag{3-9}$$

Therefore, (3-8b) is neglected in the following formulations. Two types of implications are possible with the inverse problem of (3-7):

- $v = Bu$ has no solutions – an attempt is made to minimize the squared error between v and Bu, or
- $v = Bu$ has infinitely many solutions – the input u is picked that is closest to the desired set point for the input vector u_d (containing elements corresponding to those of u), in the Euclidean norm sense, subjected to a weighting of coordinates.

This is done by a Sequential Least Squares (SLS) problem given by

$$\begin{cases} u' = \arg\min\limits_{\underline{u} \leq u \leq \bar{u}} \left\| W_v (Bu - v) \right\|^2, \quad u' \in \mathcal{U} & \text{(3-10a)} \\ u = \arg\min\limits_{u \in \mathcal{U}} \left\| W_u (u - u_d) \right\|^2 & \text{(3-10b)} \end{cases}$$

where $\mathcal{U}$ is the possibly uncountable set of all optimal solutions u' of (3-10a). Furthermore, W_u and W_v are (diagonal) weighting matrices. This can be reduced to a Weighted Least Squares (WLS) problem requiring fewer solution steps:

$$u = \arg\min_{\underline{u} \leq u \leq \bar{u}} \left\| W_u (u - u_d) \right\|^2 + \lambda \left\| W_v (Bu - v) \right\|^2 \tag{3-11}$$

where $\lambda \in \mathbb{R}$ is a weighting parameter – as elaborated in [26], a higher λ brings the problem (3-11) closer to (3-10), but can pose numerical implications. Figure 3-5 shows how the formulation (3-11) fits into the closed-loop vehicle control.

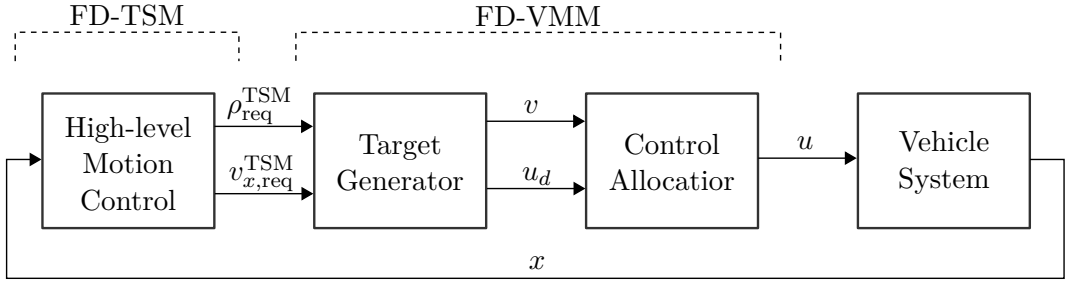

Figure 3-5: A simplified functional overview of the control loop based on CA

Description of the currently used setting It is a common approach in the literature (see [14]) to define the high-level system dynamics (3-6a) so that the virtual input v yields as a vector of forces and moments. Nevertheless, in our current application, v is defined as kinematic requests:

$$v = \begin{bmatrix} a_{x,1,\text{req}} & \ddot{\psi}_{1,\text{req}} & \ddot{\gamma}_{\text{req}} \end{bmatrix}^T \in \mathbb{R}^3 \tag{3-12}$$

where $a_{x,1,\text{req}}$ is the longitudinal acceleration request of the tractor unit, $\ddot{\psi}_{1,\text{req}}$ the yaw angular acceleration request of the tractor unit and $\ddot{\gamma}_{\text{req}}$ is the articulation angular acceleration request. The input vector u is defined according to the used vehicle combination configuration's available actuators:

$$u = \begin{bmatrix} \delta & u_e & u_{F,l} & u_{F,r} & u_{R,l} & u_{R,r} & u_T \end{bmatrix}^T \in \mathbb{R}^7 \tag{3-13}$$

where u_e is the engine torque, $u_{F/R,l/r}$ are braking torques on the first/rear axle of the tractor, on left/right wheels, accordingly. The three trailer axles and six wheels are lumped into a single, virtual wheel having six times the effectiveness of a normal wheel. The braking torque of this wheel is $u_T^{\text{lumped}} = 6 \cdot u_T$. The input set-point will not be used and therefore is set to $u_d = \begin{bmatrix} 0 & \cdots & 0 \end{bmatrix}^T \in \mathbb{R}^7$. Correspondingly, the weighting matrices are defined as follows:

$$W_v = \text{diag}\left(\begin{bmatrix} w_a & w_\psi & w_\gamma \end{bmatrix}^T \right) \in \mathbb{R}^{3\times 3} \tag{3-14a}$$

$$W_u = \text{diag}\left(\begin{bmatrix} w_\delta & w_e & w_{F,l} & w_{F,r} & w_{R,l} & w_{R,r} & w_T\sqrt{6} \end{bmatrix}^T \right) \in \mathbb{R}^{7\times 7} \tag{3-14b}$$

In general, it is hard to come up with weighting matrices that suit all use cases. Our setting will schedule the weighting factors $w_i \in \{w_{F,l}, w_{F,r}, w_{R,l}, w_{R,r}, w_T\}$ corresponding to the brakes, according to the available tyre capabilities:

$$w_i(k) = \sqrt{\frac{\sum\limits_i \bar{M}_i(k)}{\bar{M}_i(k)}} w_u \tag{3-15}$$

where $\bar{M}_i$ is calculated as it will be shown in (3-16) and $w_u \in \mathbb{R}$ is – just as a rest of the weights – a constant, see Table 3-1.

Table 3-1: Default static, dimensionless parameter values of the current Control Allocation setting

Parameter	Value	Parameter	Value	Parameter	Value
w_a	1	w_δ	1	w_u	0.2
w_ψ	1	w_e	0.1	λ	10^8
w_γ	10^{-4}				

Therefore, managing prioritization between actuators happens via *constraints*, rather than weight scheduling. This means that the actuator constraints (3-8a) can be dynamically recalculated at each time step, according the following:

- Individual tyre capability limitations, based on the combined slip phenomenon described in Chapter 2

$$\max\left(-\bar{M}_i(k), -\bar{u}_i\right) \leq u_i(k) \leq 0 \tag{3-16a}$$

where $u_i \in \mathbb{R} \leq 0$ is the braking torque of wheel i (including trailer wheels), $\bar{u}_i \in \mathbb{R} \geq 0$ is the physical limit of the brakes and the maximal torque $\bar{M}_i$ resulting from tyre capability is calculated as follows, recalling the friction circle (2-12)

$$\bar{M}_i(k) = R_{e,i}\bar{F}_{x,i}(k) = R_{e,i}\sqrt{\left(\hat{\mu}_i(k)\hat{F}_{z,i}(k)\right)^2 - F_{y,i}^2(k)} \tag{3-16b}$$

where $\hat{\mu}_i$ and $\hat{F}_{z,i}$ are the friction coefficient and vertical tyre force estimates associated with tyre i, and $F_{y,i}$ is obtained using the tyre model $f_{\text{Dugoff}} : \mathbb{R}^3 \to \mathbb{R}$ according to (2-9):

$$F_{y,i}(k) = f_{\text{Dugoff}}\left(\hat{\mu}_i(k), C_{\alpha,i}, \hat{\alpha}_i(k)\right) \tag{3-16c}$$

where $\hat{\alpha}_i$ is the corresponding slip angle estimate.

- Steering limitation based on tractor front axle slip levels

$$\max\left(\underline{\delta}, \beta_F(k) - \bar{\beta}_F\right) \leq \delta(k) \leq \min\left(\bar{\delta}, \beta_F(k) + \bar{\beta}_F\right) \tag{3-17}$$

where $\bar{\delta}$, $\underline{\delta}$ are physical actuator limits, β_F the front axle side slip and $\bar{\beta_F}$ the pre-defined, allowed side slip.

- Powertrain limitation, based on tyre capabilities

$$0 \leq u_e(k) \leq \min\left(\max_i\left(\bar{M}_i(k)\right), \bar{u}_e\right) \tag{3-18}$$

with $\bar{u}_e$ being the maximal torque of on the powertrain

- Physical actuator rate constraints

$$\underline{\dot{\delta}} \leq \dot{\delta}(k) \leq \bar{\dot{\delta}} \tag{3-19}$$
$$\underline{\dot{u}}_e \leq \dot{u}_e(k) \leq \bar{\dot{u}}_e \tag{3-20}$$
$$\underline{\dot{u}}_i \leq \dot{u}_i(k) \leq \bar{\dot{u}}_i \tag{3-21}$$

which will be translated to upper and lower actuator limitations, using (3-9).

By introducing control objectives as CA constraints, different control objectives (Yaw Stability Control, Anti-Lock Braking System (ABS)) can inherently be achieved and merged into one, concise formulation.

Let us consider the following norm:

$$\|W_v(Bu - v)\| = \left\| \underbrace{\begin{bmatrix} w_a & 0 & 0 \\ 0 & w_\psi & 0 \\ 0 & 0 & w_\gamma \end{bmatrix}}_{=W_v} \left(\underbrace{\begin{bmatrix} a_{x,1,\text{ach}} \\ \ddot{\psi}_{1,\text{ach}} \\ \ddot{\gamma}_{\text{ach}} \end{bmatrix}}_{=Bu} - \begin{bmatrix} a_{x,1,\text{req}} \\ \ddot{\psi}_{1,\text{req}} \\ \ddot{\gamma}_{\text{req}} \end{bmatrix} \right) \right\| \tag{3-22}$$

here, $a_{x,1,\text{ach}}$, $\ddot{\psi}_{1,\text{ach}}$, $\ddot{\gamma}_{\text{ach}}$ are the achieved virtual inputs by the optimal solution u of (3-11), which is highly dependent on the appropriate choice of the control efficiency matrix B. This matrix is calculated at each time step k to linearly approximate the non-linear dynamics in (3-6b) at the current set-point of (estimated) vehicle states $\left\{\hat{F}_{z,i}(k), \delta(k), \gamma(k)\right\}$. Matrix B can account for a four-wheeled tractor and a trailer with lumped wheel, according to (3-13).

The WLS (3-11) is solved as an optimization problem, using the qpOASES [27] toolbox. For more information about the numerical solution, the reader is referred to [14].

Limitations of the current CA formulation The currently used formulation is under continuous development and has flaws. The one having the biggest impact on RSC synthesis is the lack of control authority over trailer dynamics. The current description in (3-6b) (and in B, correspondingly) does not make it possible to impose kinematic requests on the trailer unit. Instead, trailer behaviour is grasped trough articulation requests. Furthermore, only linear constraints are allowed using qpOASES – nevertheless, it can handle constraints of the form

$$\underline{b} \leq A_{\mathrm{CA}} \cdot u \leq \bar{b} \tag{3-23}$$

where $A_{\mathrm{CA}} \in \mathbb{R}^{w \times m}$, $w \in \mathbb{Z}^+$ defines a linear combination of elements of u and $\underline{b}, \bar{b} \in \mathbb{R}^w$ are bound vectors. This is by default not exploited.

3-4-2 Target generation for Control Allocation

Looking at Figure 3-5, the Target Generator fills the gap between the high-level motion requests based on the truck's relation to the generated trajectory reference ($\rho_{\mathrm{req}}^{\mathrm{TSM}}, v_{\mathrm{req}}^{\mathrm{TSM}}$) and kinematic motion requests v ("virtual input"), passed to the Control Allocator. This is done by means of two decoupled controllers.

Corrective yaw controller

Also called the "curvature control". Firstly, FD-TSM's curvature request gets translated to a steering request, according to (2-21):

$$\delta^{\mathrm{ff}}(k) = \tan^{-1}\left(l_{wb} \cdot \rho_{\mathrm{req}}^{\mathrm{TSM}}(k)\right) \tag{3-24}$$

where δ^{ff} is interpreted as a feed-forward steering command, resulting from the Pure-Pursuit algorithm. Subsequently, this request is converted to a yaw rate request, based on the current tractor speed:

$$\dot{\psi}_{1,\mathrm{req}}^{\mathrm{TSM}}(k) = v_{x,1}(k) \cdot \rho_{\mathrm{req}}^{\mathrm{TSM}}(k) \tag{3-25}$$

and the yaw rate error $e_{\dot{\psi}}$ is obtained as:

$$e_{\dot{\psi}}(k) = \dot{\psi}_{1,\mathrm{req}}^{\mathrm{TSM}}(k) - \dot{\psi}_1(k) \tag{3-26}$$

The corrective control algorithms takes into account the yaw rate error dynamics, using a PD controller represented by $C_{\psi}^{\mathrm{PD}} : \mathbb{R}^2 \to \mathbb{R}$. The feed-forward term δ^{ff} is also added:

$$\delta_{\mathrm{req}}^{\mathrm{VMM}}(k) = C_{\psi}^{\mathrm{PD}}\left(e_{\dot{\psi}}(k), \hat{\dot{e}}_{\dot{\psi}}(k)\right) + \delta^{\mathrm{ff}}(k) \tag{3-27}$$

where $\hat{\dot{e}}$ is a numerically approximated, appropriately filtered estimate of the yaw rate error. Based on the controller's output $\delta_{\mathrm{req}}^{\mathrm{VMM}}(k)$, one can determine the virtual inputs determining the yaw motion of the vehicle combination:

$$v_2(k) = \ddot{\psi}_{1,\mathrm{req}}(k) = h_{\psi}\left(\delta_{\mathrm{req}}^{\mathrm{VMM}}(k)\right) \tag{3-28}$$

$$v_3(k) = \ddot{\gamma}_{\mathrm{req}}(k) = h_{\gamma}\left(\delta_{\mathrm{req}}^{\mathrm{VMM}}(k)\right) \tag{3-29}$$

where the functions $h_{\psi}, h_{\gamma} : \mathbb{R} \to \mathbb{R}$ describe the relation between the steering input and the tractor unit's yaw angular acceleration response, as well as the truck combination's articulation response.

Cruise controller

Firstly, the controller gradually reduces the speed request $v_{x,\text{req}}^{\text{TSM}}$ if any of the tractor axles are saturated, obtaining $v_{\text{req}}^{\text{VMM}}$. Based on the error

$$e_v(k) = v_{\text{req}}^{\text{VMM}}(k) - v_{x,1}(k) \tag{3-30}$$

a PI controller $C_v^{\text{PI}} : \mathbb{R}^2 \to \mathbb{R}$ and a feed-forward term $a_{x,1}^{\text{ff}}$ create the needed acceleration request:

$$v_1(k) = a_{x,1,\text{req}}(k) = C_v^{\text{PI}}\left(e_v(k), \sum_k e_v(k)\right) + a_{x,1}^{\text{ff}}(k) \tag{3-31}$$

where $a_{x,1}^{\text{ff}}(k) = C_v^{\text{ff}}(x(k))$ and the feed-forward cruise control function $C_v^{\text{ff}} : \mathbb{R}^n \to \mathbb{R}$ implies compensation of road pitch angle, steering angle, roll resistance of tyres and air drag.

Using equations (3-31), (3-28), (3-29) and $u_d = \begin{bmatrix} 0 & \cdots & 0 \end{bmatrix}^T$, it is possible to create the needed inputs for Control Allocation.

3-5 Problem formulation

This section will reflect on the previously described, existing framework and will propose problem formulations – Roll Stability Control will be synthesized by solving these problems. The formulations are divided into pro- and reactive algorithms. Both should be developed as individually applicable functional entities being fully independent from the one another. The solution methods should be validated with real-life tests.

3-5-1 Proactive Roll Stability Control

Let us consider the reference trajectory description $f_r : \mathbb{R} \to \mathbb{R}^q$, $q \in \mathbb{Z}^+$

$$f_r(s), \quad s \in [0, s_H] \tag{3-32}$$

on a spatial horizon of length s_H, containing at least the following reference information:

$$\psi_{\text{ref}}(s) = f_\psi(s) \text{ or } \dot{\psi}_{\text{ref}}(s) = f_{\dot{\psi}}(s) \tag{3-33}$$

$$v_{x,\text{ref}}(s) = f_v(s), \quad s \in [0, s_H] \tag{3-34}$$

where $f_\psi : \mathbb{R} \to \mathbb{R}$ (or $f_{\dot{\psi}} : \mathbb{R} \to \mathbb{R}$) and $f_v : \mathbb{R} \to \mathbb{R}$ are heading (or heading rate) and speed references – therefore, $q \geq 2$. Let us assume that there exists a transformation $\Upsilon : \mathbb{R}^q \to \mathbb{R}^q$:

$$r(k) = \Upsilon\left(f_r(s)\right) \tag{3-35}$$

where $r(k) \in \mathbb{R}^q$ is one point of the reference trajectory at time instance k, with $s \in [0, s_H]$ and $kT_s \in [0, t_H]$, t_H being the temporal time horizon length corresponding to s_H, $kT_s = 0$ signifies the time point, when the generated trajectory gets passed to the tracking controller.

Furthermore, an appropriate description of a plant model for a tractor-semitrailer combination will be regarded in closed-loop (see Figure 3-6) with a suitable reference tracking controller, $f_{cl} : \mathbb{R}^n \times \mathbb{R}^q \to \mathbb{R}^n$

$$x(k+1) = f_{cl}\left(r(k), x(0)\right) \tag{3-36}$$

where $x(0) \in \mathbb{R}^n$ is the vector of initial states. Let $C_y \in \mathbb{R}^{q \times n}$ be the matrix that selects the

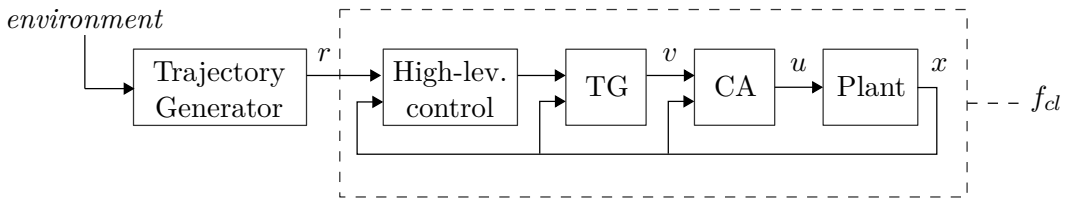

Figure 3-6: Definition of the closed-loop system represented by f_{cl}

system states that will be considered as the plant's output vector y_r:

$$y_r(k) = C_y x(k) \tag{3-37}$$

where the elements of $y_r \in \mathbb{R}^q$ contain the same physical information as those of r, correspondingly. The reference r may be the product of any sort of generator algorithm, and the closed-loop system f_{cl} may utilize any control method, provided that the following holds:

$$\|r(k) - y_r(k)\| < \varepsilon \quad \forall k T_s \in [0, t_H] \tag{3-38}$$

where $\varepsilon \in \mathbb{R} \geq 0$ is sufficiently small – i.e. the generated trajectory is possible to follow within physically acceptable margins and the utilized controller is capable of doing so, with an acceptable performance. Unfortunately, the assumption (3-38) does not always hold, see for instance the MPC-based trajectory generation algorithm designed for long heavy vehicle combinations in [22].

Tasks

1. Find the transformation (3-35) to obtain the generated reference trajectory parametrized along a temporal time horizon.
2. Find a suitable approximation of the closed-loop dynamics $\hat{f}_{cl}$, based on FD-VMM's communicated capability and status information (see Figure 3-3).
3. Predict the closed-loop system's states $\tilde{x}(k+1) = \hat{f}_{cl}(r(k), x(0))$ along the reference trajectory, $kT_s \in [0, t_H]$.
4. Define an appropriate measure proportional to the danger of rolling over, called Rollover Index (ROI) as a function of vehicle states, $\mathrm{ROI}(k) = f_{\mathrm{ROI}}(x(k))$, $f_{\mathrm{ROI}} : \mathbb{R}^n \to \mathbb{R}$ and analyze the predicted danger $f_{\mathrm{ROI}}(\tilde{x}(k))$ on the prediction horizon.
5. Synthesize an intervention method that ensures $\mathrm{ROI}(k) \leq \overline{\mathrm{ROI}} \quad \forall k T_s \in [0, t_H]$ by modifying f_r and so, FD-TSM's requests $\rho_{\mathrm{req}}^{\mathrm{TSM}}$, $v_{x,\mathrm{req}}^{\mathrm{TSM}}$.

3-5-2 Reactive Roll Stability Control

To begin with, the currently used Control Allocation paradigm will be looked at. One is given a system representation (3-6) and the approximation of the actuator-chassis interaction (3-7). FD-VMM achieves vehicle motion control based on the CA formulation (3-11).

Tasks

1. Analyze the broad possibilities of vehicle actuation in terms of rollover prevention.
2. A rollover danger detection algorithm shall be developed, which is independent of the Rollover Index used by proactive RSC. This is to ensure redundancy.
3. Extend the currently existing set of functionalities of FD-VMM realized by the constraint functions (3-16)-(3-21), scheduling of weighting matrices (3-14) and control laws (3-27), (3-31). A similar behaviour is to be achieved as with commercial Electronic Stability Control (ESC) systems, but within the Control Allocation setting. This makes it possible to integrate roll safety to the motion control systems of autonomous trucks. The proposed method shall examine the possibility of incorporating new constraints implying roll stability, introducing constraints of the from (3-23).

3-6 Summary

This chapter attempted to familiarize the reader with Volvo's current control architecture and reference framework for Autonomous Vehicles. Several flow charts visualized the signal flow between functional entities. The two main Functionality Domains used in this work (Traffic Situation Management and Vehicle Motion Management) were separately described and their interaction emphasised. Knowing the requirements from Chapter 1, the controlled system from Chapter 2 and the now the existing framework, as well, mathematical problem formulation and plan of approach was proposed for both pro- and reactive Roll Stability Control methods.

Chapter 4

Rollover analysis

Chapter 2 presented modelling techniques that helped understand the main characteristics of elements that influence a truck's roll motion. These are general effects resulting from component properties and use cases that are not specific for automated vehicles. With no human driver being involved, current methods of rollover detection and mitigation will not be completely adaptable, as they are principally based on the presupposition of having a well-trained person behind the steering wheel.

It is crucial to detect (or even better, predict) rollover danger by means of on-board measurable signals (eg. yaw rate, lateral acceleration, roll angle, and roll rate). The previously written literature survey [14] has collected the state-of-the-art in rollover detection, presenting several ways of defining Rollover Indices (ROI's). This Chapter will introduce the Lateral Load Transfer Ratio (LTR) as Rollover Index and explain how it can be utilized as a predictable measure that is proportional to the rollover propensity. Furthermore, it is also essential to understand the effect of vehicle dynamic behaviour and parameters on roll performance. The goal of this chapter is to present the most important phenomena that occur during rollovers in terms of system states and to analyze the related implications through appropriate test cases.

4-1 Mechanics of roll stability

4-1-1 Important factors and phenomena

Extensive studies (e.g. [28],[7]) have been carried out to investigate vehicle parameters affecting roll performance. These generally mention the following factors to play a vital role:

- Centre of Gravity height of tractor and trailer,
- roll centre height of tractor and trailer,
- axle roll stiffness of tractor and trailer,

- effective track width of tractor and trailer (including dual tyre spacing),
- fifth wheel height and roll stiffness, coupling design,
- vehicle mass,
- tyre stiffness characteristics (vertical, lateral and overturning),
- frame flexibility, especially for trailer.

These parameters are always set as a result of certain design trade-offs, therefore it is not possible to optimize the truck configuration for roll stability alone. For instance, a high axle roll stiffness would be advantageous from a roll safety perspective, but would be unacceptable to authorities due to the imposed road damage. Similarly, certain use cases will always demand carrying loads that yield an extremely high CoG height, e.g. mining applications. In the following, the most important factors of roll stability will be laid out, which will be considered during controller synthesis.

CoG height to track width ratio

As the effective track width is usually defined by standards, the CoG height remains an important stability factor. In our simulations, the configuration will possess track width and CoG height values according to Table 4-1. In real-life tests, the CoG height could not be

Table 4-1: Track width and CoG height (from ground to sprung chassis body CoG) values used in simulations – $l_{t,F/R/T}$ correspond to front, rear and trailer axles, $h_{cg,1/2}$ to tractor and trailer units; tractor rear axle has dual tyres

Parameter	Value [m]
$l_{t,F}$	2.05
$l_{t,R}$	1.85
$l_{t,T}$	2.05
$h_{cg,1}$	0.9676
$h_{cg,2}$	2.3512

guaranteed to be exactly at the same level. For details, see Chapter 7. As the (laden) trailer has a higher CoG height to track width ratio, it will be more prone to rolling over than the tractor.

Soft front axle suspension

The implication due to different suspension stiffness values per axle will not be explicitly regarded during controller design, therefore it is hereby only briefly mentioned. For comfort reasons, the front tractor axle is typically lower in roll stiffness. An optimal vehicle loading implies axle loads proportional to their roll stiffnesses. During intense braking interventions however (which are typical for rollover mitigation), longitudinal load transfer happens and the front axle gets exposed to a high vertical load. This yields that the overall roll stiffness

of the unit reduces, hence the same lateral acceleration will produce a higher roll angle (see (2-18)).

Hence, a too hard braking can also lead to an unintended behaviour and vehicle rollover. An example of this is given in the Appendix, Section A-1 (see Figures A-5 and A-8) – here, one can observe a "peak" in ϕ at the first moment of intense deceleration, due to the reduced overall roll stiffness of the tractor unit. This increased roll angle will interfere with the trailer, which was already on the edge of wheel lift-off, yielding rollover. Although longitudinal load transfer is not modelled in this thesis project, it is required that a braking intervention is never more aggressive than necessary, especially, when the load transfer of the trailer is high.

Rearward Amplification (RWA)

The phenomenon in which the lateral acceleration amplifies as it traverses through a sequence of vehicle units resulting from steering input is called Rearward Amplification (RWA) [29]. Formally, the RWA of unit i is defined as the ratio between its peak lateral acceleration and that of the tractor ($i = 0$):

$$\mathrm{RWA}_i = \frac{|a_{y,\mathrm{peak},i}|}{|a_{y,\mathrm{peak},0}|} \tag{4-1}$$

This ratio is dependent on the steering input (excitation) frequency and vehicle speed (high speeds typically yield high RWA). Hence, it becomes especially important when the frequency content of steering (manoeuvring) overlaps with the natural frequency of the combination's yaw motion. In other words, excitation of frequencies associated with a high RWA value shall be avoided. Table 4-2 describes the effect of parameter changes on Rearward Amplification. For our particular vehicle combination configuration and parameters, a simulation example is given by Figure 4-1, showing RWA during a slalom manoeuvre. For more information about

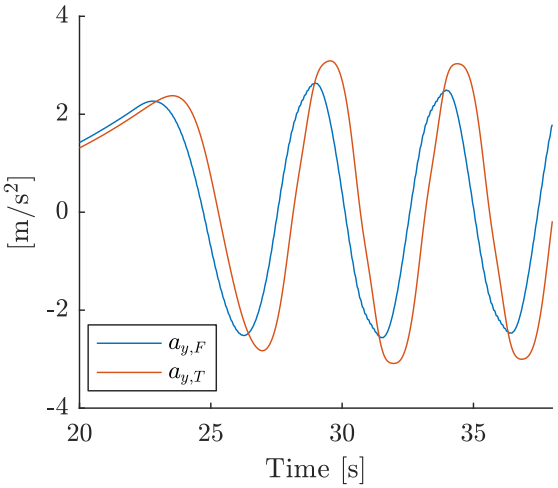

Figure 4-1: Lateral acceleration of the tractor's front axle and the trailer's axle group, during a slalom manoeuvre, at $v_x = 75$ [km/h]

the Rearward Amplification phenomenon, see the previously written literature survey [14].

Table 4-2: Effects of parameter changes on the vehicle combination's Rearward Amplification, according to [3]

Parameter	Action	Effect on RWA
Number of articulation joints	Increase	↗
Coupling position	Moving it closer to the rear axles	↘
Drawbar length	Increase	↘
Trailer wheelbase	Increase width	↘
Steered trailer axles	Utilization	↗
Mass distribution	Moving the load rearwards	↗
Tyre cornering stiffness	Increase	↘

Excited eigenmodes of roll motion

As suggested by (2-18), the system dynamics from a_y to ϕ is approximately of second-order. This implies two issues: Firstly, rapidly changing a_y inputs will be followed by a delayed input in ϕ. This implies that a Rollover Index solely based on ϕ would not be not a practical approach. Secondly, for the considered vehicle combination, roll motion excitation (via a_y) at a frequency on range 0.2 - 0.8 Hz will yield an amplifying roll motion. This range is mentioned in the scientific literature (e.g. [8]), but will also be confirmed by this thesis project, during identification of the roll motion model (2-18). Unfortunately, this frequency range overlaps with the frequency content of typical emergency manoeuvres (about 0.5 Hz [30]). The phenomenon is represented by a simulation shown by Figure 4-2, where one can observe both the mentioned phase delay and the amplifying roll angle on the front axle signals $a_{y,F}$, ϕ_F.

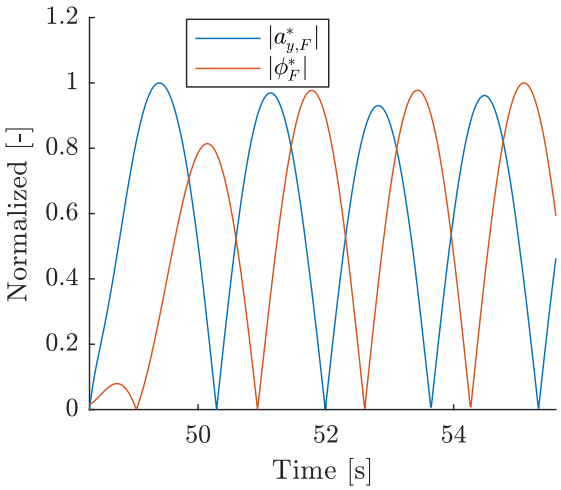

Figure 4-2: Roll angle response of the front axle to its lateral acceleration – the signals are normalized with their maximum value

4-1-2 Rollover indicators

Steady-State Rollover Threshold

Let us recall (2-15):

$$a_y^{\mathrm{SRT}} = \frac{l_t g}{2h_{cg}} \tag{4-2}$$

according to which one can calculate the static rollover propensity of each unit, using the values of Table 4-1 and $l_{t,1} := (l_{t,F} + l_{t,R})/2$ as the effective track width of the whole tractor unit – see Table 4-3. These numbers tell us that the laden trailer is (with rigid body and quasi-

Table 4-3: Steady-State Rollover Threshold values of the vehicle units

Parameter	Value [m/s^2]
$a_{y,1}^{\mathrm{SRT}}$	9.89
$a_{y,2}^{\mathrm{SRT}}$	4.28

static manoeuvre assumptions) more than two times more prone to rolling over compared to the tractor unit. This motivates that as long as untripped rollovers are concerned, rollover indication analysis shall be focusing on trailer states.

Load Transfer Ratio

The dimensionless lateral **Load Transfer Ratio** LTR [31] is defined for each axle as the lateral load transfer normalized by the total vertical load

$$\Delta F_z^* = \frac{F_{z,l} - F_{z,r}}{F_{z,l} + F_{z,r}} \tag{4-3}$$

$\Delta F_z^* = \pm 100\%$ corresponds to wheel lift off on the corresponding axle – which will be our conservative definition of a rollover event. The big advantage of LTR as Rollover Index compared to SRT is that it directly incorporates roll dynamics in terms of (2-17), which means capturing the possibly excited eigenmodes, as well (see Figure 4-2). To ensure roll safety, the allowed lateral load transfer can be set to a safe value. It is possible to instrument an axle to provide an estimate of the vertical tyre forces, and, therefore, of LTR, as done in [32]. The limitation of the approach is the necessity of a more sophisticated measurement setup. It is possible to estimate the vertical tyre forces $\hat{F}_{z,i}$ directly – in fact, a relatively accurate vertical tyre force is implemented within Volvo's framework. Nevertheless, these estimators are typically obtained based on complex vehicle models and need system states that are not necessarily predictable in a robust way.

The interest of this thesis work lies in a formulation that is an accurate approximation of LTR in terms of measurable or accurately estimated signals that can also be predicted based on the trajectory information (3-32). It should also possess a reasonable level of simplicity so that it can be tested in real-life within the scope of the thesis project. The chosen method is based on an idea of the book [4]. Using the model (2-18), one can express the difference and the sum of tyre forces in terms of the roll angle:

$$\Delta F_z^* = \frac{F_{z,l} - F_{z,r}}{F_{z,l} + F_{z,r}} = \frac{k_\phi l_t \sin\phi + b_\phi l_t \dot{\phi} \cos\phi}{mg} \tag{4-4}$$

This formulation is dependent on the measured roll rate and estimated roll angle, but obtaining the parameters k_ϕ, b_ϕ would need sophisticated measurements for each vehicle unit, which would lead to highly inefficient use cases. Instead, by ignoring transient dynamics by setting $\ddot{\phi} = 0$ in (2-18), one can write:

$$k_\phi l_t \sin\phi + b_\phi l_t \dot{\phi} \cos\phi = \frac{2ma_y h_{cg} \cos\phi + 2mgh_{cg} \sin\phi}{l_t} \tag{4-5}$$

using (4-4) and (4-5) at each unit i and axle j, one arrives to our final formulation:

$$\Delta\hat{F}^*_{z,j} = \underbrace{\frac{2h_{cg,i}}{l_{t,i}}}_{:=X_i} \left(\frac{a_{y,j}}{g} \cos\phi_j + \sin\phi_j \right) \tag{4-6}$$

where $\Delta\hat{F}^*_{z,j}$ is the approximated Load Transfer Ratio of axle j and X_i is a dimensionless constant feature of vehicle unit i, depending on its CoG height and effective track width. To

Table 4-4: X values of the vehicle units

Parameter	Value [-]
X_1	0.9924
X_2	2.2939

account for the neglected transient dynamics $\ddot{\phi} = 0$ and (in real-life) uncertainty in h_{cg}, a safety factor can be applied:

$$\hat{X}_1 = c_{s,1} X_1 \tag{4-7a}$$

$$\hat{X}_2 = c_{s,2} X_2 \tag{4-7b}$$

where $c_{s,1/2}$ are safety factors corresponding to tractor and trailer $X_{1/2}$ constants, respectively.

Remark: In case an accurate CoG height estimator were implemented (obtaining $\hat{h}_{cg,i}$), it can be incorporated into the formulation (4-6).

4-1-3 Choosing safety factors

According to (4-7), the choice of $c_{s,i}$ will define the allowed driving envelope in terms of $\{a_y, \phi\}$. To get a grasp about the safe envelope, a Monte Carlo simulation has been carried out with 1000 different test cases (with manoeuvres defined in Sections 4-2 and A-1) using different speed profiles – not all of the tests ended with rollover. At the moment k of wheel lift-off, the values $\left\{ a_{y,R/T}(k), \phi_{R/T}(k), \dot{\phi}_{R/T}(k) \right\}$ were saved and analyzed – as it turned out, $\dot{\phi}_{R/T}$ values were not useful in limiting the safe envelope any further, therefore the design choice of relying only on $\{a_y, \phi\}$ in terms of (4-6) was justified. To begin with, one has to point out that trusting X_1 is a naive approach as it does not take into account the trailer's effect on the tractor. Therefore, $\hat{X}_1$ is chosen based on simulation data shown in Figure 4-3. Whereas trailer axle group lift-offs are well aligned with the assumption in (2-17) (i.e. wheel lift-off principally depends on roll angle), points applying for the tractor are more scattered.

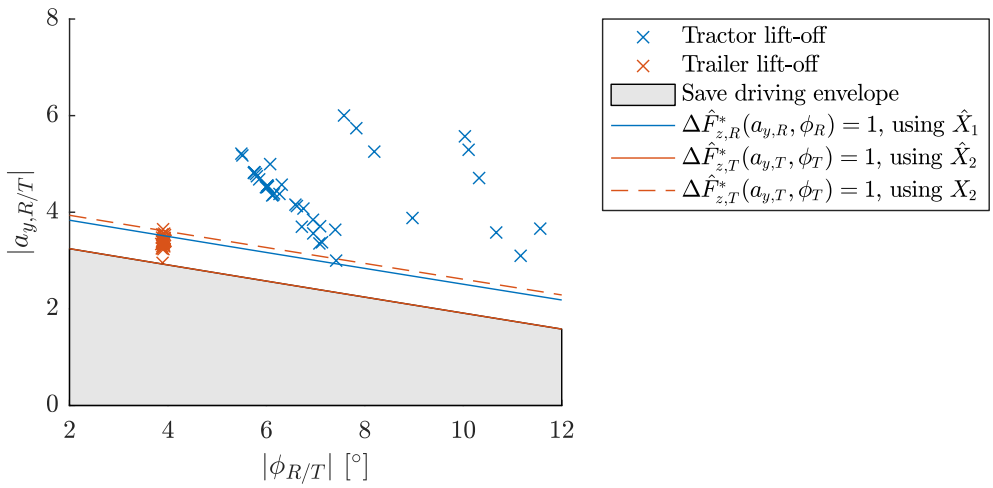

Figure 4-3: Monte Carlo simulation results – (a_y, ϕ) data points at the moments of wheel lift-offs, used to define a safe driving envelope

This is due to the fact that the tractor's rollover is always influenced by the trailer's motion. Based on this data, it is safe to say that in the following one should only be concerned about trailer rollovers, and only use the tractor's signals to make deductions regarding the trailer's state. Hence, (4-6) will only be considered for the trailer axle group and the only concern is to choose $c_{s,2}$.

Looking at the data, the average turnover point for the trailer is ($a_{y,T} = 3.4$ m/s^2 , $\phi_T = 3.9°$). The rollover threshold estimate $\Delta\hat{F}^*_{z,T}(a_{y,T}, \phi_T) = 1$ already explains this pretty well using X_2 – the small deviation from the average point could be due to the assumption $\ddot{\phi} = 0$. The trailer wheel lift-off event happening at extremely low lateral acceleration ($|a_{y,T}| < 3$) – as well as some others – are caused by hard retardation during a cornering manoeuvres. For the results without these edge cases and with modified suspension stiffness and CoG height, see Appendix A-2 (Figures A-9, A-10 and A-11). To account for edge cases, a design choice of

$$\hat{X}_2 = c_{s,2} \cdot X_2 = 1.25 \cdot 2.2939 = 2.88 \tag{4-8}$$

was applied, to have a relatively conservative estimate of LTR, yielding a safe driving envelope that covers all our (untripped) test cases.

4-1-4 Actuation possibilities for rollover mitigation

Let us recall the equation (2-24a). The lateral acceleration inducing roll motion is expressed as:

$$a_y = \dot{v}_y + v_x\dot{\psi} \tag{4-9}$$

In the paper [33] it is proven (for a single unit vehicle, assuming steady-state) that it is not possible to reduce the rollover risk by reallocating tyre forces without changing the yaw rate or the vehicle speed. In terms of this finding and (4-9) it is safe to say that the actuation possibilities (without Active Roll Control) are (differential) braking – or just a mild retardation to reduce speed – and counter-steering.

4-2 Test cases for roll stability

In this section, relevant test cases will be defined. The "hook" manoeuvre will represent quasi-static cornering scenarios. The "double lane change" can emphasise complex dynamics and tractor-trailer interaction. Lastly, the "evasion at high speed" will show how the system behaves when the lateral acceleration suddenly becomes extreme.

4-2-1 Hook manoeuvre

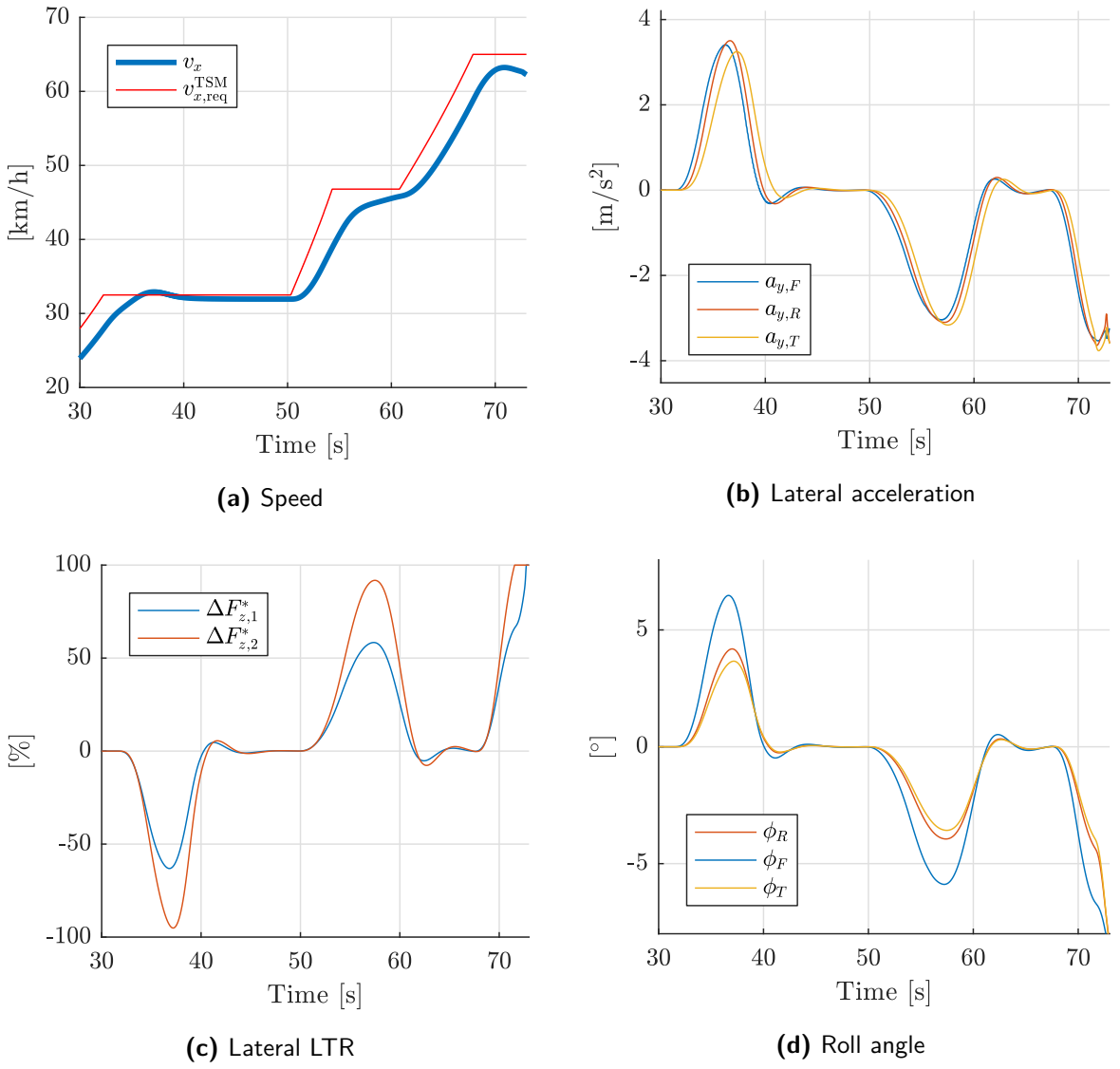

(a) Speed

(b) Lateral acceleration

(c) Lateral LTR

(d) Roll angle

Figure 4-4: Signals related to hook manoeuvre; $|\Delta F_z^*| = 100\%$ signifies wheel lift-off, happens at $a_{y,T} = 3.3$ m/s^2

The path depicted by Figure A-1 consists of three cornering manoeuvres, each at different speeds. Lateral dynamics is can here be regarded as quasi-static. Note that the load transfer

of the trailer is much more intense than that of the tractor unit – in the quasi-static case this is due to $h_{cg,1} < h_{cg,2}$. In fact, the trailer almost rolls over already in the first (sharp) turn at only $v_x = 32$ [km/h]. In addition, the first axle roll angle ϕ_F is much higher than the rest: This is due to the soft cab suspension. Still, it possesses the same dynamic characteristics as $\phi_{R/T}$: During this manoeuvre, $\phi_{R/T}$ and $a_{y,R/T}$ can be modelled as a scaled and delayed version of the corresponding front axle signal. Furthermore, RWA < 1 applies to the first, slow cornering, whereas at higher speeds RWA > 1. Wheel lift-off of the trailer axle group happens at $a_{y,T} = 3.3$ m/s^2 , which indicates that $a_{y,2}^{\mathrm{SRT}}$ gives merely a rough figure of the allowed lateral acceleration at small roll angles. The higher the CoG, the more difference the roll motion makes.

4-2-2 Double lane change

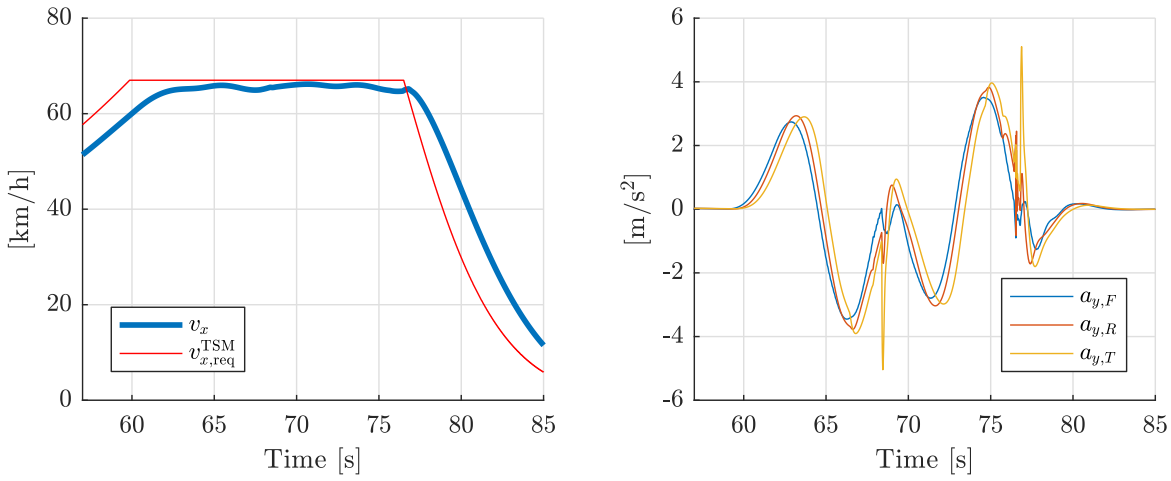

(a) Speed

(b) Lateral acceleration

(c) Lateral LTR

(d) Roll angle

Figure 4-5: Signals related to double lane change manoeuvre; $|\Delta F_z^*| = 100\%$ signifies wheel lift-off, happens at $a_{y,T} = 3.2$ m/s^2 , twice

The following test case (see Figure A-2) is the well-known double lane change, which is one of the riskiest driving tasks, involving complex dynamics with high frequency steering excitation at a constant speed. In the presented situation, Interaction between the tractor and trailer is a lot more intense. Aggressive trailer wheel lift-offs have a twisting effect on the fifth wheel, and so, further increasing the lateral load transfer of the tractor. At 76 seconds, both units are subjected to momentary wheel lift-off. The vividness of the situation is much better explained by looking at the LTR evolution than by simply considering trends in a_y, as commercialized ESC systems would do.

4-2-3 Evasion at high speed

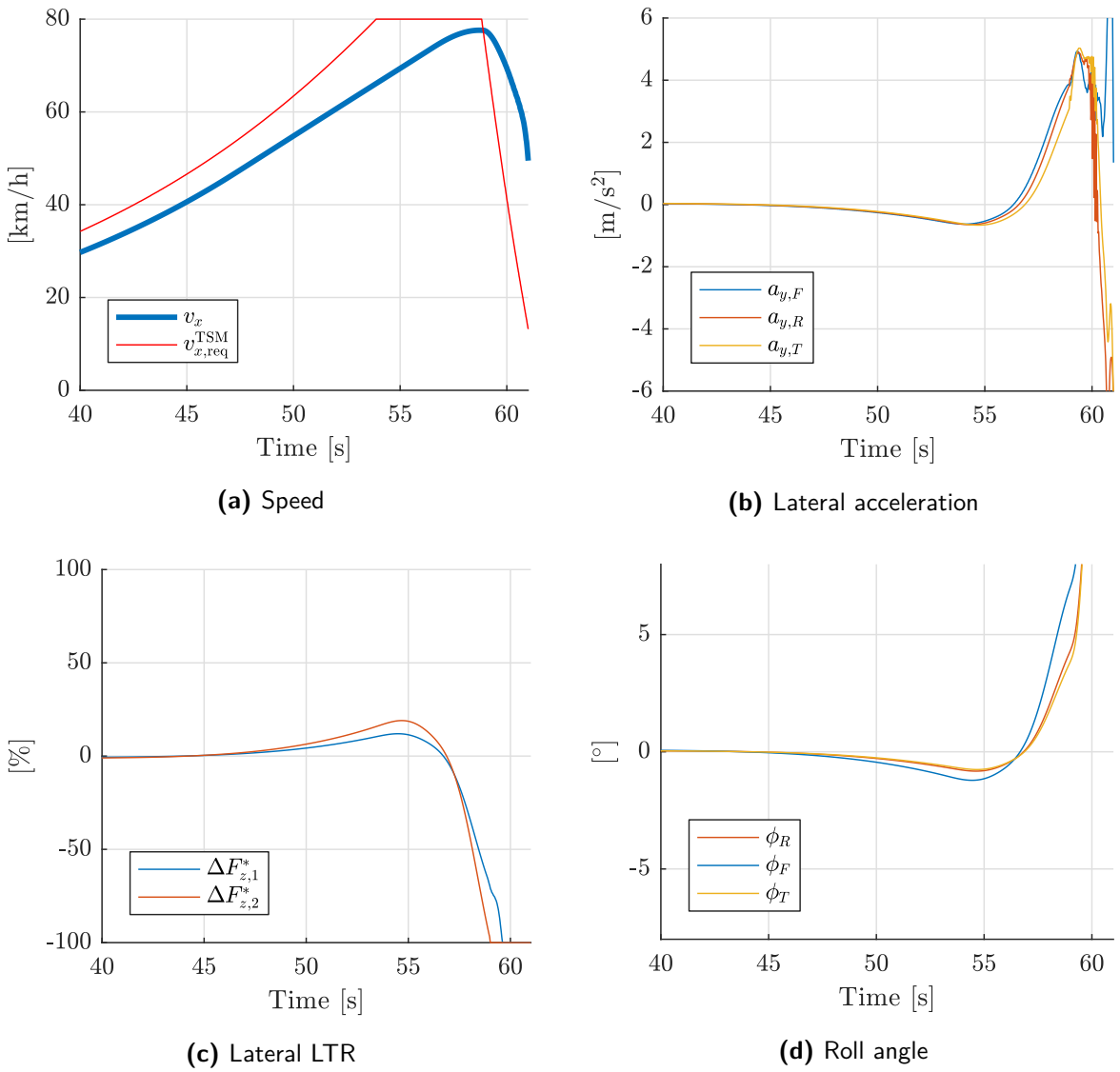

(a) Speed

(b) Lateral acceleration

(c) Lateral LTR

(d) Roll angle

Figure 4-6: Signals related to evasion manoeuvre at high speed; $|\Delta F_z^*| = 100\%$ signifies wheel lift-off, happens at $a_{y,T} = 3.1$ m/s^2

This test case (see Figure A-3) represents an evasion manoeuvre at a highway. Rollover

happens at $a_{y,T} = 3.1$ m/s^2 , way below $a_{y,2}^{\mathrm{SRT}}$ and within a matter of moments. Both units roll over simultaneously. The main challenge in preventing a rollover like this is the short time that is given to intervene. In addition, a fixed spatial horizon at high speeds might reduce significantly in time and a model that is updated based on past data might not have time to adapt to the new situation.

Additional, interesting test cases inducing high frequency oscillations in trailer lateral acceleration or hard braking during cornering resulting in rollovers can be found in the Appendix, Section A-1. In the following, only the hook manoeuvre will be presented as a way of testing control performance. The algorithms will of course be run on the rest of the test cases, as well. These results will be given in Appendix A. The developed algorithms performed well on in other test cases, as well. Still, these three comprise all important phenomena that need to be covered.

4-3 Conclusions

Concluding our investigations so far, one can make the following claims:

1. Due to the relatively low roll stiffness of trucks, rollovers happen at lateral accelerations below the Steady-State Rollover Threshold. The real threshold can vary depending on the actual roll motion states of the vehicle. Hence, to ensure absolute roll safety, a hard a_y limitation is not sufficient. One has to capture the dynamics of roll motion, as well – and incorporate it into predictions, if there are any.

2. As long as untripped rollovers are concerned, it makes sense to mainly focus on trailer behaviour, as dynamic effects and (especially in laden case) its higher Centre of Gravity make it far more likely to be exposed to wheel lift-off sooner than the tractor.

3. In cases of untripped rollovers, the trailer's lateral acceleration and roll angle states can be approximated as an amplified and phase-delayed version of the corresponding tractor rear axle signals (at low articulation angles, with typically applies, as rollovers happen at high speeds). This approximation, combined with knowledge of trailer's effective track width and CoG height (i.e. X_2) allows to conservatively ensure trailer roll stability by only measuring tractor rear axle signals. This is important, because not all trailers are equipped with the needed sensors.[1] In addition, roll angle estimation in our framework is currently only available on the cab.

4. Due to the lower roll stiffness of the front axle, a rollover intervention that involves retardation might induce a temporary peak in ϕ, and therefore, in ΔF_z^*. Thus, there has to be a margin of load transfer when triggering an intervention.

These statements will be validated in a quasi-static case by real-life measurements in Chapter 7.

[1] With dedicated hardware, there is a possibility to exploit the known articulation angle between the units and kinematically deduce the trailer's lateral acceleration. In practice however, this turned out to be unwise due to low robustness against measurement noise.

4-4 Summary and contributions

In this chapter, important factors and phenomena contributing to heavy vehicle rollovers were listed. The most important of these factors (CoG height to track width ratio, soft front axle suspension, Rearward Amplification and excited roll motion) were explicitly shown on the example of our chosen vehicle combination configuration, through simulation charts and parameter values. Subsequently, the necessity of a dynamic Rollover Index was explained and the chosen index derived in terms of measurable and predictable systems states. Monte Carlo simulations were carried out to define a safe driving envelope with the chosen vehicle configuration. Subsequently, its results were used to tune the detection algorithm. To get an understanding about rollovers in general and how the relevant vehicle states evolve wheel lift-offs, pre-defined test cases were shown, pointing out important aspects of roll safety. Lastly, conclusions were drawn that will be used as a starting point in the next chapters, during controller synthesis.

Chapter 5

Proactive Roll Stability Control

This Chapter will present the main ideas and design steps behind the proactive RSC, following the guidelines of the problem formulation given in Section 3-5. The controller shall be placed within the Functionality Domain - Traffic Situation Management and impose vehicle motion limitations based on an analysis of the generated reference trajectory and current vehicle states. Figure 5-1 shows, how this functionality fits into the control loop realized by FD-TSM and FD-VMM. The aim is to prevent sending requests to the lower-level Vehicle Motion

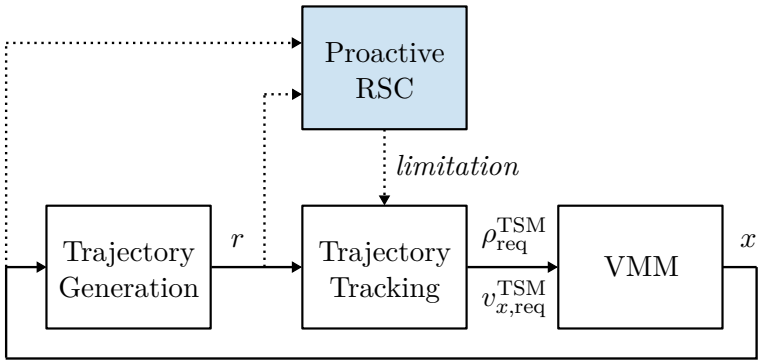

Figure 5-1: A high-level overview of the proactive RSC's functionality – the controller receives the generated trajectory and current vehicle states, and outputs safety requirements on FD-TSM's requests

Management that could potentially lead to wheel lift-off of any axle. In the following, the explanation will cover the related functional requirements, the prediction model and the intervention algorithm. Finally, simulation results will be given and conclusions will be drawn.

5-1 Requirements and assumptions

Most importantly, the utilization of the controller shall be sufficient to avoid untripped rollovers in itself, without the additional safety layer of reactive RSC (see Chapter 6). A

wide range of manoeuvres and speeds shall be covered and their safety ensured – this should be implied by a sufficient performance in all the defined test cases. Nevertheless, the interventions shall not be unnecessarily conservative: Vehicle mission performance should not be significantly limited. As it was previously pointed out in Chapter 4, achieving roll safety in a broader sense is only possible if one regards the load transfer phenomenon. Thus, the model-based predictions shall categorically focus on obtaining accurate (lateral) Load Transfer Ratio projections, not merely on roll motion states, such as lateral acceleration, roll angle and roll rate. Ideally, the proactive RSC shall constitute a separate functional entity or module that works independently of the nature of the trajectory generator in FD-TSM and the controllers in FD-VMM, as long as the prerequisite (3-38) holds. The implementation shall strive to meet this requirement, although this property will not be explicitly tested within the scope of this project. Furthermore, it should be possible to incorporate roadway bank into the vehicle motion limitations.

In order to meet the above requirements, one has to introduce some assumptions. Firstly, the mathematical steps in Section 5-3 will assume a differentiable heading description in $f_\psi(s)$, or the yaw rate reference to be prepared by the trajectory generator. In the same section, it will be assumed that neglecting lateral skidding during cornering is an insignificant simplification in terms of reference tracking. Secondly, a flat road surface will be presumed with zero road pitch angle. Since the proactive RSC will not be tested in real-life within the scope of this thesis, it will be assumed that the tractor's chassis roll angle ϕ_R is measured or accurately estimated (in reality, an accurate estimate of cab roll angle ϕ_F is available). Finally, the predictions will be based on linear models. Therefore, the closed-loop system behaviour has to be such that is possible to approximate it via a (constantly updated) linear model.

Two important, additional points are to regard both tractor and trailer unit roll stability and that the uncertainty of the Centre of Gravity height shall be accounted for. These were – with some compromises – dealt with in Chapter 4: Based on simulated test cases, it was argued that trailer stability implies safe tractor dynamics, as well. Furthermore, due to the lack of a reliable CoG height estimator, a safety factor (4-8) was introduced in the LTR calculations (4-6), based on Monte Carlo simulations.

5-2 Overview of controller architecture

Based on the findings in Chapter 4, the prediction goal is to acquire the approximate evolution of $\Delta F^*_{z,T}(k)$ on the prediction horizon $kT_s \in [0, t_H]$, denoted $\Delta \tilde{F}^*_{z,T}(k)$. In terms of (4-6), this can approximately be achieved by making predictions for $a_{y,T}$ and ϕ_T. Using conclusion number 3. of the previous Chapter 4, $a_{y,R}$ and ϕ_R will be predicted and the scaling $\hat{X}_2$ applied to deduce the trailer's lateral load transfer. The phase delay between the tractor rear axle and trailer axle signals will be neglected – in rollover detection, one is interested in obtaining accurate amplitudes as soon as possible.

Remark: This approach has one significant benefit: It allows the proactive algorithm to work with different trailer units, provided the parameter X_2 is accurately known and the safety factor $c_{s,2}$ is accordingly chosen.

Since coupled vehicle motion models are too complex to use as prediction models, a design choice is made to come up with decoupled yaw and roll motion models. Here, the yaw planar model would describe how the lateral acceleration evolves whilst tracking the predefined reference trajectory, which will be the input of the roll planar prediction model. This architecture is depicted by Figure 5-2. Let us define a reference trajectory description along the time horizon t_H as

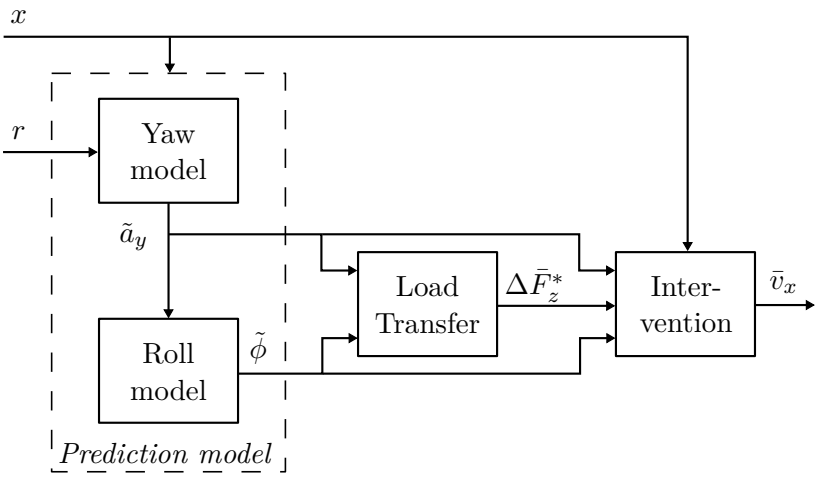

Figure 5-2: Signal flow of proactive Roll Stability Control

$$R_r(k) = \begin{bmatrix} r(k) & r(k+1) & \cdots & r(k+n_H) \end{bmatrix} \in \mathbb{R}^{q\times(n_H+1)} \tag{5-1}$$

where $n_H = t_H/T_s$ and it is assumed that $n_H \in \mathbb{N}$ always applies. Let us also define the following:

$$\tilde{\Lambda}(k) = \begin{bmatrix} \tilde{a}_y(k) & \tilde{a}_y(k+1) & \cdots & \tilde{a}_y(k+n_H) \end{bmatrix}^T = f_\Lambda(R_r(k), x(k)) \tag{5-2a}$$

$$\tilde{\Phi}(k) = \begin{bmatrix} \tilde{\phi}(k) & \tilde{\phi}(k+1) & \cdots & \tilde{\phi}(k+n_H) \end{bmatrix}^T = f_\Phi\left(f_\Lambda(x(k), R_r(k)), x(k)\right) \tag{5-2b}$$

with $f_\Lambda : \mathbb{R}^{q\times(n_H+1)} \times \mathbb{R}^n \to \mathbb{R}^{n_H+1}$, $f_\Phi : \mathbb{R}^{n_H+1} \times \mathbb{R}^n \to \mathbb{R}^{n_H+1}$. Based on $\tilde{\Lambda}(k)$ and $\tilde{\Phi}(k)$, the Rollover Index $\Delta\bar{F}_z^*(k) \in \mathbb{R}$ is calculated:

$$\Delta\bar{F}_z^*(k) = f_{\text{ROI}}\left(\tilde{\Lambda}(k), \tilde{\Phi}(k)\right) \tag{5-3}$$

which is the maximal, predicted LTR along the prediction horizon, with $f_{\text{ROI}} : \mathbb{R}^{n_H+1} \times \mathbb{R}^{n_H+1} \to \mathbb{R}$. Based on $\Delta\bar{F}_z^*$, an appropriate vehicle motion limitation should be obtained. If the horizon length t_H is sufficiently long, rollover danger could be detected soon enough so that no hard braking event is needed, nor a counter-steering intervention. Ideally, a mild reference speed reduction to a safe level before intense cornering shall suffice. This is equivalent to writing:

$$v_{x,\text{req}}^{\text{TSM}}(k) = \min\left(v_{x,\text{ref}}(k), \bar{v}_x(k)\right) \tag{5-4a}$$

$$\bar{v}_x(k) = f_{\text{int}}\left(\tilde{\Lambda}(k), \tilde{\Phi}(k), \Delta\bar{F}_z^*(k), x(k)\right) \qquad \forall k \in \mathbb{Z}^+ \tag{5-4b}$$

where $v_{x,\text{req}}^{\text{TSM}}(k)$ is the speed request sent by FD-TSM to FD-VMM, $v_{x,\text{ref}}(k)$ is the current reference speed in $r(k)$ (see (3-34) and (3-35)) and $\bar{v}_x(k)$ is a speed limitation ensuring roll safety, based on the intervention function $f_{\text{int}} : \mathbb{R}^{n_H+1} \times \mathbb{R}^{n_H+1} \times \mathbb{R} \times \mathbb{R}^n \to \mathbb{R}$. This intervention calculation will take into account the currently measured vehicle states $x(k)$, which closes the control loop.

In the following four sections, the functional blocks of the proactive RSC will be discussed in detail.

5-3 Horizontal motion prediction

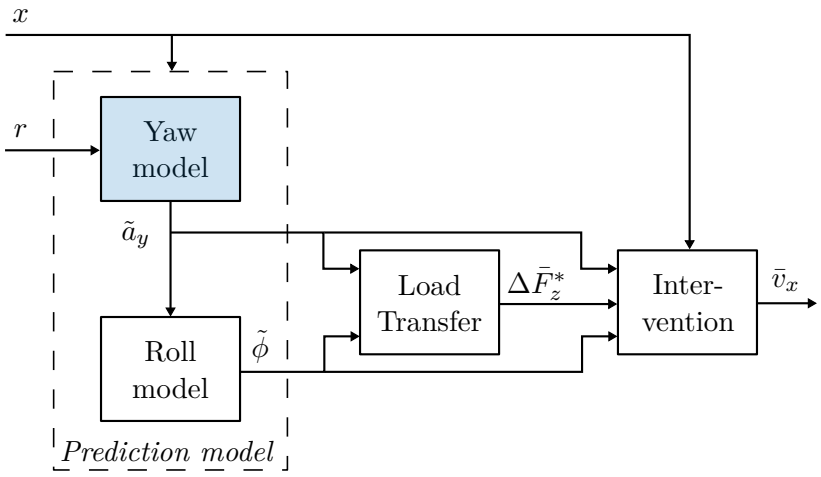

Figure 5-3: Signal flow of proactive Roll Stability Control – focusing on horizontal motion prediction

In this section, predicting the closed-loop behaviour of the vehicle in the horizontal plane will be in focus, on a prediction horizon corresponding to the reference trajectory $f_r(s), \quad s \in [0, s_H]$ (horizon length $s_H = 35$ m, by definition). This of course implies knowledge about the underlying control algorithm within the closed loop. As mentioned several times earlier, the predictions should be accurate regardless of the used tracking algorithm. In practice, this means that the design process should use as little information about yaw control as possible, which implies that some level of abstraction will be needed.

It is important to recognize that from a roll safety perspective, one solely cares about the dynamics of $a_y(k)$, as this signal will serve as excitation to the roll motion prediction model. Thus, the used model can be greatly simplified, which has an other benefit, namely that identification of a detailed yaw motion model can be avoided, which typically uses a high number of parameters (see examples in Chapter 2). Doing so, one can neglect other vehicle states such as global position and heading.

In this thesis, these problems are resolved by transforming the reference trajectory $r(k)$ into an abstract lateral acceleration reference $a_{y,\text{ref}}(k)$, that is being tracked by a likewise abstract second order system. The result of tracking $a_{y,\text{ref}}(k)$ is the prediction $\tilde{a}_y(k)$, which resembles the closed-loop behaviour of $a_y(k)$ on the time horizon $kT_s \in [0, t_H]$.

5-3-1 Translation of the reference trajectory to lateral acceleration reference

The following reference information is given, recalling (3-34):

$$\psi_{\text{ref}}(s) = f_{\psi}(s) \tag{5-5}$$
$$v_{x,\text{ref}}(s) = f_{v}(s), \quad s \in [0, s_H] \tag{5-6}$$

If one carries out the transformation $\Upsilon : \mathbb{R}^q \to \mathbb{R}^q$, recalling (3-35):

$$r(k) = \Upsilon\left(f_r(s)\right) \tag{5-7}$$

and so, obtains $\psi'_{\text{ref}}(k)$ and $v'_{x,\text{ref}}(k)$ (which contain the same information as $\psi_{\text{ref}}(s)$ and $v_{x,\text{ref}}(s)$, using time parametrization), it is possible to use (2-24a) to deduce the lateral acceleration that needs to be achieved in order to follow the required path with the desired speed profile. Assuming that $a_{y,\text{ref}}(k)$ does not account for non-ideal path following and lateral skidding, $\dot{v}_y = 0$ can be set, thus:

$$a_{y,\text{ref}}(k) = v'_{x,\text{ref}}(k)\dot{\psi}'_{\text{ref}}(k) \tag{5-8}$$

While this seems to be straight forward, the transformation Υ still has to be found. The formula

$$s_i = \int_0^{t_i} v_x(\tau)d\tau \qquad 0 \leq t_i \leq t_H,\ 0 \leq s_i \leq s_H \tag{5-9}$$

will be used to create an association between the time points t_i and the corresponding curve lengths s_i. The problem is that using $v_x(t)$ assumes knowledge of the vehicle speed along the prediction horizon, which is dependent on the closed-loop behaviour including cruise control (see (3-31)). Assuming a small tracking error, using the information[1] in $v_{x,\text{ref}}$ could be an option. Nevertheless, as it turned out during simulations, the currently used setup oftentimes allows a large delay between the actual speed and its reference, which can cause significant absolute deviations in $v_{x,\text{ref}}(k) - v_x(k)$ during high longitudinal acceleration levels, deteriorating (5-9) – see for instance Figure 4-4.

An acceptable performance has been achieved by linearly extrapolating v_x:

$$\hat{v}_x(t) = v_x(0) + a_x(0)t \qquad t \in [0, t_H] \tag{5-10}$$

where $\hat{v}_x(t)$ is the estimated future speed profile, based on the current speed and longitudinal acceleration – see Figure 5-4. In addition, this approach is very general and is independent of the used cruise control method. Now, one can evaluate the integral

$$s_k = \int_0^{t_k} \hat{v}_x(\tau)d\tau \qquad 0 \leq t_k \leq t_H,\ 0 \leq s_k \leq s_H \tag{5-11}$$

at each time step $\{t_k = kT_s | k \in \mathbb{Z}^+ \leq t_H/T_s\}$ to obtain the corresponding s_k lengths. Then, one can hope to get:

$$\psi'_{\text{ref}}(t_k) \approx \psi_{\text{ref}}(s_k) \tag{5-12}$$

[1] This could mean using the slope information of the reference to deduce the expected evolution of the speed in the future. Nevertheless, attempts to expoit this were proven to be unsuccessful, for the mentioned reason.

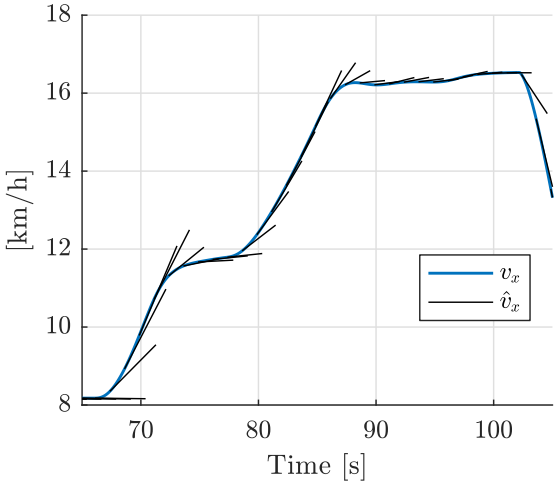

Figure 5-4: Prediction of speed, based on extrapolation – during a hook manoeuvre (every 100th prediction is plotted)

where the accuracy will depend on how well v_x is approximated by $\hat{v}_x$. In this thesis work, for the relatively short horizon $s_H = 35$ m, this is a reasonable assumption that will only yield noticeable errors during intense longitudinal accelerations. From a numerical perspective, the s_k obtained by (5-11) is likely to fall between the points $\{s_i = i\Delta s | i \in \mathbb{Z}^+ \leq s_H/\Delta s\}$ (with Δs being the fixed spatial step length), where the reference trajectory is defined. Therefore, interpolating ψ_{ref} is needed.

Remark: The numerical challenge in these calculations is handling the changing time horizon length t_H in a real-time embedded software environment. Initially, the time horizon in (5-10) is set to 10 s, which is then adjusted in (5-11), when $s_k > 35$m is satisfied. Once (5-10) and (5-12) (and its appropriately filtered numerical derivative) are numerically pre-calculated, one can write in terms of (5-8):

$$\hat{a}_{y,\text{ref}}(k) = \hat{v}_x(k)\dot{\psi}'_{\text{ref}}(k) \tag{5-13}$$

which yields the abstract lateral acceleration "reference". As Figure 5-5 shows, tracking a trajectory (path following is illustrated by Figure 5-5a) can be interpreted (from the Roll Stability Control perspective) as if $a_y(k)$ were tracking its reference signal $\hat{a}_{y,\text{ref}}(k)$ – for better visualization, only the last two turns are plotted on Figure 5-5b.

5-3-2 Prediction of lateral acceleration

Looking at Figure 5-5 it becomes obvious that $a_{y,R}$ can approximately be predicted for the next t_H seconds, only by regarding $\hat{a}_{y,\text{ref}}$. However, the reference does not tell us anything about the closed-loop dynamics. The aforementioned figure proves the importance of this: In some cases (on the figure, at about 90 seconds), $a_{y,R}$ can indeed overshoot its abstract reference.

The model that is utilized to approximate the expected closed-loop behaviour shall be as simple as possible, keeping the real-time requirements, flexibility, generality and ease of implementation in mind – the first approach will be a linear system description. Nevertheless,

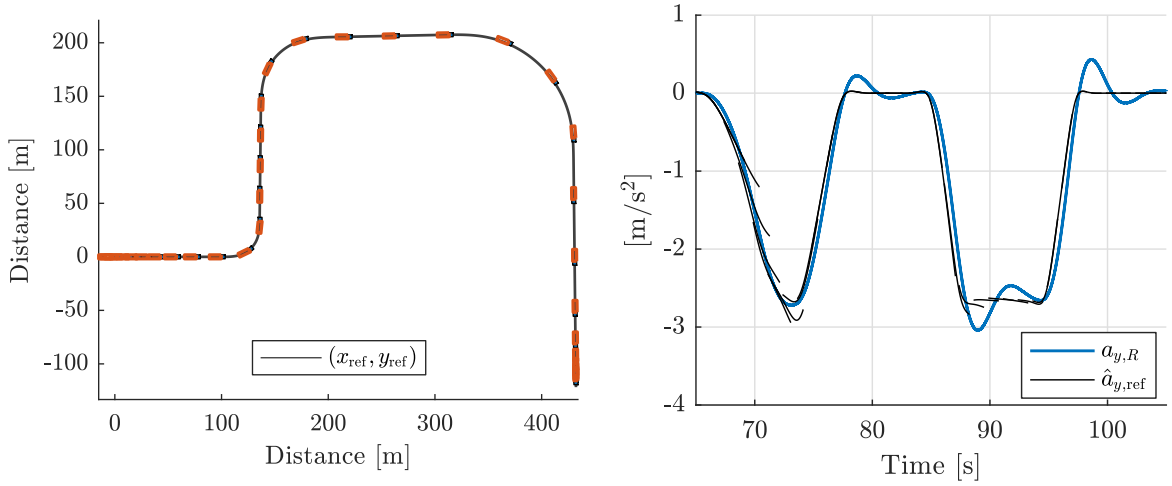

(a) Original (path) tracking problem

(b) Translated tracking problem (last two turns)

Figure 5-5: Lateral acceleration reference trajectories, "tracked" by lateral acceleration – during a hook manoeuvre (every 100th $\hat{a}_{y,\text{ref}}$ trajectory is plotted)

it should still be able to capture the "swings" in the a_y signal, i.e. should exhibit oscillations and overshoot, an intuitive equivalent of "momentum". This implies accounting for *lateral jerk*. The simplest linear system that meets these criteria is second order, having no zeros. The following standard SISO transfer function description is assigned to it:

$$G_a(\breve{s}) = \frac{\tilde{A}_{y,R}(\breve{s})}{\hat{A}_{y,\text{ref}}(\breve{s})} = \frac{A_G \omega_n^2}{\breve{s}^2 + 2\xi\omega_n \breve{s} + \omega_n^2} \tag{5-14}$$

where G_a is a Laplace-domain transfer function, $\tilde{A}_{y,R}$ and $\hat{A}_{y,\text{ref}}$ the Laplace-transforms of the corresponding acceleration signals, $\breve{s}$ a complex number, A_G the steady-state gain of the system, ξ the damping factor and ω_n the undamped natural frequency. Choosing these parameters is key. Both input and output signals have the dimension m/s^2 and steady-state offset is undesired. Furthermore, a reasonable amount of overshoot should be made possible. These motivate the parameter choices according to Table 5-1. For simplicity, the tracking quality will be incorporated solely into the parameter ω_n. This is of course an

Table 5-1: Chosen parameters of the acceleration model

Parameter	Value
A_G	1
ξ	$1/\sqrt{2}$
ω_n	$0.5 \ldots 3$ rad/s

oversimplification of the real dynamics, but as it was pointed out earlier, the goal is predicting the right magnitude of a_y during tracking – from a roll safety perspective, it is far more important than accurate dynamics. Thus, an interval of ω_n values is set – for the scope of the these project, intuitively, based on the test cases of Chapter 4, to cover cases with low and high frequency behaviour in a_y. Then, the prediction algorithm can calculate the worst-case scenario from a rollover perspective. Generally, this interval can be adjusted according to

the bandwidth capabilities of the applied yaw controller (this would fit the FD-TSM/VMM interaction scheme depicted by Figure 3-3). If the yaw controller exhibits an aggressive behaviour, FD-VMM can communicate a high expected a_y bandwidth to FD-TSM, and the sudden changes will be accounted for by the prediction model (5-14).

The predicted lateral acceleration of the rear axle is obtained by subjecting the prediction model (5-14) to the acceleration reference (5-13):

$$\tilde{a}_{y,R}(t) = \max_i \left(\left| \mathcal{L}^{-1} \left\{ G_{a,i}(\breve{s}) \hat{A}_{y,\mathrm{ref}}(\breve{s}) \right\} \right| \right) \tag{5-15}$$

where $\mathcal{L}^{-1}$ is the inverse-Laplace transformation, and $G_{a,i}$ corresponds to the prediction model with bandwidth $\omega_{n,i} \in [\omega_n^{\min}, \omega_n^{\max}]$. In practice, this prediction is calculated at discrete k time points, by discretizing a finite number of models $G_{a,i}$ using zero-order-hold, obtaining the form

$$H_{a,i}(q^{-1}) = \frac{n_{1,i} + n_{2,i} q^{-1}}{d_{1,i} + d_{2,i} q^{-1} + d_{3,i} q^{-2}} \tag{5-16}$$

with $H_{a,i}$ being the discretized transfer function $G_{a,i}$, q the time-shift operator and $n_{1/2,i}$, $d_{1/2/3,i}$ scalar coefficients, corresponding to a particular $\omega_{n,i}$ bandwidth. This leads to the difference equation

$$\tilde{a}^i_{y,R}(k+1) = -\frac{d_{2,i}}{d_{1,i}} \tilde{a}^i_{y,R}(k) - \frac{d_{3,i}}{d_{1,i}} \tilde{a}^i_{y,R}(k-1) + \frac{n_{1,i}}{d_{1,i}} \hat{a}_{y,\mathrm{ref}}(k) + \frac{n_{2,i}}{d_{1,i}} \hat{a}_{y,\mathrm{ref}}(k-1) \tag{5-17a}$$

$$\tilde{a}_{y,R}(k+1) = \max_i \left(\left| \tilde{a}^i_{y,R}(k+1) \right| \right), \qquad kT_s \in [0, t_H] \tag{5-17b}$$

A very important issue here that needs to be addressed is the choice of the initial conditions $\tilde{a}^i_{y,R}(0)$, $\tilde{a}^i_{y,R}(-1)$. The association $\tilde{a}^i_{y,R}(0) = a_{y,R}(0)$ is intuitively straight forward. Setting $\tilde{a}^i_{y,R}(-1) = a_{y,R}(-1)$ is equivalent to numerical differentiation of $a_{y,R}$, which reduces robustness against noise and causes accuracy problems even during simulated test cases – ideally, measurement of lateral jerk would be required, which is unavailable. In the current project, this problem is dealt with as follows:

$$\Delta \hat{a}_y(0) = \hat{a}_{y,\mathrm{ref}}(0) - \hat{a}_{y,\mathrm{ref}}(-1) \tag{5-18a}$$

$$\tilde{a}^i_{y,R}(-1) = \lambda_a \left(a_{y,R}(0) - \Delta \hat{a}_y(0) \right) + (1 - \lambda_a) a_{y,R}(-1) \tag{5-18b}$$

where $\Delta \hat{a}_y$ represents the change (slope) in the acceleration reference (which is inherently noise-free) and the filtering factor λ_a can be used to prioritize between potential accuracy and robustness. In the tested cases, a $\lambda_a = 0.5$ returned satisfactory performance. Prediction results for the test case used in Figure 5-5 are shown by Figure 5-6 – $\lambda_a = 0$ would yield even more accurate predictions in a quasi-static case like this one.

Remark: The predictions (5-17) are based on current a_y measurements, which are dependent on the chassis roll angle due to sensor mounting (see Figure 5-7). Still, according to the model 2-16, a horizontal input force on the chassis' CoG is assumed. According to the findings in Chapter 4, with the current truck configuration, wheel lift-offs happen below $\phi_T = 4^\circ$, hence even in the worst case scenario, the relative error caused by sensor roll is $1 - a_y / a_y^{\mathrm{meas}} = 1 - \cos(4^\circ) = 0.0024$. Therefore, this difference will be neglected.

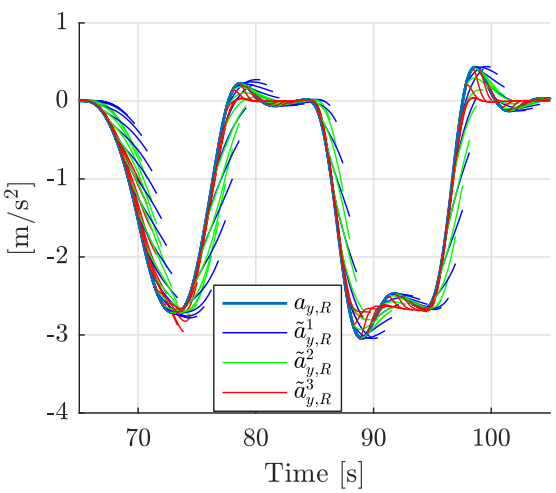

(a) Prediction results according to $\omega_{n,1} = 0.5$ rad/s, $\omega_{n,2} = 1$ rad/s, $\omega_{n,3} = 3$ rad/s

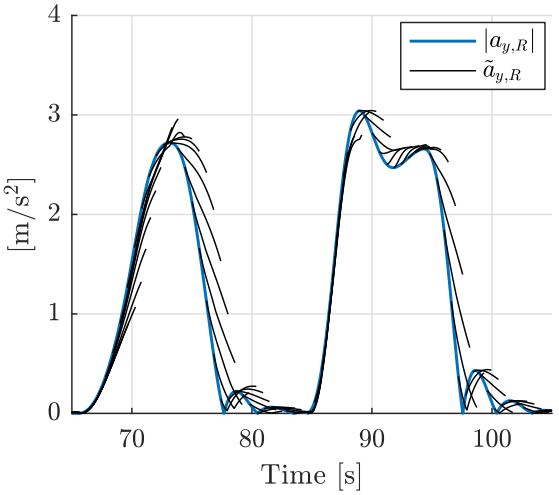

(b) Final prediction, according to $\tilde{a}_{y,R} = \max_i(|\tilde{a}^i_{y,R}|)$

Figure 5-6: Lateral acceleration predictions – during a hook manoeuvre (every 60th trajectory is plotted); the speed varies between 10-16 m/s, which yields prediction horizons of length 2.2-3.5 s

5-4 Roll motion prediction

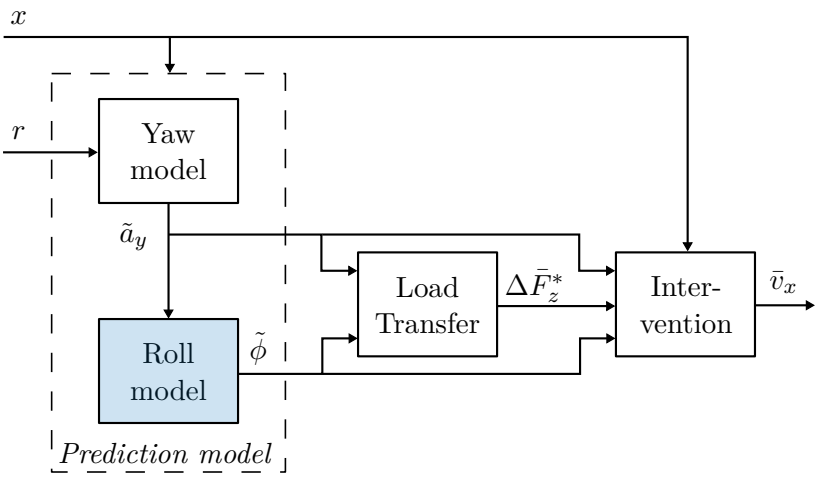

Figure 5-8: Signal flow of proactive Roll Stability Control – focusing on roll motion prediction

The roll prediction model will be based on the previously introduced heavy vehicle roll motion description (2-18). As it was concluded in Chapter 4, rollovers typically happen around 4° roll angle (which is confirmed by real-life tests, see Chapter 7), therefore linearization of (2-18) is a reasonable simplification, as long as wheel lift-off does not happen at any axle. The linearized differential equation of motion at the rear of the tractor chassis will become:

$$(I_{xx} + mh_{cg}^2)\ddot{\phi}_R = ma_{y,R}h_{cg} + \left(mgh_{cg} - \frac{1}{2}k_\phi l_t^2\right)\phi_R - \frac{1}{2}b_\phi l_t^2\dot{\phi}_R \tag{5-19}$$

Here, the parameters k_ϕ, b_ϕ, h_{cg} are especially hard to obtain by means of conventional mea-

surement techniques. In this section, the linearized prediction model (5-19) will be constantly updated online, implicitly estimating the above-mentioned parameters. Then, a method will be presented to apply the identified model to predict the roll motion along $\tilde{a}_{y,R}(k)$, $kT_s \in [0, t_H]$. As mentioned earlier, for the proactive controller design, ϕ_R is assumed to be measured.

5-4-1 Roll motion model identification

Firstly, let us rewrite to model (5-19) to a more convenient, standard form:

$$\ddot{\phi}_R + c_1\dot{\phi}_R + c_2\phi_R = c_3 a_{y,R} \tag{5-20}$$

where $c_{1/2/3}$ are scalar coefficients. For real-time implementation, the above model will need to be discretized. Since $\dot{\phi}_R$ is typically measured, it is straight forward to write (5-20) in state-space form, which makes the choice of prediction initial conditions $\tilde{\phi}_R(0) = \dot{\phi}_R(0)$, $\tilde{\phi}_R(0) = \phi_R(0)$ straight forward, opposed to a discrete-time transfer function description. The continuous-time state-space form of (5-20) is:

$$\begin{bmatrix}\dot{\phi}_R(t)\\ \ddot{\phi}_R(t)\end{bmatrix} = \underbrace{\begin{bmatrix}0 & 1\\ -c_2 & -c_1\end{bmatrix}}_{=A_c}\begin{bmatrix}\phi_R(t)\\ \dot{\phi}_R(t)\end{bmatrix} + \underbrace{\begin{bmatrix}0\\ c_3\end{bmatrix}}_{=B_c} a_{y,R}(t) \tag{5-21}$$

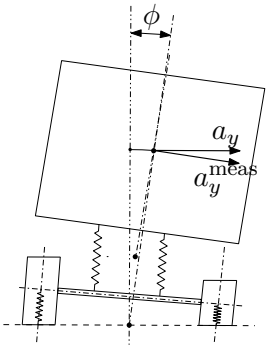

Figure 5-7: Differentiation between the lateral acceleration resulting from the D'Alembert force and the one measured, based on [7]

where A_c, B_c are system matrices. Using zero-order-hold, these system matrices can be discretized, yielding:

$$\begin{bmatrix}\phi_R(k+1)\\ \dot{\phi}_R(k+1)\end{bmatrix} = \underbrace{\begin{bmatrix}a_{d,11} & a_{d,12}\\ a_{d,21} & a_{d,22}\end{bmatrix}}_{=A_d}\underbrace{\begin{bmatrix}\phi_R(k)\\ \dot{\phi}_R(k)\end{bmatrix}}_{=x_\phi(k)} + \underbrace{\begin{bmatrix}b_{d,1}\\ b_{d,2}\end{bmatrix}}_{=B_d} a_{y,R}(k) \tag{5-22}$$

where $x_\phi(k)$ is the discrete-time system state vector of the roll motion model, A_d, B_d are discretized system matrices with the corresponding $a_{d,ij}$, $b_{d,i}$ scalar coefficients – the goal of roll motion identification is estimating these coefficients.

Formulation of the identification problem

To do so, let us define the following, according to the standard Recursive Least Squares (RLS) notation (see e.g. [34]):

$$y(k) = x_\phi^T(k) \tag{5-23a}$$

$$\varphi(k) = \begin{bmatrix}x_\phi(k-1)\\ a_{y,R}(k-1)\end{bmatrix} \tag{5-23b}$$

$$\Theta(k) = \begin{bmatrix}\hat{A}_d^T(k)\\ \hat{B}_d^T(k)\end{bmatrix} \tag{5-23c}$$

where $y(k) \in \mathbb{R}^{1\times 2}$ is the measurement vector, $\varphi(k) \in \mathbb{R}^3$ is the data vector (constituted by previous measurements and previous input), $\Theta(k) \in \mathbb{R}^{3\times 2}$ is the parameter estimate matrix. Recalling (5-22), one can write the following parameter identification formulation:

$$y(k) = \varphi(k)^T \Theta(k) + e_{id}(k) \tag{5-24}$$

where $e_{id}(k) \in \mathbb{R}^{1\times 2}$ is the identification error vector between the measured $y(k)$ and estimation $\varphi(k)^T\Theta(k)$. The Recursive Least Squares identification procedure will be carried out at each time step k as follows:

1. Save the previous states and input $\varphi(k)$, measure the system output $y(k)$
2. Calculate the error $e_{id}(k)$ using the previously estimated model parameters $\Theta(k-1)$

$$e_{id}(k) = y(k) - \varphi^T(k)\Theta(k-1) \tag{5-25}$$

3. Calculate the update gain vector $K(k)$ and update the tuning matrix $C_{id}(k)$

$$K(k) = \frac{C_{id}(k-1)\varphi(k)}{\lambda_{id} + \varphi^T(k)C_{id}(k-1)\varphi(k)} \tag{5-26}$$

$$C_{id}(k) = \frac{1}{\lambda_{id}}\left(C_{id}(k-1) - \frac{C_{id}(k-1)\varphi(k)\varphi^T(k)C_{id}(k-1)}{\lambda_{id} + \varphi^T(k)C_{id}(k-1)\varphi(k)}\right) \tag{5-27}$$

4. Update the parameter estimate matrix

$$\Theta(k) = \Theta(k-1) + K(k)e_{id}(k) \tag{5-28}$$

where $\lambda_{id} \in \mathbb{R} > 0$ is the exponential forgetting factor, ensuring that recent measurements are stronger weighted than older ones. Tuning this value ensures prediction accuracy and fast convergence time. A too low value will lead to underfitting data, whereas a too high setting will not incorporate enough measurements to be able to predict the future. Given the dataset $\{\varphi(0), \varphi(1), \ldots, \varphi(k)\}$, $C_{id} \in \mathbb{R}^{3\times 3}$ would be calculated as:

$$C_{id}(k) = \left[\sum_{i=0}^{k} \lambda_{id}^{k-i}\varphi(i)\varphi(i)^T\right]^{-1} \tag{5-29}$$

For derivation, more details about the RLS algorithm and the initialization of C_{id} and Θ, see [35].

Initialization of RLS

According to this, the following design decisions are made:

$$C_{id}(0) = 1000\hat{C}_\varphi \tag{5-30}$$

$$\Theta(0) = 0_{3,2} \tag{5-31}$$

where $\hat{C}_\varphi$ is the covariance matrix of $\varphi(k)$ numerically calculated on the short time window $kT_s \in [-t_W, 0]$. The intuitive explanation behind this choice (according to [35]) is that the

matrix $C_{id}(k)$ is proportional to the matrix $C_\Theta(k) = E[(\Theta(k) - E[\Theta(k)])(\Theta(k) - E[\Theta(k)])^T]$ and at early time steps, $\hat{C}_\Theta(k) \approx \hat{C}_\varphi(k)$. Since the knowledge of these parameters at $k = 0$ is vague, high covariance values are expected. The exact initialization of C_{id} requires matrix inversion (see (5-29)), which might not be guaranteed to exist on based on the data gathered during the window $kT_s \in [-t_W, 0]$. $\Theta(0) = 0_{3,2}$ assumes no prior knowledge of the system coefficients.

Activation and adjustment of RLS

For the parameter updates given by (5-28) to converge, the system needs to be excited. In the extreme case, when the input sequence $a_{y,R}(k) = 0$ (and, therefore $\varphi(k) = 0$) $\forall k \in \mathbb{Z}$, no information about the transfer from $a_{y,R}(k)$ to $y(k)$ can be retrieved. This implies that the input sequence $\varphi(k)$ has to be "rich" enough, which is called *persistency of excitation* of the input [36]. The activation condition

$$(v_x(k) > 5 \text{ km/h}) \wedge \left(|a_{y,R}(k)| > 0.5 \text{ m/s}^2\right) \tag{5-32}$$

turned out to be effective to ensure a sufficient level of persistency of excitation. In the following, prediction results will not be plotted, when the condition (5-32) is unsatisfied.

Furthermore, it is known that – with all wheels on the road – the roll motion of a heavy vehicle unit is inherently stable. This prior knowledge can be incorporated into the identification process by rejecting solutions that would imply an unstable system[2]. Using the partitioning in (5-23c), one can retrieve $\hat{A}_d(k)$ from $\Theta(k)$. The identified linear discrete-time system is asymptotically stable if and only if:

$$\forall \lambda_i \in \mathbb{C} \text{ that satisfy } |\hat{A}_d(k) - \lambda_i I| = 0,\ |\lambda_i| < 1 \tag{5-33}$$

applies, where λ_i is an eigenvalue of $\hat{A}_d(k)$, I is the identity matrix. Then, the step (5-28) can be modified as follows:

$$\Theta(k) = \begin{cases} \Theta(k-1) + K(k)e_{id}(k), & \text{if (5-33) applies} \\ \Theta(k-1), & \text{otherwise} \end{cases} \tag{5-34}$$

In turns out that implementing this adjustment improves identification accuracy a great deal.

Identification results

Figure 5-9 shows Bode magnitude plots and eigenvalues of the identified (and continuously updated), second-order systems, after initial convergence, using $t_W = 5$ s and $\lambda_{id} = 0.97$. The plots correspond to the scenario covered by Figures 5-5 and 5-6. The predominantly identified system is shown by the dashed line – only some cases differ significantly. The largely deviating system descriptions might cause a "blow-up" phenomenon in the predictions. As it will be seen in Section 5-6, the intervention design is prepared for such cases not to cause unexpected behaviour.

[2]The fact that systems with $\mathfrak{Re}(\lambda_i) < 0$ do not have a continuous-time equivalent will be disregarded: In practice, using this as constraint was proven to be too limiting for fast convergence.

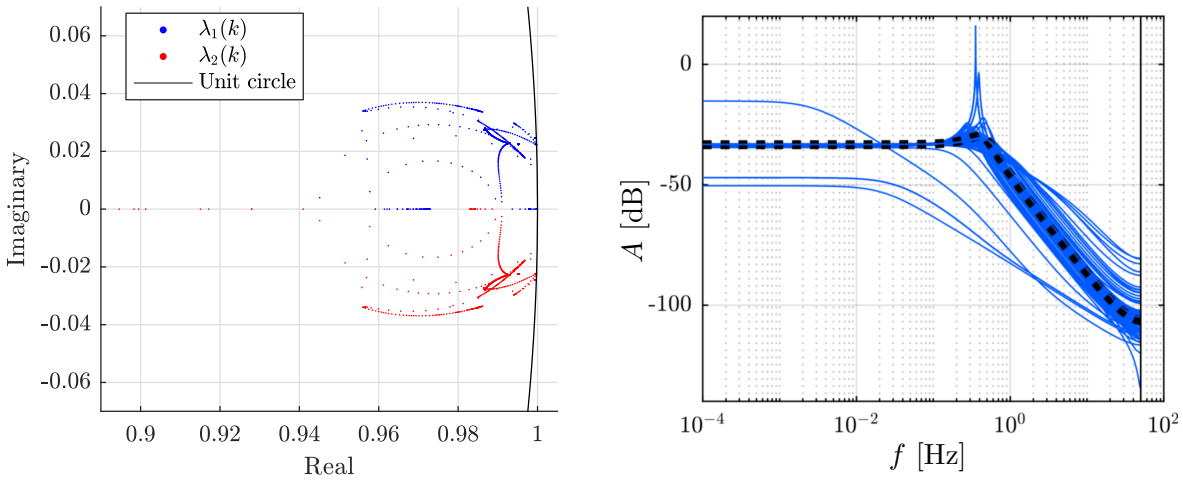

(a) Eigenvalues **(b)** Bode magnitude plots

Figure 5-9: Characteristics of updated models from $a_{y,R}$ [m/s^2] to ϕ_R [rad] – during a hook manoeuvre, after after initial RLS convergence; the most commonly identified system is highlighted

One can observe that the prevailing identified system has a natural frequency within the range 0.2 - 0.8 Hz, which (as mentioned in Chapter 2) is typical for heavy vehicle roll motion eigenmodes. Validation of the updates models will happen by evaluating prediction performance.

5-4-2 Prediction of roll angle

At time step k with $kT_s \in [0, t_H]$, the identified model will possess the system matrices $\hat{A}_d(k)$, $\hat{B}_d(k)$. The roll motion prediction model will be applied along the (predicted) lateral acceleration trajectories $\tilde{a}^i_{y,R}(k)$ corresponding to the bandwidth values $\omega_{n,i}$ – and not along $\tilde{a}_{y,R}(k)$, as this might include discontinuities due to the "max" operation, see (5-17). Recalling (5-22), the prediction model becomes:

$$\begin{bmatrix} \tilde{\phi}^i_R(k+1) \\ \dot{\tilde{\phi}}^i_R(k+1) \end{bmatrix} = \hat{A}_d(k) \underbrace{\begin{bmatrix} \tilde{\phi}^i_R(k) \\ \dot{\tilde{\phi}}^i_R(k) \end{bmatrix}}_{=\tilde{x}_{\phi,i}(k)} + \hat{B}_d(k)\tilde{a}^i_{y,R}(k) \tag{5-35a}$$

$$\tilde{\phi}_R(k+1) = \max_i \left(|\tilde{\phi}^i_R(k+1)| \right), \qquad kT_s \in [0, t_H] \tag{5-35b}$$

with the initial conditions $\tilde{\phi}^i_R(0) = \phi_R(0)$ and $\dot{\tilde{\phi}}^i_R(0) = \dot{\phi}_R(0)$. Prediction results are depicted by Figure 5-10. This time, to visualize RLS convergence, a wider time range is presented: One can observe the improving prediction performance over time. In the pre-defined test cases, reasonable performance could be achieved with $\lambda_{id} = 0.97 \ldots 0.98$. In this thesis work, all presented results were achieved using $\lambda_{id} = 0.97$, but in cases, where the lateral acceleration was changing with high frequencies (e.g. during a reactive intervention, see Chapter 6) a slightly higher λ_{id} resulted in faster convergence, thus, in more accurate predictions. For this reason and for avoidance of the blow-up phenomenon (infinite increase of the covariance matrix (5-27)), as well as for a faster adaptation to a changed setpoint of the vehicle states, the implementation of an adaptive forgetting factor is highly recommended. This has also been

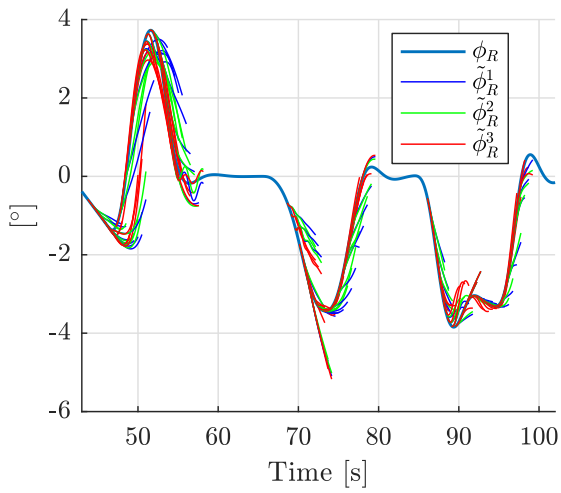

(a) Prediction results according to $\omega_{n,1} = 0.5$ rad/s, $\omega_{n,2} = 1$ rad/s, $\omega_{n,3} = 3$ rad/s

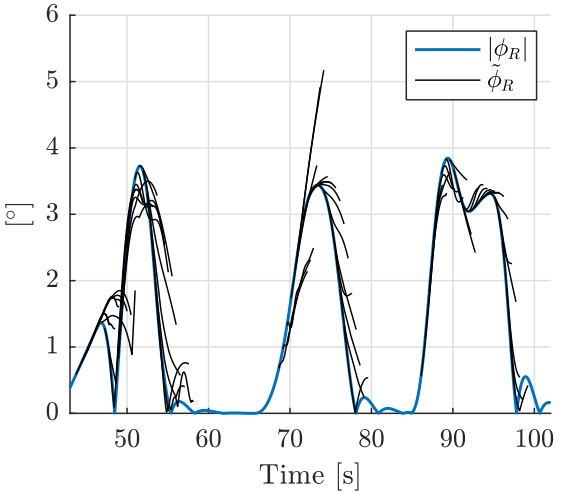

(b) Final prediction, according to $\tilde{\phi}_R = \max_i(|\tilde{\phi}_R^i|)$

Figure 5-10: Roll angle predictions – during a hook manoeuvre (every 60th trajectory is plotted); the speed varies between 10-16 m/s, which yields prediction horizons of length 2.2-3.5 s

pointed out by the scientific literature, see for instance [37] on a similar topic. In addition, appropriate preprocessing of RLS regression signals in φ would likely be necessary for real-life applications.

5-5 Prediction of lateral load transfer ratio

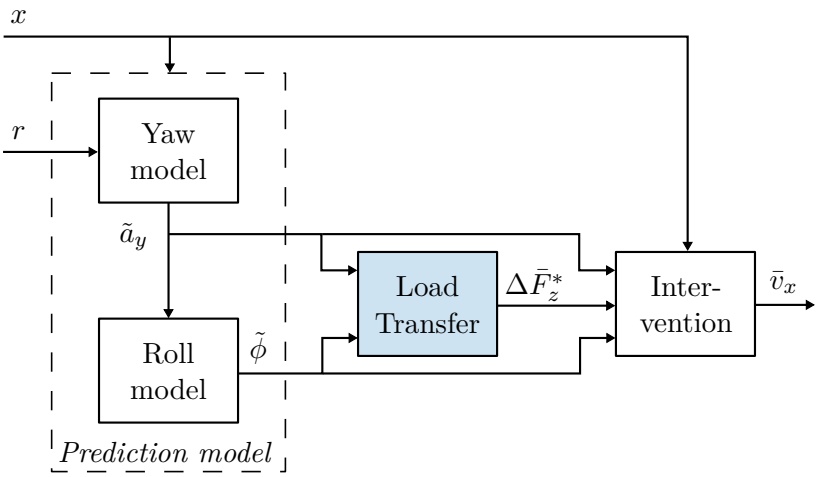

Figure 5-11: Signal flow of proactive Roll Stability Control – focusing on lateral load transfer prediction

In the previous sections, prediction of lateral acceleration $\tilde{a}_{y,R}^i$ and roll angle $\tilde{\phi}_R^i$ was carried out, corresponding to a range of bandwidth values $\omega_{n,i}$ that are assumed to be communicated by the low-level yaw controller in FD-VMM, according to its current capability. In this section,

k_0 will stand for the current time step instead of the index zero. Recalling the approximate lateral Load Transfer Ratio formula (4-6) and the reasoning in Chapter 4 about $a_{y,R} \approx a_{y,T}$, $\phi_R \approx \phi_T$, one can write:

$$\Delta\tilde{F}^{i,*}_{z,T}(k) \approx \underbrace{c_{s,2}\frac{2h_{cg,2}}{l_{t,2}}}_{:=\hat{X}_2}\left(\frac{\tilde{a}^i_{y,R}(k)}{g}\cos\tilde{\phi}^i_R(k) + \sin\tilde{\phi}^i_R(k)\right), \quad kT_s \in [k_0T_s, k_0T_s + t_H] \tag{5-36}$$

which combines the predictions of lateral acceleration and roll angle of the rear tractor axle with the trailer's geometrical parameters and the corresponding safety factor[3] $c_{s,2}$ to arrive at a predicted, approximate lateral Load Transfer Ratio of the trailer axle group. Similarly to (5-17b) and (5-35b), the final prediction of LTR is obtained by assuming the worst-case scenario:

$$\Delta\tilde{F}^*_{z,T}(k) = \max_i\left(|\Delta\tilde{F}^{i,*}_{z,T}(k)|\right), \quad kT_s \in [k_0T_s, k_0T_s + t_H] \tag{5-37}$$

The Rollover Index (ROI) at the current time step $k = k_0$ will be chosen as the largest Load Transfer Ratio along the prediction horizon:

$$\text{ROI}(k_0) = \Delta\bar{F}^*_{z,T}(k_0) = \max_k\left(\Delta\tilde{F}^*_{z,T}(k)\right), \quad kT_s \in [k_0T_s, k_0T_s + t_H] \tag{5-38}$$

Depending on the horizon length t_H, this scalar can indicate rollover danger a lot sooner before a wheel lift-off could happen. This mechanism is shown by Figure 5-12. It is important to

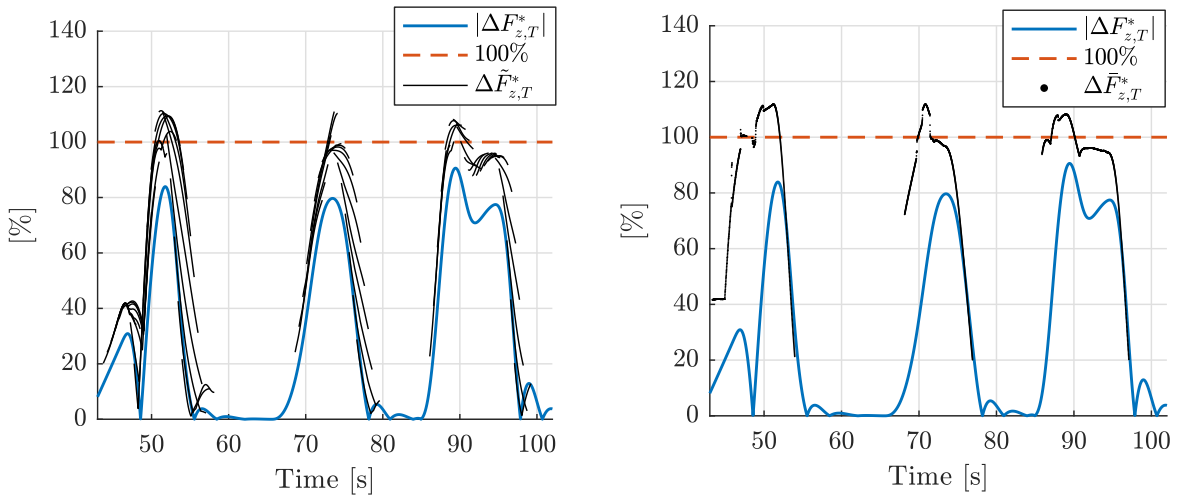

(a) LTR predictions according to (5-37)

(b) ROI values according to (5-38)

Figure 5-12: Rollover Index calculation based on predictions of lateral Load Transfer Ratio – during a hook manoeuvre (every 60th trajectory is plotted); dangerous LTR values are predicted seconds before they occur

note that the apparent conservativeness of the LTR predictions is due to the choice of $c_{s,2}$. As it will be seen in the next section, these predictions will not be directly proportionate to the intensity of rollover interventions, therefore the conservativeness in $c_{s,2}$ – which was chosen based on the data shown by Figure 4-3 – does not limit the diving envelope more than necessary.

[3]The choice of the safety factor was argued for and derived in Chapter 4.

5-6 Design of proactive Roll Stability Control intervention

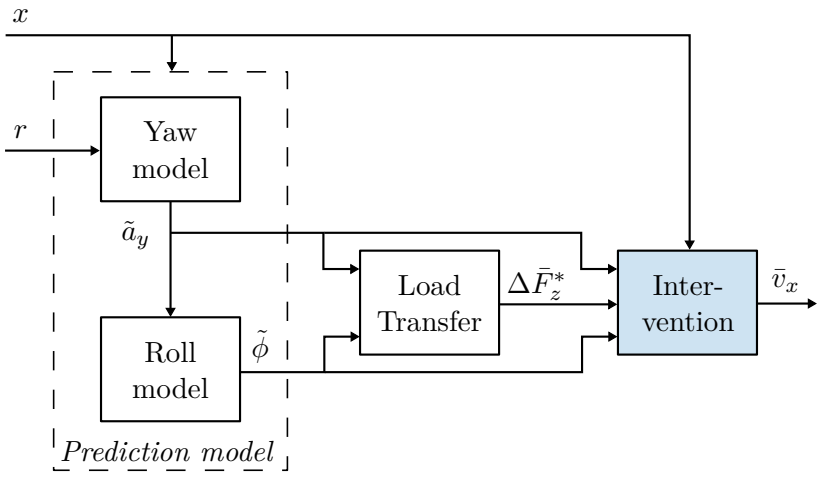

Figure 5-13: Signal flow of proactive Roll Stability Control – focusing on intervention design

Activation of intervention

Triggering a rollover mitigation intervention is traditionally based on lateral acceleration thresholds. In this project, the predefined threshold will be a maximally allowed load transfer, $\Delta\bar{F}^*_{z,\text{pro}}$. To guarantee rollover-free motion, a value lower than 100% should be set. This work will use

$$\Delta\bar{F}^*_{z,\text{pro}} = 80\% \tag{5-39}$$

for the proactive Roll Stability Control. Recalling (5-38), if $\Delta\bar{F}^*_{z,T} > \Delta\bar{F}^*_{z,\text{pro}}$, a triggering signal is applied. If this signal is active during ten consecutive time steps (plausibility check), an intervention is turned on and held at least during the current time horizon length t_H.

Intervention mechanism

As it has been pointed out several times, the goal of the proactive intervention is to avoid having to use aggressive (differential) braking and counter-steering policies. Instead, if one possesses knowledge of $\Delta\tilde{F}^*_{z,T}(k)$ (and therefore $\Delta\bar{F}^*_{z,T}$) seconds before the danger occurs, a speed request reduction to a rollover-safe level shall suffice – recalling the proposition (5-4). This approach would also avoid the implications associated with unnecessarily hard braking – see Section 4-1 and Figures A-5 and A-8. This way, the algorithm can be less conservative but more stable at the same time.

The proactive RSC aims to find $\bar{v}_x$, which will pose a limitation to $v^{\text{TSM}}_{x,\text{req}}$. Firstly, one obtains a safe lateral acceleration level corresponding to the worst-case ϕ_T that can occur on the prediction horizon and the predefined threshold $\Delta\bar{F}^*_{z,\text{pro}}$, by using (5-35b) and rearranging (5-36):

$$\bar{a}_{y,R}(k_0) = \frac{g}{\cos\bar{\phi}_R(k_0)}\left(\frac{\Delta\bar{F}^*_{z,\text{pro}}}{\hat{X}_2} - \sin\bar{\phi}_R(k_0)\right) \tag{5-40a}$$

where k_0 is the current time step and

$$\bar{\phi}_R(k_0) = \max_k \left(\tilde{\phi}_R(k)\right), \quad kT_s \in [k_0T_s, k_0T_s + t_H] \tag{5-40b}$$

Recalling (4-9) and the simplification $\dot{v}_{y,R} \approx 0$:

$$\bar{v}_x(k_0) = \frac{\bar{a}_{y,R}(k_0)}{\bar{\dot{\psi}}(k_0)} \tag{5-40c}$$

where

$$\bar{\dot{\psi}}(k_0) = \max_k \left(\left|\frac{\tilde{a}_{y,R}(k)}{\hat{v}_x(k)}\right|\right), \quad kT_s \in [k_0T_s, k_0T_s + t_H] \tag{5-40d}$$

The maximum yaw rate along the prediction horizon $\bar{\dot{\psi}}$ is obtained using the closed-loop lateral acceleration prediction and the extrapolated speed profile (5-10).

Remark: The allowed lateral acceleration calculation in (5-40a) can be extended with the incorporation of *roadway cross slope*:

$$\bar{a}'_{y,R}(k_0) = \bar{a}_{y,R}(k_0) - \sin(\phi_{\text{bank}}(k_0))g \tag{5-41}$$

and then, by plugging the adjusted maximal lateral acceleration $\bar{a}'_{y,R}$ into (5-40c). This corresponds to Figure 2-10 – however, the effect of ϕ on the allowed lateral acceleration is already accounted for by (5-40a). Here, ϕ_{bank} could be obtained along the prediction horizon using e.g. GPS data. Nevertheless, an even better solution would be to include road bank to the prediction model (5-17).

The last step is calculating[4] the speed request of FD-TSM, which will be communicated to FD-VMM:

$$v_{x,\text{req}}^{\text{TSM}}(k) = \min\left(v_{x,\text{ref}}(k), \bar{v}_x(k)\right), \quad k \in \mathbb{Z}^+ \tag{5-42}$$

One might notice that the maximum values $\bar{\phi}_R$ (therefore, $\bar{a}_{y,R}$) and $\bar{\dot{\psi}}$ do not necessarily belong to the same time step k of the prediction horizon. In other words, it can happen that at a time step $kT_s \in [k_0T_s, k_0T_s + t_H]$, $|\phi(k)|$ is indeed equal to $\bar{\phi}_R(k_0)$, but at the same time, $|\dot{\psi}(k)|$ is lower than $\bar{\dot{\psi}}(k_0)$. This is to ensure conservativeness of the calculation of $\bar{v}_x$. Nevertheless, as the truck starts slowing down, the projected roll angle (and $\bar{\phi}_R$ with it) will also decrease. Thus, the allowed speed $\bar{v}_x$ will increase during intervention to a value which ensures a Load Transfer Ratio close to the predefined threshold.

5-7 Simulation results of proactive Roll Stability Control

In this section, simulation results of the proactive Roll Stability Control are given on the example of a hook manoeuvre. For other test cases, see Appendix A, Section A-3. Firstly, the proactive algorithm is applied on a reference trajectory that would request up to 75 km/h speeds along the defined "hook" path, which would lead to rollovers at all three turns –

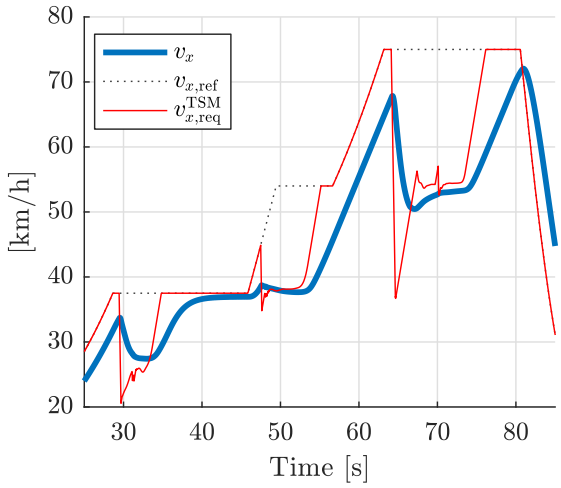

(a) Speed

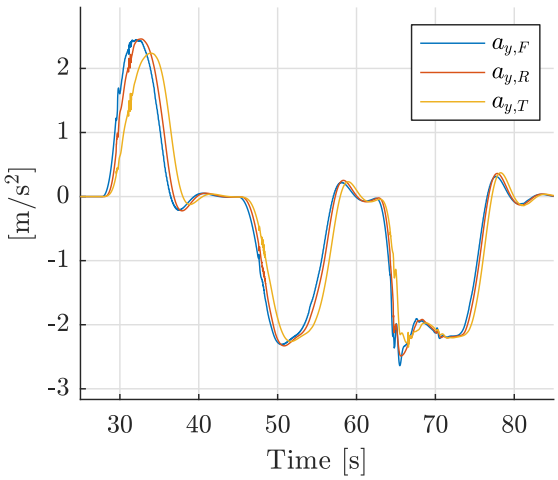

(b) Lateral acceleration

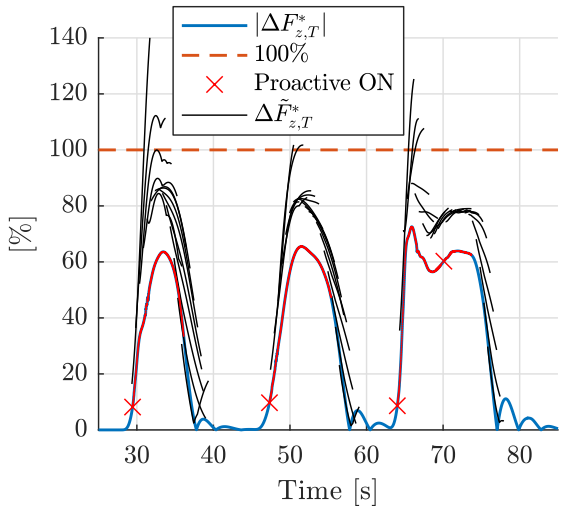

(c) Lateral LTR – red line: RSC active

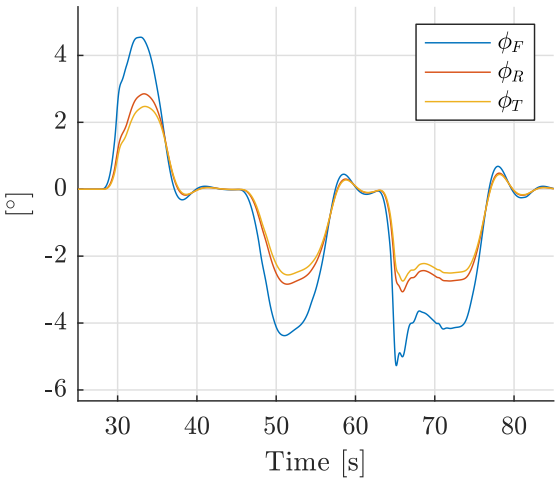

(d) Roll angle

Figure 5-14: Proactive Roll Stability Control during an intense hook manoeuvre, $\Delta \bar{F}_{z,\mathrm{pro}}^* = 80\%$, $c_{s,2} = 1.25$

see Figure 5-14. The first notable thing on the controller's behaviour is that it intervenes *sooner than the vehicle would even enter the corner*. The following mechanism takes course before every turn: Using the initial speed extrapolation and expected lateral accelerations based on the reference trajectory (and the fitted roll motion model), the algorithm predicts extreme load transfers. Accordingly, a massive speed reduction is requested. As the truck's speed decreases, LTR predictions also become milder. This leads to a phenomenon, where $\bar{v}_x$ converges to a speed level, which ensures that $\Delta \tilde{F}_{z,T}^* \approx \Delta \bar{F}_{z,\mathrm{pro}}^*$. Since a safety factor of $c_{s,2} = 1.25$ was used in the load transfer calculations (based on the argumentation of Chapter

[4]Due to the nature of the used predictions, a low-pass filter was applied to the speed limitation $\bar{v}_x$. Edge cases, such as division by zero or blow-up phenomena in the roll angle predictions were accounted for in the real-time implementation framework.

4, the actual LTR values are about 25% lower than the threshold ($\Delta\bar{F}^*_{z,\text{pro}} = 80\%$). Thus, for a less dynamic manoeuvre (such as this one), the safety factor is not necessary.

This is confirmed by the results depicted by Figure 5-15, where no safety factor was used ($c_{s,2} = 1$). This way, the predictions align with the actual LTR values, a higher speed can safely be allowed. This is a valid approach for less dynamic use cases, where the neglections, simplifications and assumptions made do not play a vital role in prediction accuracy. More

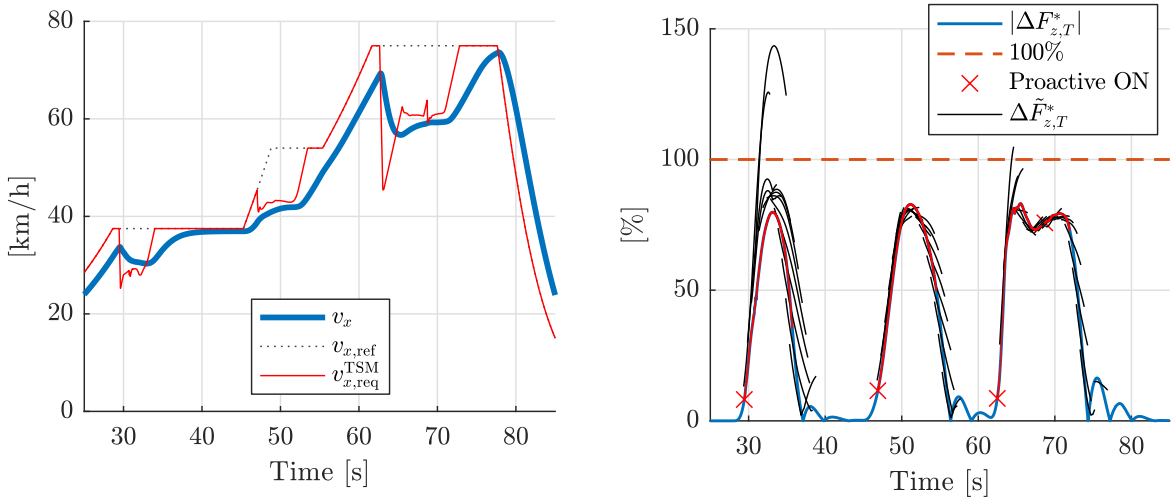

(a) Speed

(b) Lateral LTR – red line: RSC active

Figure 5-15: Proactive Roll Stability Control during an intense hook manoeuvre, $\Delta\bar{F}^*_{z,\text{pro}} = 80\%$, $c_{s,2} = 1$

dynamic test cases and corresponding conclusions can be found in Appendix A, see Figures A-12 and A-13. A comparison with an approach using a hard lateral acceleration constraint instead of roll motion is made in Section A-3, see Figure A-14.

5-8 Limitations

Next to the promising results so far, the method's limitations in its current state are just as important to note. These are can be summarized in the following points:

- First of all, the trailer motion and *tractor-trailer interaction* are not explicitly modelled in this application (only via empirical observations and the different geometric parameters described by $X_{1/2}$). For example, since the assumption $\phi_R \approx \phi_T$ is made, an excited trailer roll motion can only be detected, if it is (at least to some extent) transferred to the tractor chassis through the fifth wheel. Thus, measuring trailer $a_{y,T}$ and ϕ_T would be safer – this is possible with expensive equipment, as shown during tests in Chapter 7 and the algorithm in its current implementation is prepared for handling separate trailer measurements. The current assumptions could be used, if the trailer gets replaced by one, which does not possess sophisticated sensors. Nevertheless, one can make the claim that future self-driving trucks might need on-board ϕ estimation on the trailer(s), as well – especially for longer combinations.

- A significant limitation of the current implementation is the *fixed spatial horizon length* ($s_H = 35$ m). This is due to toolchain limitations. Since in the defined test cases the proactive RSC performs well using this length, no effort has been devoted to changing it. Nevertheless, there are some implications involved: If the current speed is high, the fixed 35 m prediction horizon becomes very short in time (at 80 km/h, the horizon length is only 1.6 s). This yields an intense speed reduction request, which does not align with the ideal behaviour of the proactive RSC, overlapping with the Functionality Domain of the reactive RSC. Furthermore, Recursive Least Squares needs to be exposed to safe *roll motion excitation* with an appropriate persistency in the beginning to learn the prediction model. If the roll model has not converged yet, predictions are inaccurate. If both conditions (no convergence and short horizon due to high speed) apply, the proactive RSC is more likely to fail. Nevertheless, in real-life scenarios, reaching a speed corresponding to highway operation (> 70 km/h) is not likely to be achieved without exciting roll motion.
- Beside convergence issues, there are other factors affecting *prediction accuracy*. Although for the relevant range of ϕ (up to 4°) the linear roll motion model is reasonable to use, the lateral LTR calculation is based on the assumption of $\ddot{\phi} = 0$ which results inaccurate predictions, when they would be most needed – during intensely dynamic cases. Furthermore, the roll motion identification is highly sensitive for changes in the forgetting factor λ_{id} – an adaptively set value would be a great added value, as pointed out in Section 5-4. Furthermore, in simulations, the excitation input a_y has been an ideal, noise-free signal. As it will be seen in the next chapter, aggressive interventions can cause noisy acceleration measurements, which may corrupt the regression of the RLS. Thus, in real-life applications, an appropriate signal preprocessing will needed. Another distorting factor is the assumption implied by (5-10), namely that a_x will remain constant along the prediction horizon – this causes inaccuracy in calculating the temporal parameterization of the reference trajectory during sudden changes in v_x.
- The proposed algorithm is only functional, if the generated *heading reference trajectory* is close to what the vehicle will actually achieve in closed-loop. This condition does not hold for all trajectory generation algorithms. In some cases for example, a Model Predictive Control-based algorithm might output references that are far from the actual closed-loop behaviour (see e.g. [22]).
- The effects of the environmental factors of road slope and crosswind were not included to the controller design.
- Lastly, *real-life issues* have not been tested. Calculation of the safe speed limitation $\bar{v}_x$ has already involved the need for a low-pass filter design and the handling of many numerical edge cases yielding from the requirements of the implementation framework. It is likely that real, noisy measurements will demand a more robust numerical implementation.

5-9 Summary and contributions

In this chapter, a novel approach for rollover mitigation of autonomous heavy vehicle combinations (up to tractor-semitrailer configuration) was mathematically described, implemented

in a real-time framework and simulated using Volvo's high fidelity simulator. The proposed control algorithm was able to prevent rollovers in a wide scale of manoeuvres (all the test cases were covered) with various reference speed profiles, detecting the danger of rollover up to 35 metres before they happen. This thesis work accomplished the design process from receiving a reference trajectory of FD-TSM to adjusting the high-level speed request sent to FD-VMM.

This synthesis involved translating the heading information of the generated reference trajectory to an abstract lateral acceleration "reference". A prediction model was developed, projecting the expected closed-loop behaviour of lateral acceleration and roll dynamics along the horizon. Subsequently, the predictions were translated into the expected lateral load transfer, which was defined as the rollover propensity. Based on the expected danger of rollover, an intervention mechanism establishes the maximally allowable speed request that can be sent to the lower-level controllers in FD-VMM.

The most important part of the algorithm is also the simplest: The lateral acceleration predictions utilize calculations that are lightweight and robust against noise – lateral jerk can be calculated from the reference trajectory. The algorithm as a whole is easily adaptable to different vehicle configurations and its conservativeness can be tuned using a safety factor. The roll motion prediction model is recursively updated at each time step without the need of storing large datasets and is able to capture roll motion excitation, which makes the controller able to tackle problems that a conventional RSC with hard a_Y limits could not. Except for the roll angle (which is accurately estimated in the current setting), all the used signals can be measured by commercially available sensors ($\dot{\phi}$, a_x, a_y, v_x).

Finally, given that the above-mentioned limitations are accounted for, the designed proactive Roll Stability Control could be used as a separate functional entity or product, regardless of the used tracking controller and trajectory generator, without the need to incorporate roll motion to the existing algorithms.

Chapter 6

Reactive Roll Stability Control

This chapter presents the design process and simulation results of the reactive Roll Stability Control. This shall constitute the next, redundant roll safety layer after the proactive RSC, and should work as a separate functional entity. Firstly, the related requirements will be articulated. Subsequently, as the first step of controller synthesis, the reactive algorithm's rollover detection method will be presented. This will be followed by describing how the needed interventions can be implemented within the Control Allocation paradigm. Lastly, simulations will show the effectiveness of the approach.

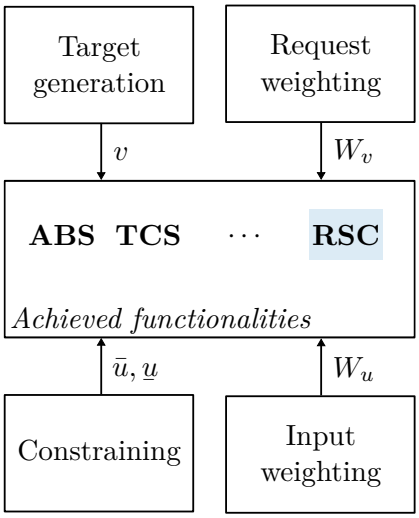

Figure 6-1: Tools to achieve motion control objectives within the Control Allocation paradigm – e.g. Anti-Lock Braking System (ABS), Traction Control System (TCS) and Roll Stability Control (RSC)

The Functionality Domain-Vehicle Motion Management and the Control Allocation framework were introduced in Section 3-4. An important property of this paradigm is that it offers a self-contained way to merge different motion control objectives that traditionally are implemented as separate functionalities. The CA formulation offers a broad variety of ways to incorporate Roll Stability Control. Implementing the needed actuations can happen by means of four factors: Changing the control laws of target generation, introducing new constraints on the CA problem, as well as request and input weight scheduling – this concept is depicted by Figure 6-1.

This chapter will present a proof of concept; a simple and intuitive method to achieve roll stability of the chosen heavy vehicle combination configuration, testable in real-life within the scope of the thesis.

6-1 Requirements and assumptions

The proposed reactive Roll Stability Control shall satisfy a set of requirements. These have been mentioned throughout the thesis and can be summarized in the following points:

- Independence of the proactive RSC. This implies that the detection algorithm should not rely on the predictions of FD-TSM and should be robust and reliable: It has to detect events that could not be predicted. Furthermore, the intervention method should be inherently different compared to the proactive controller (which was merely lowering a speed request).
- The reactive intervention shall be sufficient to mitigate imminent rollovers, without an unnecessarily extreme level of braking. Nevertheless, since the reactive Roll Stability Control would ideally be running in parallel with the proactive RSC, if the reactive controller has to be activated, it is safe to state that a mild intervention is not sensible: Gentle speed reduction belongs to the functionality domain of the proactive controller. A compromise has to be found in the severity of the interventions and it shall be ensured that it does not interfere with the requests of the proactive controller.
- The needed functionalities shall be realized within the CA paradigm. The implementation has to be simple and intuitive so that it can be tested in real-life within the time constraints of the thesis

These prerequisites can be fulfilled, if the following assumptions are made:

- A sufficiently well-functioning $F_{z,i}$ (i stands for a particular tyre) estimation[1] for tyre force allocation.
- The presupposition that $\mu = 1$ is a reasonable approximation of the friction coefficient corresponding to the contact between dry asphalt and the tyres.
- Flat road surface, zero road pitch angle, zero road bank angle – this is a significant assumption, as high road pitch/bank angles might demand a very different intervention policy.

6-2 Design of imminent rollover detection

Since the claims of Chapter 4 do not only apply for a predictive approach, using the lateral Load Transfer Ratio as Rollover Index is a reasonable choice for an imminent rollover detection, as well. According to the formulation (4-6), LTR can be approximated using *lateral acceleration* and *roll angle* signals. The idea of deducing trailer LTR by means of tractor rear axle signals and the scaling factor X_2 is a less reliable approach in the reactive controller's case, as the events that need a reactive intervention tend to involve complex tractor-trailer

[1] The currently available tyre force estimator offers sufficient performance for control allocation, but it cannot follow the fast dynamics during a rollover event. In addition, it is unable to supply information about the expected changes in the Load Transfer Ratio, which would be needed for effective detection.

interaction[2]. Nevertheless, to meet the requirement of real-life testability, the algorithm will only make use of signals that are available without external measurement equipment[3]. The task hereby is to choose appropriate a_y and ϕ signals for the LTR calculations; ideally, these should incorporate a certain level of predictive effect, so that rollover detection can happen as soon as possible.

As it was pointed out in Section 2-3, it is possible to approximate the tractor rear axle lateral acceleration $a_{y,R}^{\text{kin}}$ from the steering angle, using the kinematic bicycle model – see (2-23). As this model neglects tyre dynamics (zero slip), it offers a way to estimate $a_{y,R}$ typically about one second sooner than it would appear. The more dynamic the manoeuvre, the larger this delay becomes, as the tyres need time to build up lateral slip, producing lateral forces. Since there is an additional a phase delay between $a_{y,R}$ and $a_{y,T}$, using $a_{y,R}^{\text{kin}}$ offers a significant predictive advantage. This phenomenon is depicted by Figure 6-2, corresponding to the hook and double lane change test cases outlined by Figures 4-4 and 4-5, respectively. For

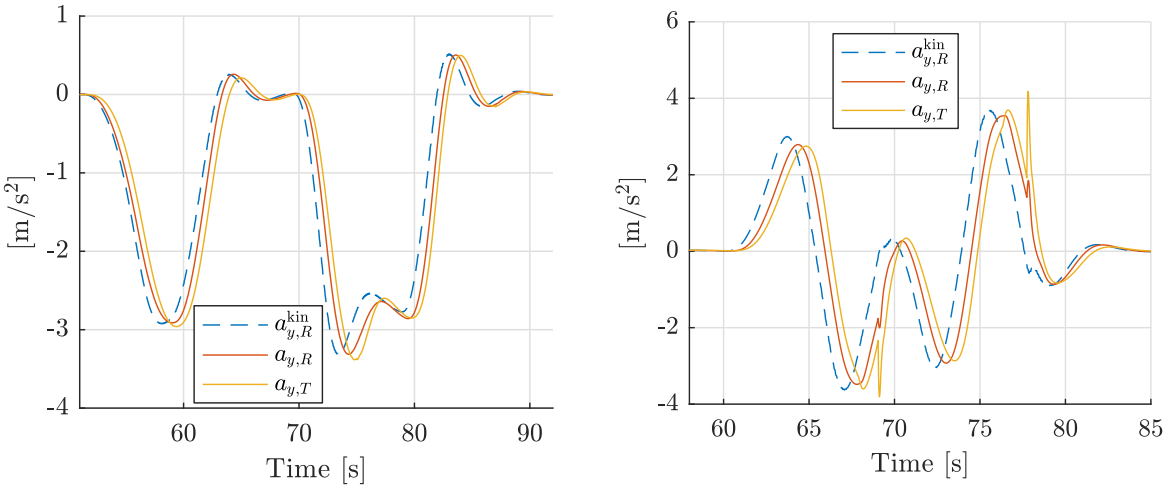

(a) During a hook manoeuvre, corresponding to Figure 4-4

(b) During a double lane change manoeuvre, corresponding to Figure 4-5

Figure 6-2: Kinematically estimated $a_{y,R}^{\text{kin}}$ in comparison with $a_{y,R}$ and $a_{y,T}$

conservativeness and because the direct measurement $a_{y,R}$ can be seen as ground truth, the acceleration value used in the LTR calculation is chosen as follows:

$$a_{y,R}^{\text{re}}(k) = \max\left(\left|a_{y,R}^{\text{kin}}(k)\right|, \left|a_{y,R}(k)\right|\right) \tag{6-1}$$

where $a_{y,R}^{\text{re}}(k)$ is the lateral acceleration used by the detection algorithm of the reactive controller, at time instance k. Furthermore, the design choice of using the available $\hat{\phi}_F$ cab roll angle estimate was made, as it is the only accurate roll angle estimate currently available in our framework, using GPS antennas mounted on the cab. This means that the safety factor $c_{s,2}$ in (4-7) shall be reduced, due to the fact that ϕ_F tends to show larger values than ϕ_T,

[2]For this reason, commercially available RSC modules are supplied separately for both tractor and trailer units.

[3]Tractor rear axle and trailer axle group roll angles, as well as accelerations will be measured by means of externally supplied devices, but these will not be in production and hence only serve as means of validation.

thanks to the reduced roll stiffness of the front axle and the relatively soft cab suspension – see Chapter 4 ($c_{s,2} = 1.1$ proved to be satisfactory). The benefit of using the cab roll angle for imminent rollover detection is that it also introduces a predictive effect, as it will be the first part of the vehicle exposed to lateral acceleration – and therefore, to roll motion – when it enters a corner. Consequently, the load transfer calculation will become:

$$\Delta\hat{F}^*_{z,T}(k) = \underbrace{c_{s,2}\frac{2h_{cg,2}}{l_{t,2}}}_{:=\hat{X}_2}\left(\frac{a^{\text{re}}_{y,R}(k)}{g}\cos|\hat{\phi}_F(k)| + \sin|\hat{\phi}_F(k)|\right), \quad k \in \mathbb{Z}^+ \tag{6-2}$$

where $\Delta\hat{F}^*_{z,T}$ is the approximate lateral Load Transfer Ratio of the trailer axle group – if this value is larger than the load transfer threshold used for the reactive RSC $\Delta\bar{F}^*_{z,\text{re}} = 80\%$ (for ten consecutive time steps), an intervention is triggered.

Remark: When the pro- and reactive controllers are used in parallel, $\Delta\bar{F}^*_{z,\text{pro}} < \Delta\bar{F}^*_{z,\text{re}}$ should apply. Doing so, the reactive RSC will only interfere if the proactive approach failed.

6-3 Intervention implementation using Target Generator and Control Allocation

As it was pointed out in Chapter 4 it is not possible to reduce the rollover risk without changing yaw rate or vehicle speed. The actuation possibilities (without Active Roll Control) are (differential) braking and counter-steering. Differential braking has a double effect: It reduces the speed and yaw rate at the same time. In this section, the implementation of actuation policies utilizing differential braking and counter-steering within the Control Allocation paradigm will be presented.

According to the description of FD-VMM from Section 3-4, the formulation (3-11) is used. Recalling the quadratic programming problem:

$$u = \arg\min_{\underline{u}\le u\le\bar{u}} \|W_u(u-u_d)\|^2 + \lambda\|W_v(Bu-v)\|^2 \tag{6-3}$$

using the constraints (3-16)-(3-21). The goal of using Control Allocation is to obtain a concise, continuous (i.e. not rule-based) control formulation that integrates all needed motion control functionalities. This framework offers a large flexibility in terms of the possible ways of achieving a particular control objective – as it was shown by Figure 6-1. This great variety of adjustable factors make it a challenge to find an adequate implementation of Roll Stability Control that ensures that the previously developed and tested software functionalities still perform after integrating add-ons – in other words, to ensure non-regression of the changes made. Due to scope and time constraints of the thesis project, the reactive RSC's design will be focused on finding a simple solution that meets the requirements of Section 6-1, ensuring roll stability of the test cases defined in Chapter 4 – even if the approach involves using a rule-based switching of control laws. For the same reasons, the yaw and cruise controllers of FD-VMM and their control gains will remain unchanged. Instead, the virtual input vector $v = \begin{bmatrix} a_{x,1,\text{req}} & \ddot{\psi}_{1,\text{req}} & \ddot{\gamma}_{\text{req}} \end{bmatrix}^T$ will be changed directly, overriding the controllers' requests,

when the danger of rolling over is imminent. The required vehicle behaviour can be fine-tuned by adjusting the weights of the matrices W_v and W_u. Ideally, the transition should be implemented either by means of constraints[4] or by a continuous weight scheduling, which would avoid having to use a switching of control laws.

Concept of reactive interventions

The main idea behind defining the control laws realizing reactive Roll Stability Control is that the severity of intervention should be proportional to the danger of wheel lift-off. According to this principle, reducing vehicle speed shall be prioritized over reducing yaw rate, which would enlarge the path tracking error. In other words, leaving the required track can only be a last resort, as this poses additional, unpredictable risks, such as injuring pedestrians or drifting onto the opposite side of a highway.

During cornering, lateral load transfer will naturally happen. In terms of the weight calculation (3-15), the tyres having a higher vertical load (hence, larger braking torque capability $\hat{M}_i$) will be less "expensive" to utilize in (3-11), therefore differential braking (on the tractor) will inherently happen. At this point, it shall be ensured that the yaw request $v_2 = \ddot{\psi}_{1,\text{req}}$ remains unchanged, which will force the steering to compensate for the turning effect of this inherent differential braking. This will be irrelevant for the trailer brakes, due to the lumped trailer axle group model in B. Furthermore, as it was pointed out in the previously written literature survey [14], differential braking is counterproductive to use on the trailer unit. Furthermore, as mentioned in Section 6-1, the goal of the reactive intervention is to ensure roll safety at all cost. Therefore, a method is needed that will only intervene at scenarios which could not be handled by the proactive algorithm. This implies an aggressive overall behaviour.

The possibility of including individual tyre braking capabilities (see (3-16)) gives rise to a sophisticated intervention mechanism: Using the trailer's braking capacity to mitigate rollovers, when the tractor is subjected to a sudden, intense cornering. In a scenario like that, the tractor axles (especially that in the front) will have lost a significant amount of longitudinal capacity, whereas the trailer axle is still low on slip levels. Then, a hard braking intervention on the trailer axle can act as an "anchor" and normalize the dangerous tractor behaviour[5]. This functionality would however require accurate estimates of slip levels on each vehicle axle, as well as accurately obtained axle vertical loads. After thorough investigations however, it turned out that the side-slip estimates during intense interventions were unreliable, causing a chattering actuator behaviour. Therefore, the following design simplification had to be made, replacing the CA constraint (3-16):

$$\max\left(-\bar{M}_i(k), -\bar{u}_i\right) \leq u_i(k) \leq 0 \tag{6-4a}$$

$$\bar{M}_i(k) = R_{e,i}\hat{\mu}_i(k)\hat{F}_{z,i}(k) \tag{6-4b}$$

[4]During the thesis work, incorporation of RSC functionalities via Control Allocation constraints of the form (3-23) has been investigated. Within the given time constraints, a formulation that yields feasible solutions could not be obtained.

[5]Commercial braking modules equipped with ESC systems are oftentimes installed on each vehicle unit. In the described scenario, the trailer can initiate its own intervention program.

where i corresponds to either of the vehicle tyres. This resulted in a much smoother actuator control. Nonetheless, the total braking force on the tractor and the trailer tends to be equal, which means that the above-mentioned feature remains unexploited[6].

In traditional ESC's, if the efforts to stabilize roll motion by brake usage fail, there is a possibility to lock up (i.e. saturate) the front tyres, which will prohibit the driver to take any more steering action. In our driverless case (with a sufficiently quick steering actuator), one can open up steering, hence directly reducing lateral forces (at a cost of leaving the desired vehicle path). Implementing actuations needed for rollover mitigation will happen via braking and steering policies, based on estimate $\Delta\hat{F}^*_{z,T}$ and the threshold $\Delta\bar{F}^*_{z,\mathrm{re}}$.

Braking and steering policies

If $\Delta\hat{F}^*_{z,T}(k) > \Delta\bar{F}^*_{z,\mathrm{re}}$ applies for ten consecutive time steps), an intervention is triggered and kept until $\Delta\hat{F}^*_{z,T}(k) < \Delta\bar{F}^*_{z,\mathrm{re}} - \Delta H$, where $\Delta H = 0.05$ realizes a hysteresis, to avoid chattering of the intervention trigger signal. When the reactive RSC is active, the control law (3-31) is overridden by

$$a_{x,1,\mathrm{req}}(k) = \begin{cases} P_a\hat{\mu}(k)\left(\Delta\hat{F}^*_{z,T}(k) - \Delta\bar{F}^*_{z,\mathrm{re}}\right), & \text{if } \Delta\hat{F}^*_{z,T}(k) > \Delta\bar{F}^*_{z,\mathrm{re}} \text{ applies} \\ 0, & \text{otherwise} \end{cases} \tag{6-5a}$$

$$P_a = \frac{-g}{1 - \Delta\bar{F}^*_{z,\mathrm{re}}} \tag{6-5b}$$

where $\hat{\mu}(k)$ is the mean of the friction coefficients estimated per tyre and the proportional gain $P_a \in \mathbb{R}$ ensures that the maximally achievable longitudinal acceleration of the tractor (according to (6-4)) is requested, when $\Delta\bar{F}^*_{z,\mathrm{re}} = 100\%$ (i.e. at wheel lift-off).

Similarly, the control law (3-27) is overridden by

$$\delta^{\mathrm{VMM}}_{\mathrm{req}}(k) = 0 \tag{6-6}$$

if $\Delta\hat{F}^*_{z,T} > 1$ applies, which – as mentioned several times – is a last resort of preserving roll stability.

Handling transients

As the reactive intervention realized by (6-5) and (6-5) tend to be quite aggressive, it is reasonable to account for the emerging transients. This is done by a post-intervention period starting immediately after the intervention, lasting two seconds – which empirically turned out to be sufficient. For these two seconds, the following adjustments are done:

- Wait for the roll motion transients to decay, do not use powertrain. This is realized by changing the constraint (3-18) to:

$$0 \leq u_e(k) \leq 0 \tag{6-7}$$

[6]For a more sophisticated tractor-trailer interaction, a reformulation of the Control Allocation problem might be needed.

- Reactive interventions tend to enlarge the yaw rate error (resulting from path tracking error) $e_{\dot{\psi}}$, see (3-26). If this error would naturally yield an aggressive steering correction towards the track, which again can increase lateral acceleration to a dangerous level. To avoid this, steering rate after the reactive intervention is limited, and brake actuation is preferred over steering. Therefore, if a yaw compensation is needed, it will be done by means of differential braking. This is realized by changing the constraint (3-19) to:

$$\underline{\dot{\delta}} \cdot 0.1 \leq \dot{\delta}(k) \leq \bar{\dot{\delta}} \cdot 0.1 \tag{6-8}$$

and by increasing the weights in (3-15):

$$w_i(k) = \sqrt{\frac{\sum_i \bar{M}_i(k)}{\bar{M}_i(k)} w_u} \cdot 10 \tag{6-9}$$

6-4 Simulation results of reactive Roll Stability Control design

In this section, simulation results of the reactive Roll Stability Control are given on the example of a hook manoeuvre. The required speed profile matches the one presented in Section 5-7, with the proactive RSC – the requested speeds in all turns are extremely high, which would result in rollovers at every turn. For further test cases, see Appendix A, Section A-4 – most importantly, the evasion at high speed manoeuvre is a typical test case for a reactive RSC, see Figure A-16. Figure 6-3 represents vehicle motion and the corresponding actuator usage along the reference. The signals $\hat{\phi}_F$, $a_{y,R}$, δ are used for rollover detection (i.e. to obtain $\Delta\hat{F}^*_{z,T}$). The (normally unmeasured) trailer roll angle ϕ_T of the high fidelity plant is plotted to validate the usage of $\hat{\phi}_F$ – the difference in scale was accounted for in reducing the safety factor $c_{s,2}$, their dynamics is very similar. Recall that the elements of vector u are the outputs of Control Allocation, which will be actuator demands for the individual actuators' controllers. Undoubtedly, the biggest contributor to the algorithm's good performance is the early detection of rollover danger. This is largely due to the kinematic considerations in (6-1): Based on the steering input and current speed, the dangerous lateral acceleration can indeed be recognized just a second earlier - which is enough to intervene with an LTR much below it's threshold (80%). The detection algorithm based on $\Delta\hat{F}^*_{z,T}$ is seemingly conservative – as it was explained in Chapter 5, this is because the safety factor $c_{s,2}$ was adapted to account for highly dynamic cases.

Furthermore, one may notice that the interventions are indeed a lot more aggressive in comparison with the proactive algorithm's closed-loop behaviour depicted by Figure 5-14. Firstly, the intense braking induces a temporary peak in the Load Transfer Ratio. This phenomenon is natural: As it has been explained earlier, due to the longitudinal load transfer and the reduced roll stiffness of the first tractor axle, the tractor's overall roll angle will increase during braking. This motion will affect the trailer's roll motion via the fifth wheel. As the zoomed part of Figure 6-3d makes it clear, the outer wheels are subjected to higher braking torques, aligning with (3-15). At the same time, an increased steering angle keeps the truck on track. Note that u_T stands for the torque applied to a single trailer wheel, out of the six. The post-intervention phase proved to be sufficient to account for the occurring transients.

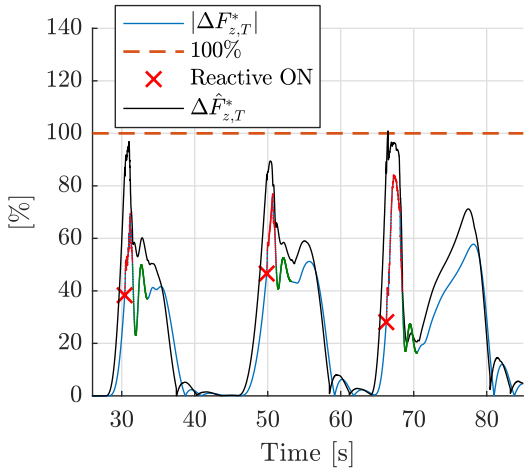

(a) Lateral LTR – red line: RSC active, green line: Post-intervention

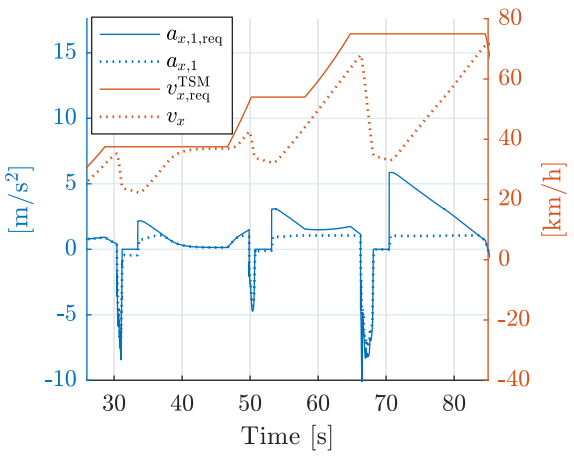

(b) Speed and longitudinal acceleration

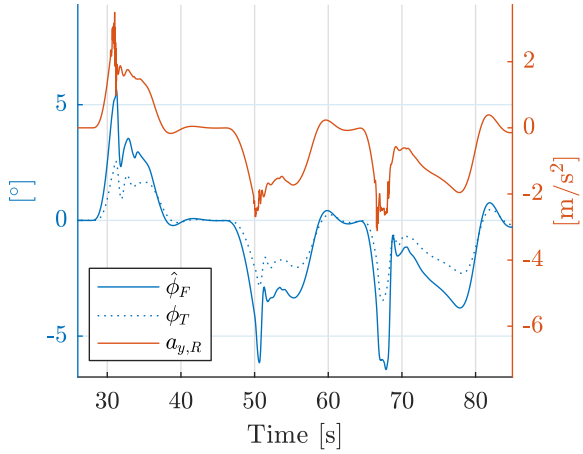

(c) Lateral acceleration and roll angle

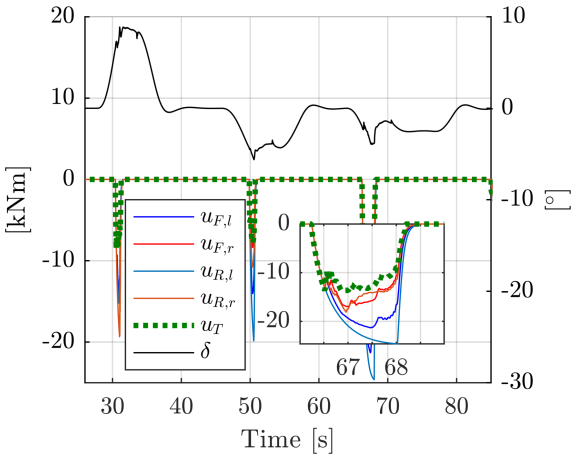

(d) Actuator usage, brakes and steer

Figure 6-3: Reactive Roll Stability Control during an intense hook manoeuvre, $\Delta \bar{F}^*_{z,\text{re}} = 80\%$, $c_{s,2} = 1.1$

All in all, the proposed reactive RSC proved to be a sufficient "safety net" of FD-VMM to account for cases, where the proactive controller fails to accurately predict the lateral load transfer. This was achieved by rigorous analysis of the used motion control system and subsequent, minimal adjustments in the Target Generator and Control Allocation settings.

6-5 Limitations

Despite the simplistic approach of the synthesized reactive Roll Stability Control, it proved to be sufficient to fulfil its requirements. Nevertheless, due to the plain design method, it does have notable limitations:

- Most importantly, the robust rollover detection performance (e.g. grasping the peaks

in LTR right after interventions) is largely thanks to the accurate estimate $\hat{\phi}_F$, which (partly) relies on *GPS signals*. At locations without this feature, an even more conservative detection algorithm will be necessary – or a roll angle estimation technique that is not reliant on GPS.

- Secondly, the current Control Allocation formulation does not allow sophisticated *trailer motion requests*. In the current setting, the trailer's motion is solely influenced via articulation requests, which are calculated based on steering actions. The performance could likely be improved by modelling the complex tractor-trailer interaction in including it in the Control Allocation formulation. This, combined with the idea of axle slip-based rollover interventions (assuming satisfactory slip estimation performance) offers a higher level of control authority over the vehicle combination.

- Furthermore, the performance was not tested on road surfaces having *non-zero bank or pitch angle*, as the design steps did not consider such use cases. Nonetheless, doing so would be essential before a commercial release of the functionality.

- Post-intervention *transients* are currently handled by restricting the rate of steering towards the track after an intervention ended (prioritizing steering by differential braking) and blocking engine usage for a fixed amount of time. While this approach proved to be satisfactory, an intervention algorithm that eliminates the need of transient handling would be preferable.

- During intense interventions, *longitudinal load transfer* reduces the overall roll stiffness of the vehicle combination (as pointed out in Chapter 4). This phenomenon should be incorporated when requesting a certain longitudinal acceleration level.

- As a last resort to preserve roll stability, the *steering action* is neutralized. There are two implication with this approach: Firstly, it assumes that the trailer's inner wheels are lifting off. This should be validated by a brake pulse test before deciding to open steering. Secondly, during autonomous operation, it shall be decided based on the environment whether it should indeed be prioritized to leave the desired path instead of allowing a rollover – in urban areas for example, a rollover might be the favourable option.

- For robustness and reduces complexity, no *friction coefficient estimation* was utilized, but the fixed value $\mu = 1$ was used.

6-6 Summary and contributions

In this chapter, a simple algorithm suitable for real-life tests within the thesis scope was developed. It consists of certain adjustments within the Control Allocation paradigm, based on the knowledge gathered throughout Chapters 3 and 4. The controller design is a result of an exhaustive research and analysis on commercially available ESC functionalities (see the previously written literature survey [14]) with the goal of finding how these (and more) could be incorporated into the currently implemented CA formulation in terms of adding a roll stability functionality.

Firstly, a rollover detection was developed, based on the principles laid out in Chapter 4, using signals that are available on the chosen truck configuration on-board (without the need of external measurement devices). It does not rely on vertical tyre force estimates, which might fail to grasp the intensely changing load transfer dynamics during a rollover event. In addition, it is completely independent of the detection algorithm used by the proactive RSC designed in Chapter 5. Subsequently, the desired vehicle combination behaviour was explained and translated into corresponding adjustments in the Control Allocation formulation. This involved defining braking and steering policies (control laws). Simulation results in our pre-defined test cases (see Section A-4 of Appendix A) suggest that the proposed algorithm is capable of preventing rollovers from happening, even in the most dynamic cases. This makes it a good candidate for the next layer of rollover prevention, after the proactive RSC.

The method fits into the CA paradigm whilst bringing the functionality of the production ESC rollover prevention, without much modification. This supports the claim that Control Allocation is an ideal basis for a motion control framework of over-actuated heavy vehicles, capable of uniting various functionalities.

Chapter 7

Rollover test and reactive Roll Stability Control implementation results

This chapter summarizes some of the most important real-life tests carried out within the scope of this thesis work. These tests had two objectives in terms of the current project: Validating the claims of Chapter 4 (which were made based on simulation results) and testing the closed-loop behaviour of the reactive Roll Stability Control, focusing on its rollover detection algorithm. The closed-loop test presented in this chapter is reproduced in simulation and can be found in Appendix A, Section A-5. Due to the matching truck configuration during simulations and tests and the very similar Centre of Gravity height, no additional tuning was necessary to reach a comparable behaviour.

7-1 Measurement setup

The used truck configuration was the same as the one used in simulation – depicted by Figure 1-4. The largest parameter deviation may be present in the total vehicle mass and the CoG height, but from the tests' standpoint, the differences turned out to be negligible. In addition, for safety reasons, the trailer was supplied with stabilizer side-wheels and hydraulically adjustable loads. A photo of the truck in standstill, on the skidpad can be seen on Figure 7-1.

The truck was fully equipped with autonomous driving functionalities (including FD-TSM and FD-VMM features described in Chapter 3) and an experienced driver was supervising the vehicle's safe motion. During the measurements presented in this chapter, the driver was not interfering with the truck's self-driving algorithms, not even whilst reaching rollover. Only once one of the side-wheels hit the ground would he take over control and bring the vehicle to a full stop.

To validate on-board measurements and estimates and to be able to log trailer states, an external measurement system (OXTS RT3000) was mounted on both the tractor and trailer

Figure 7-1: Photo of the prepared truck configuration on the skidpad

chassis. Nevertheless, as it was pointed out earlier, the control algorithms did not take advantage of these external measurement signals. Although the gathered logs were extensively analyzed to gain an adequate understanding of vehicle motion, in the following results only the signals directly related to reactive RSC will be plotted. These are the roll angles ϕ_R, ϕ_T and the lateral acceleration measured at the trailer axle group $a_{y,T}$. The rest of the signals are available in the default on-board framework.

Remark: As the test case (see next section) was quasi-static and was carried out at low speeds, using the aggressive intervention techniques utilized by the reactive RSC was not justified. Instead, the intervention was merely using the engine drag to reduce speed, when necessary. Still, the Control Allocator's brake requests were logged, and will be plotted. Due to time constraints, it was not attempted to change this setting.

7-2 Test case description

The main motivations behind choosing the real-life test case were the following:

- Choosing a case that is quasi-static, hence it is easy to analyze and compare to simulation results.
- Should be possible to test the reactive RSC, with a focus on testing the detection algorithm.
- Reproducibility should be ensured. For this reason, a dry asphalt surface is necessary, with good weather conditions – according to experience, on wet asphalt, 20 to 30 % less steering torque is needed to for the same cornering.
- There should be sufficiently large, empty area around the track, as a rollover-recovery manoeuvre might demand space.

- Restrictions due to limited availability of test tracks and certified test drivers.

It was also vital to carry out a risk assessment before the tests, comprising (among others) the following: Defining the mounting height of stabilizer wheels, safe mounting of trailer load, with special attention to hydraulics, checking the condition of tyres and other factors that help avoid the risk of slipping.

The chosen test track is a *circle with* 40 m *radius*. Following this path shall happen with a constantly increasing speed, leading to trailer wheel lift-off. This track on a skidpad can be seen on Figure 7-2, where a truck is performing a rollover. To record the reference trajectory

Figure 7-2: Photo of the truck during performing a rollover on the skidpad

for the self-driving algorithm, a manual drive was carried out along the circle. Then, the corresponding $v_{x,\text{ref}}(s)$ $s \in [0, s_l]$ speed reference was gradually scaled up, until a trajectory forcing the truck into rollover was reached. This reference was tracked autonomously, which resulted in a rollover illustrated by Figure 7-3.

The most important thing to note on the plots is the accuracy of the detection algorithm. The estimate $\Delta\hat{F}^*_{z,T}$ recognizes trailer wheel lift-off one second sooner than it happens – this means that the trailer's X_2 parameter is very close to the one used in simulations, and the safety factor $c_{s,2}$ was well chosen. This lift-off occurred at $\phi_T = 3.7°$, which aligns with previous simulation results. Nevertheless, using $a^{\text{kin}}_{y,R}$ did not prove to be useful in real life – the simplifications made by the kinematic bicycle model may be too vast for a real-life application. One can observe the general relation $a_{y,T} < a_{y,R}$ – this aligns with the statements of Section 4-2, namely that RWA < 1 applies at low speeds. It is also notable that the estimate $\hat{\phi}_F$ is accurate until wheel lift-off happens. Furthermore, there is no significant phase delay between tractor and trailer signals. These facts can lead one to believe that the assumption that tractor rear axle signals can be used to deduce the trailer's state is a viable approach. While this is true for this test case, these results do not make it possible to make the same claim for high speed, dynamic test cases.

Remark: The sudden drops in the speed signal (and in the LTR estimate, accordingly) were caused by gear shifts.

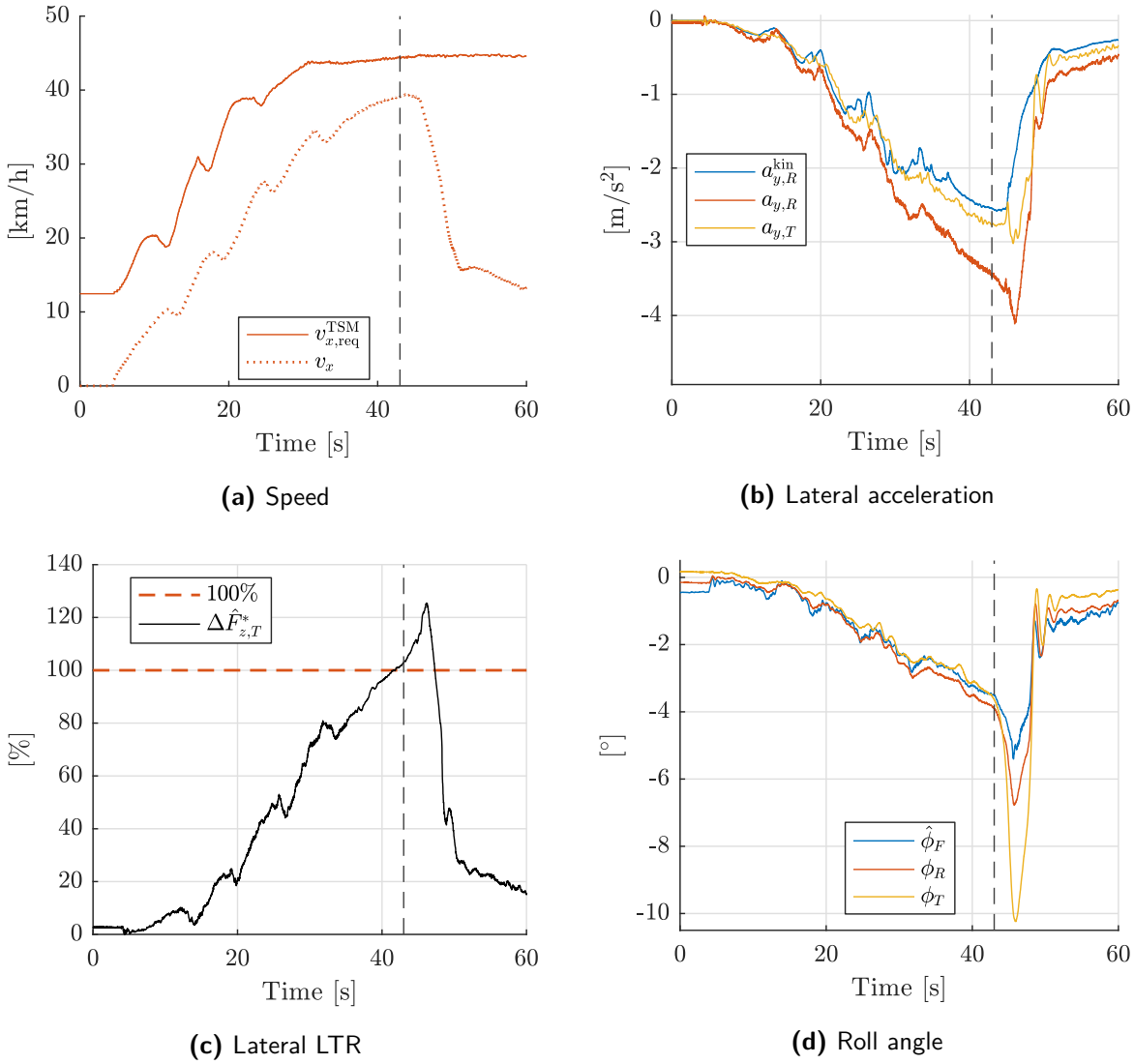

(a) Speed

(b) Lateral acceleration

(c) Lateral LTR

(d) Roll angle

Figure 7-3: Rollover test carried out in a circular path with increasing speed; the gray dashed line represents trailer wheel lift-off – $c_{s,2} = 1.1$

7-3 Test result of reactive Roll Stability Control

This section presents measurements along the same reference trajectory that was used during the rollover on Figure 7-3, but with the reactive RSC turned on. As mentioned earlier in this chapter, the brake system was turned off and the engine drag realized the needed actuation to mitigate rollovers – nonetheless, for the sake of completeness, the Control Allocation's brake demands are plotted. Therefore, the focus of these measurements lies in testing the detection algorithm in closed-loop. Changing the allowed lateral load transfer $\Delta\bar{F}_{z,\mathrm{re}}^{*}$ was handled well by the controller (during tests, multiple settings were successfully tried) – to demonstrate detection accuracy, $\Delta\bar{F}_{z,\mathrm{re}}^{*} = 85\%$ is used in the plots. The corresponding circular track, truck rear axle position during path following and the locations of interventions are depicted by Figure A-6 in Appendix A.

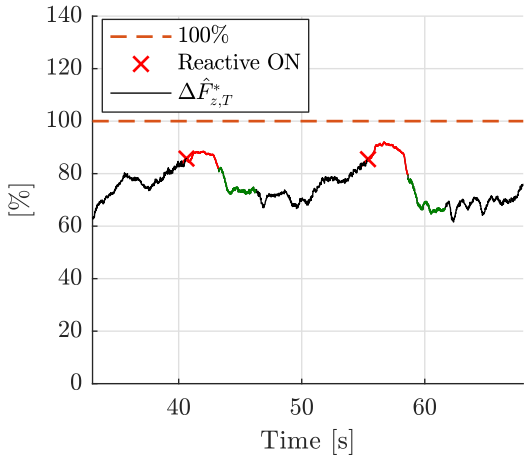

(a) Lateral LTR – red line: RSC active, green line: Post-intervention

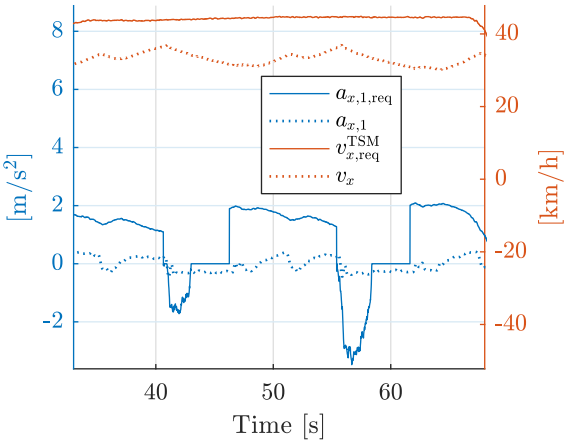

(b) Speed and longitudinal acceleration

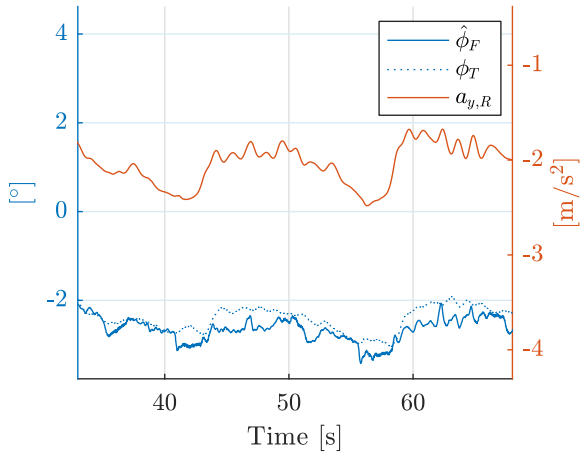

(c) Lateral acceleration and roll angle

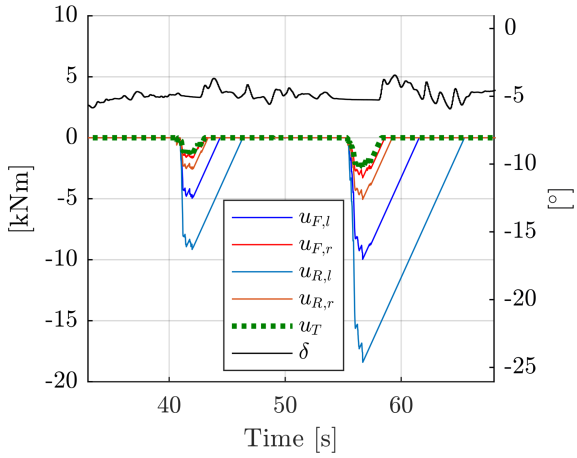

(d) Actuator usage, brakes and steer

Figure 7-4: Test results of reactive Roll Stability Control during circling on a skidpad, with increasing speed, $\Delta\bar{F}^*_{z,\text{re}} = 85\%$, $c_{s,2} = 1.1$

As the results illustrated by Figure 7-4 make it clear, the designed controller prevents rollovers. According to Volvo's handling specialist, the closed-loop vehicle behaviour using engine drag is indeed comparable to interventions initiated by commercial ESC's – these systems generally only use the brakes, when a situation demands it. Using the on-board roll angle estimate $\hat{\phi}_F$ proved to be viable even during interventions, compared to the externally measured ϕ_T as ground truth. In quasi-static circling, the difference is even less important than it was in the hook manoeuvre. An interesting confirmation of simulation results is that the temporary peaks in $\Delta\hat{F}^*_{z,T}$ after interventions are present in real-life, as well. The measurement has been reproduced in simulations, tracking the recorded reference trajectory using Volvo's high fidelity plant in closed-loop with the synthesized reactive Roll Stability Control – see Figure A-17, Appendix A

7-4 Limitations

In addition to the confinements of the reactive RSC itself (which were discussed in Chapter 6), the main limitations of its real-life tests can be summarized in four points:

- The only test case that was possible to carry out on the proving grounds was a circular path followed with increasing speed. Testing more dynamic cases, such as double lane changes might reveal further limitations in the controller design that need to be adapted.
- The Control Allocation's brake system usage could not be tested in closed-loop. The aggressive interventions seen in Chapter 6 might pose implications in real-life, which could help to adjust and fine-tune the controller and test the detecting algorithm with intensely changing acceleration and roll angle signals.
- The used yaw controller (see (3-27)) does not perform well yet in real-life. At high speeds (37 km/h+) the path follower algorithm induced sudden steering actuations, leading to immediate peaks in lateral acceleration. This is a known, non-blocking issue in the used tool chain. In these cases, the test case had to be repeated.
- Driving along the same path in the opposite direction happened with a larger off-tracking, which increased the turn radius, leading to lower lateral acceleration values at the same speeds. This led to a seemingly safer dynamics, when carrying out a counter-clockwise manoeuvre. The cause of this is most likely the fact that the clockwise turns were repeated several times before switching directions, which might have introduced a bias to the trailer suspension roll angle, slightly changing the lateral dynamics of the unit.

7-5 Summary and contributions

In this chapter, one of the many real-life rollover tests that were carried out within the scope of the thesis was presented. Effectiveness of the proposed rollover detection algorithm was confirmed. Subsequently, the designed reactive rollover prevention method was successfully tested in closed-loop, on the same test track. This test case was then reproduced in simulations.

Based on the tests represented by Figures 7-3 and 7-4, validation of the claims of Chapter 4 is possible for a quasi-static case: It is more important to focus on trailer roll stability and a wheel lift-off can accurately be detected, if its roll dynamics is grasped. Mitigating a trailer rollover is indeed possible by only measuring tractor signals. As the Load Transfer Ratio temporarily increases after interventions, the used safety margin of allowed load transfer (or lateral acceleration) has to account for this phenomenon.

Before performing these tests, a careful assembly of the test setup happened, along with the needed calibrations of the hardware and software toolchain and the management of related logistics.

Chapter 8

Conclusions and recommendations for future work

This thesis project proposed a concept of ensuring roll stability of an autonomous heavy vehicle combination. This concept entails a pro- and a reactive approach to Roll Stability Control. Both methods exploit particularities of self-driving vehicles, which enable a better performance compared to today's Electronic Stability Control techniques. The proactive controller analyzes the truck's reference trajectory from a roll safety perspective and ensures that the vehicle stays within a safe driving envelope. On the other hand, the reactive controller is designed to detect and mitigate rollovers that could not be predicted. In order to do so, it utilizes the full control authority over the self-driving truck. Subsequently, the reactive RSC was successfully tested on Volvo's proving ground.

The main contributions of this thesis are:

- Analysis of roll motion dynamics of a tractor-trailer combination,
- development and real-life tests of a rollover detection mechanism based on lateral load transfer,
- conceptualization, derivation and simulation of a proactive Roll Stability Control method, including the formulation of an adaptive roll motion model identification problem,
- extending the functionalities of an existing Control Allocation motion control framework so that it includes roll stability and testing it on a real self-driving truck.

8-1 Summary of conclusions

The main conclusions of this ten months long research project can be summarized as follows:

1. Achieving a higher level of roll stability of (autonomous) heavy vehicles is attainable, if one exploits the information contained in the reference trajectories. Judging by the truck's current state and its future reference, it is possible to prevent rollovers from happening before the vehicle would even approach a – from a rollover perspective – dangerous situation, if the generated trajectory will indeed be followed within a reasonable margin.

2. The proactive controller can be designed as a separate software module, without acquiring detailed knowledge of the used trajectory generator or the tracking algorithm.

3. One advantage of using the Control Allocation paradigm for motion control of overactuated, autonomous heavy vehicles was confirmed by this project: Extending the existing set of functionalities can be done in a short period of time.

4. By analyzing an appropriately generated motion reference and by exploiting the control authority over all actuators, untripped rollovers could be non existent for Level-4 self-driving trucks of the future.

8-2 Recommendations for future work

1. **Rollover detection** could be improved by defining a Rollover Index that is capable of detecting tripped rollovers and incorporates road slope. One possible method is given by [38], expressing the lateral Load Transfer Ratio in terms of measurable system states, road inputs and slope. Nevertheless, the method assumes the accurate knowledge of many vehicle parameters, which can make it challenging to use it in real-life.

   In addition, a viable method would be to use cameras in the vicinity of the trailer wheels to detect lift-off events.

2. **Centre of Gravity height uncertainty** is currently only accounted for by choosing a safety factor based on the data gathered through Monte Carlo simulations. Nevertheless, it could be possible to extract this information from the identified roll motion model – this might demand knowledge of the overall roll stiffness and damping coefficients. After an initial learning period, the estimated CoG height value should be saved until the next load change.

3. As mentioned in Chapter 5, the predictions of **proactive Roll Stability Control** are sensitive to changes in λ_{id}. Therefore, implementing an adaptive forgetting factor would likely be an added value. In addition, testing the Recursive Least Squares algorithm should happen on real measurement data, as well, to ensure its robustness.

   Currently, the prediction model does not consider tractor-trailer interactions. Including it may improve the accuracy of LTR predictions.

   The effect extending the fixed ($s_H = 35$ m) prediction horizon in terms of accuracy, intervention performance and real-time requirements shall be examined.

   Longitudinal load transfer during braking influences roll motion, as it was pointed our several times. This effect, along with the consequences of road pitch angle shall be incorporated into the allowed speed calculation.

Roll safety might also be achieved, if the utilized trajectory generator and tracking algorithms ensure that the neither of the vehicle units exceed a pre-defined, very conservative, hard-coded lateral acceleration limit. It was shown that such an approach might unnecessarily limit the vehicle speed during cornering. Nonetheless, an investigation could be carried out to examine how much this limitation matters during a real-life mission route – doing so, one could assess the added value of using the proposed proactive RSC algorithm.

4. The **reactive Roll Stability Control** in its current implementation prioritizes to avoid rollover at all cost, with opening the steering action if an imminent wheel lift-off is assumed. This prioritization policy could be rationalized, if the algorithm takes the environment into consideration: After all, there will be no driver to make this decision. One step in this direction could be that FD-TSM communicates to FD-VMM how much lateral corridor space would remain in the next seconds, according to its predictions. This may help to decide if opening the steer is a viable option at the moment.

   Furthermore, an accurate road surface friction estimator would supplement the rollover prevention algorithm – high friction poses the danger of a possible overturn, whereas on a low friction surface, yaw stability should be the main focus. Knowledge of μ would make it possible to adapt the Control Allocation's intervention capabilities (via constraints) according to road surface.

   By using a more robust side-slip estimator, calculating slip-based tyre capability constraints would be possible. This, combined with a Control Allocation formulation, which allows separate trailer acceleration requests could make the reactive intervention more sophisticated: The trailer could be used as an "anchor", when the tractor is suddenly exposed to high slip levels.

In general, further, more dynamic real-life test cases would be necessary to evaluate the usefulness of both rollover prevention approaches.

Appendix A

Additional simulation results

This appendix presents additional simulation results. These help to develop a better understanding of the proposed algorithms, as well as to assess their performance in various test cases.

Firstly, the paths of the pre-defined test cases will be illustrated. Two edge cases (excited roll motion during a slalom manoeuvre and rollover due to hard braking) will be shows in detail. Subsequently, repeated Monte Carlo simulation results will be given, with modified roll motion parameters of the high fidelity plant. The upcoming chapters will simulate both the pro- and reactive RSC's closed-loop behaviour during a double lane change and an evasion manoeuvre. The proactive controller will be compared to a more conventional, conservative approach. Finally, the real-life test results of Chapter 7 will be reproduced in simulations.

A-1 Additional information about test cases

This section shows the paths of the pre-defined test cases and provides a deeper insight into rollovers cased by excited roll motion and by hard braking.

A-1-1 Test case path descriptions

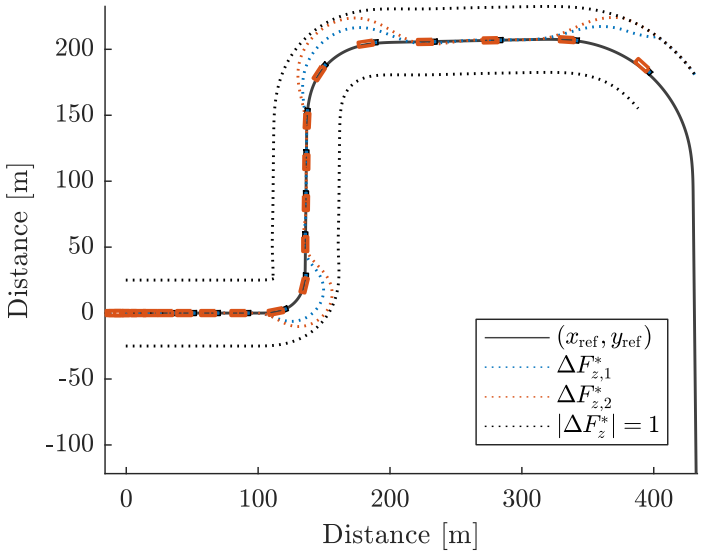

Figure A-1: Hook manoeuvre – spacing between the dotted lines and the reference path is proportionate to LTR; the black dotted lines represent and LTR equivalent to wheel lift-off

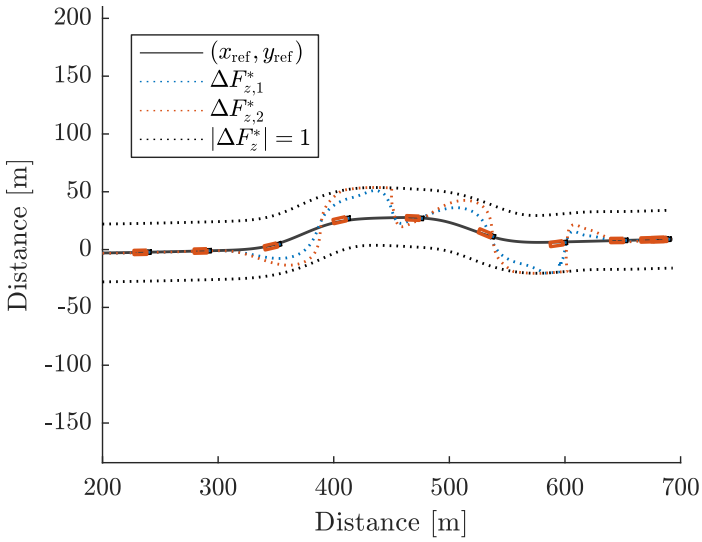

Figure A-2: Double lane change manoeuvre – spacing between the dotted lines and the reference path is proportionate to LTR; the black dotted lines represent and LTR equivalent to wheel lift-off

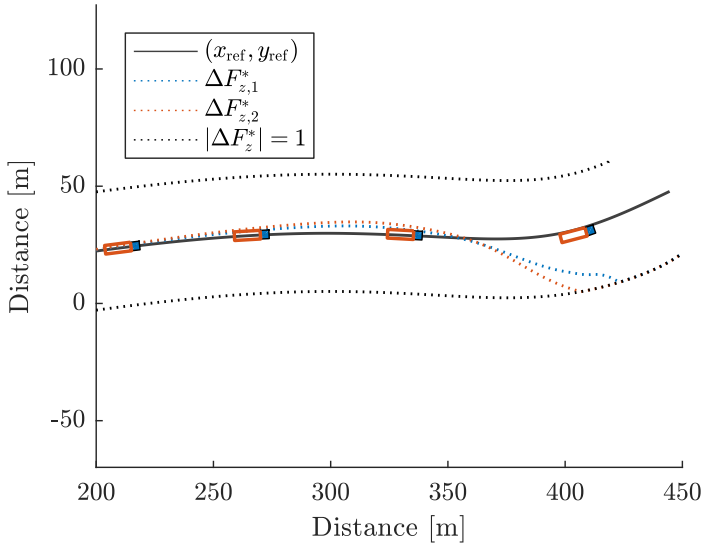

Figure A-3: Evasion manoeuvre at high speed – spacing between the dotted lines and the reference path is proportionate to LTR; the black dotted lines represent and LTR equivalent to wheel lift-off

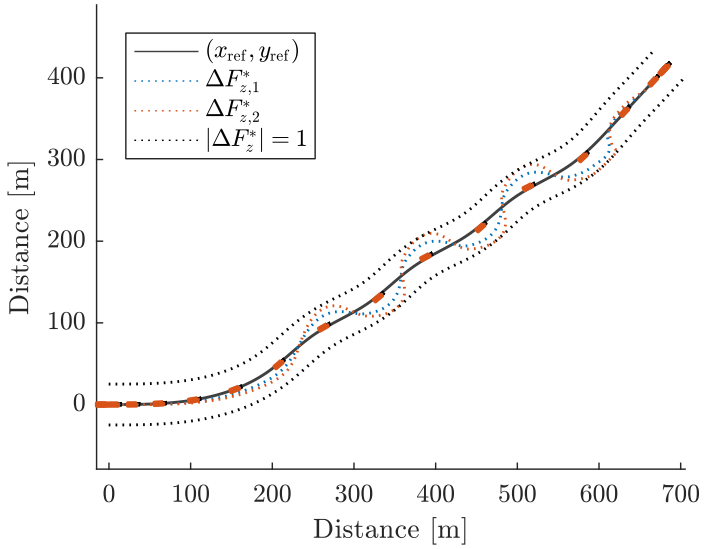

Figure A-4: Slalom manoeuvre at high speed – spacing between the dotted lines and the reference path is proportionate to LTR; the black dotted lines represent and LTR equivalent to wheel lift-off

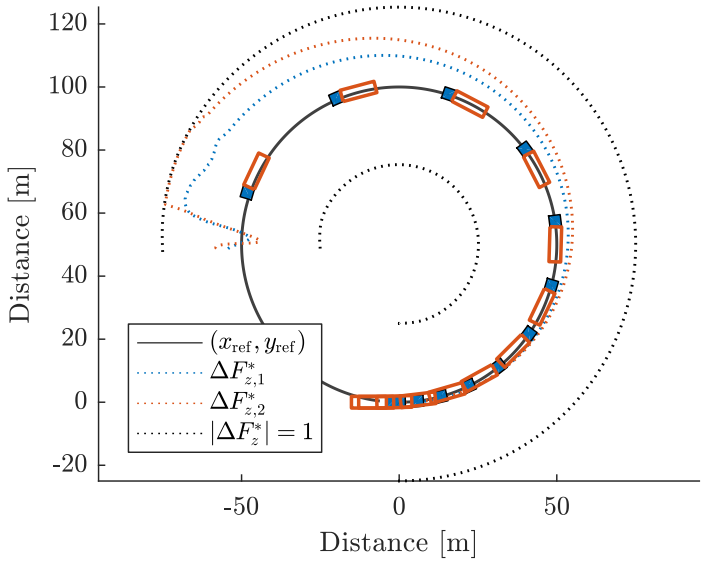

Figure A-5: Circle manoeuvre with hard braking – spacing between the dotted lines and the reference path is proportionate to LTR; the black dotted lines represent and LTR equivalent to wheel lift-off

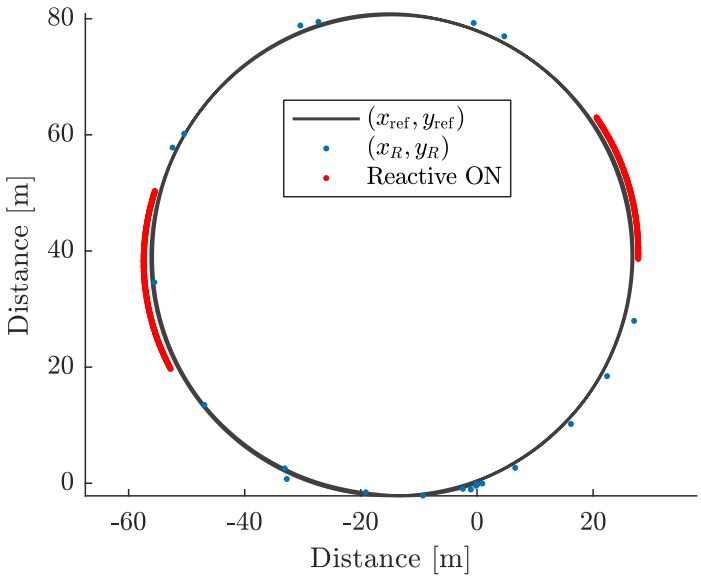

Figure A-6: The circular path recorded during real-life tests – the red points denote where the interventions took place and the spacing between the blue dots (tractor rear axle positions) is proportional to speed

A-1-2 Evolution of systems states during test cases

Rollover in slalom manoeuvre

During the slalom manoeuvre, the steering excitation happened at 1.5 Hz, with constant amplitude. This excites both yaw and roll motions, leading to trailer wheel lift-offs. By only measuring lateral acceleration, detecting rollovers may be difficult is such cases.

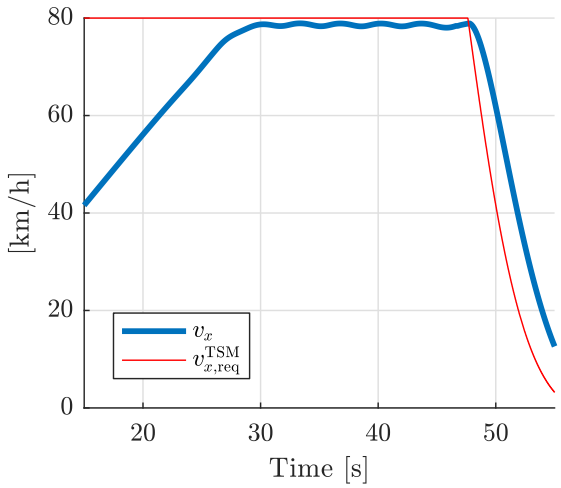

(a) Speed

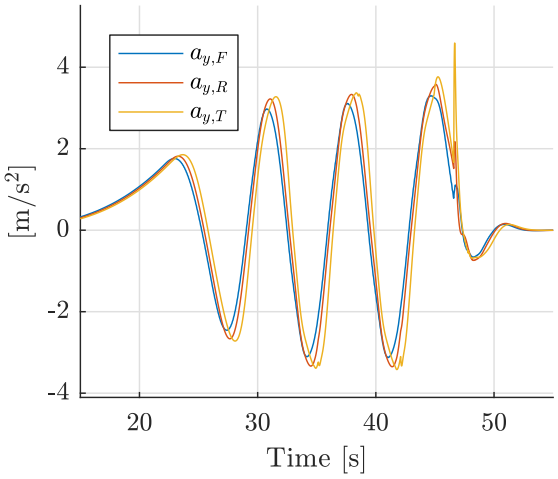

(b) Lateral acceleration

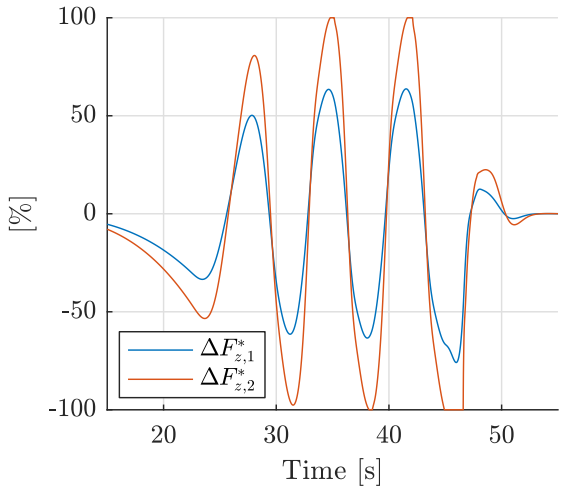

(c) Lateral LTR

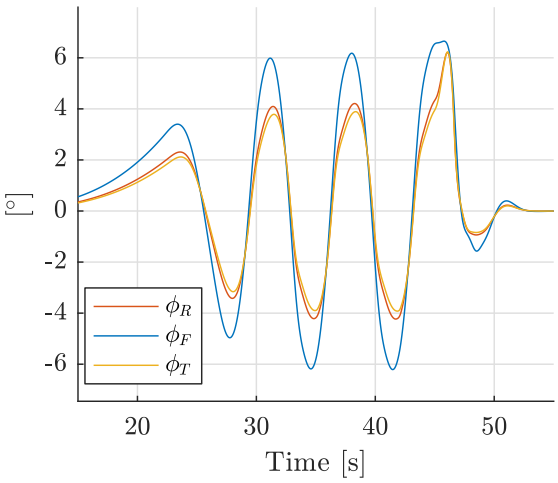

(d) Roll angle

Figure A-7: Signals related to a slalom manoeuvre; $|\Delta F_z^*| = 100\%$ signifies wheel lift-off, happens multiple times

Rollover in circle manoeuvre with hard braking

This test cases illustrates why it is essential to have a margin of LTR before triggering an intervention: Due to the typically softer front axle suspension, the overall roll stiffness of the

system reduces during braking (thanks to longitudinal load transfer).

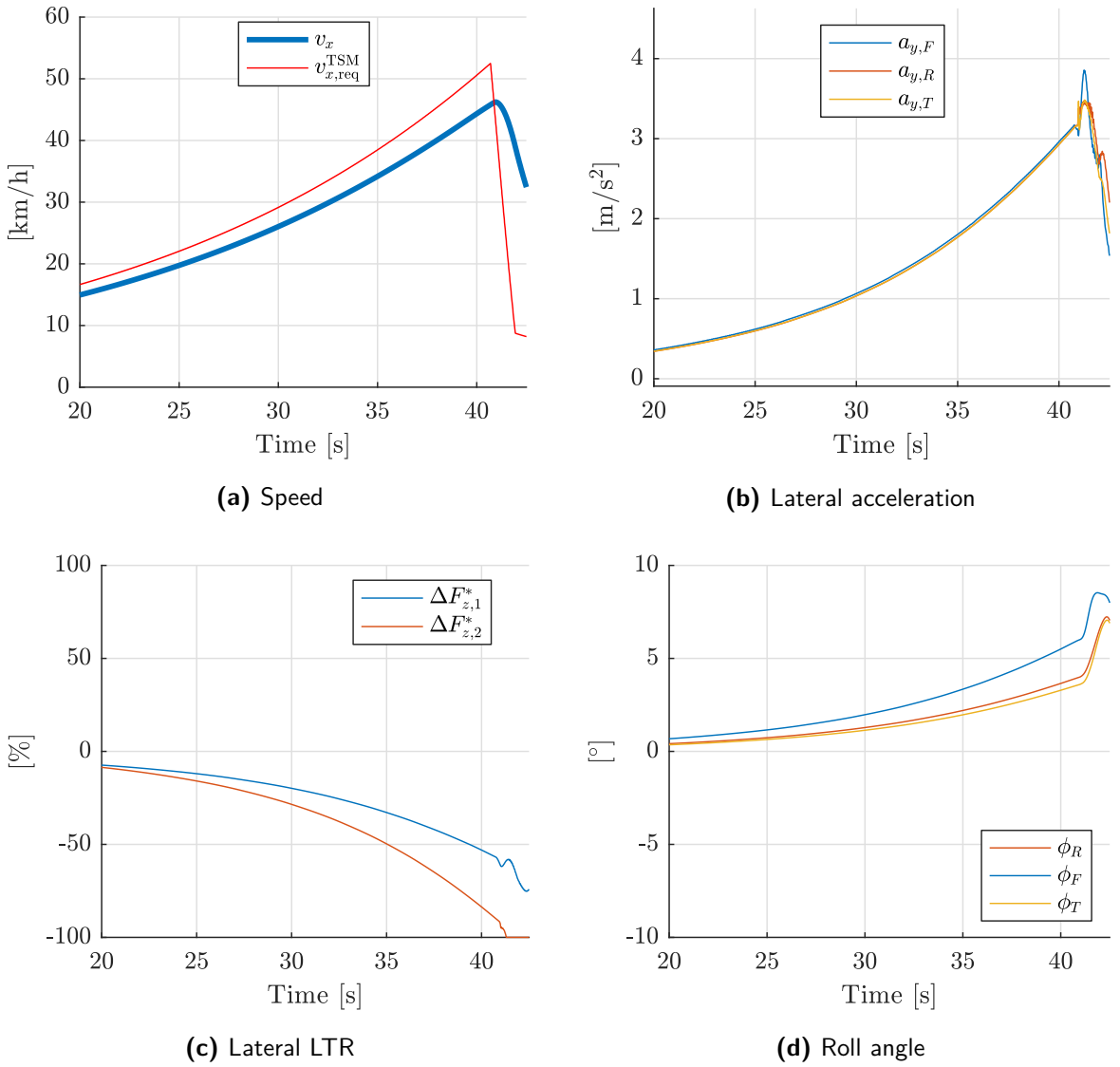

(a) Speed

(b) Lateral acceleration

(c) Lateral LTR

(d) Roll angle

Figure A-8: Signals related to a circle manoeuvre; $|\Delta F_z^*| = 100\%$ signifies wheel lift-off, when a hard braking even happens with a too small margin left in the LTR, leading to rollover

A-2 Additional results of Monte Carlo simulations

Additional Monte Carlo simulations can be found in this section, with modified initial settings. Figure captions describe the details of each case.

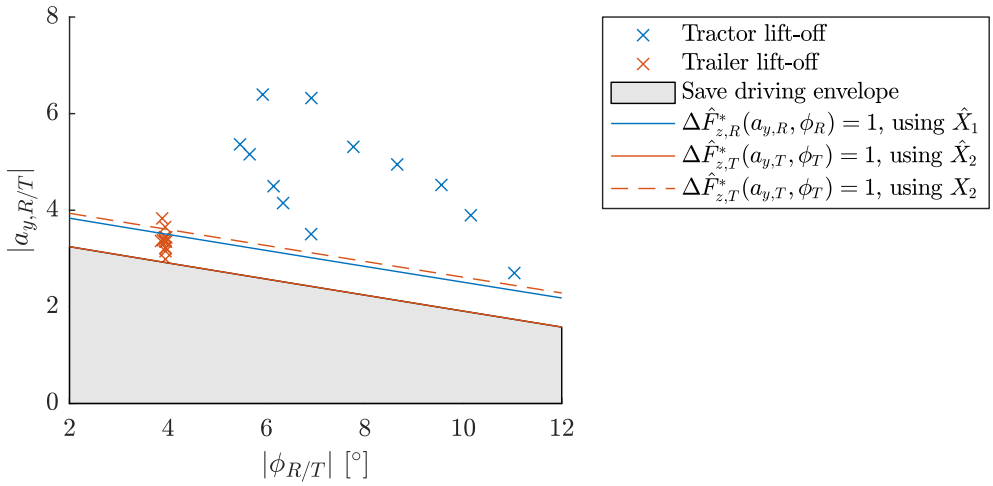

Figure A-9: Monte Carlo simulation results – (a_y, ϕ) data points at the moments of wheel lift-offs, without hard braking during cornering; some of the edge cases vanish

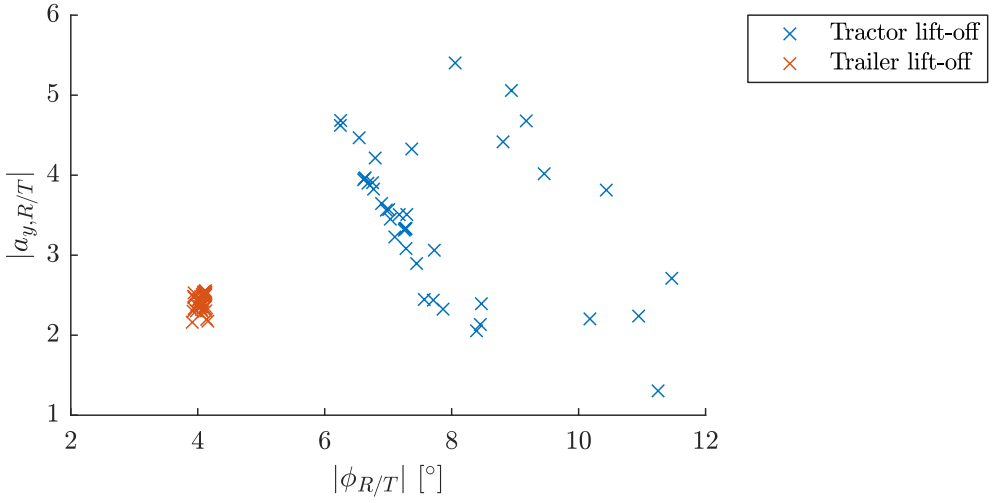

Figure A-10: Monte Carlo simulation results – (a_y, ϕ) data points at the moments of wheel lift-offs, with $h_{cg,2} = 3$ m; higher CoG results in lower acceleration limits

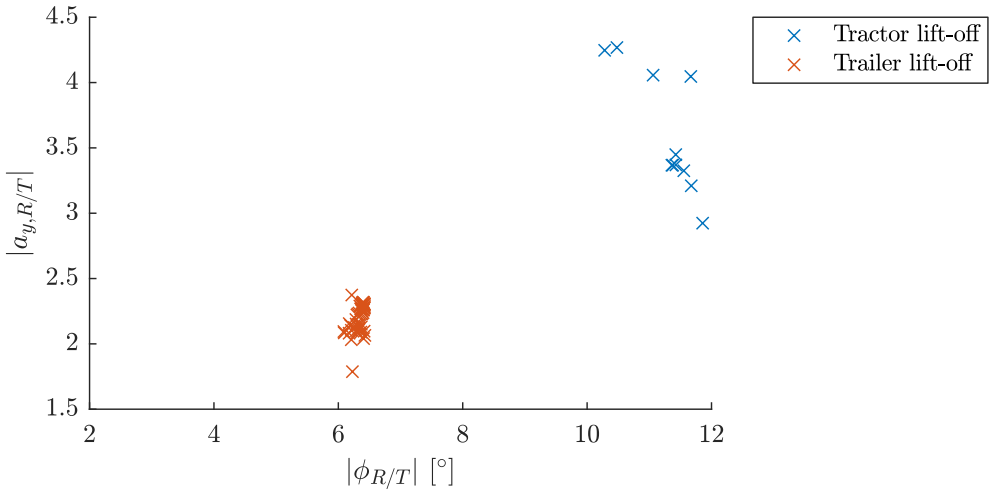

Figure A-11: Monte Carlo simulation results – (a_y, ϕ) data points at the moments of wheel lift-offs, with $h_{cg,2}$ increased with 20% and stiffness of multiple trailer suspension elements decreased by 50%

A-3 Additional results of proactive Roll Stability Control simulations

Double lane change

In this case, the reference trajectory would demand a double lane change at 80 km/h, which is an extreme speed for such an intense manoeuvre. Still, rollover could effectively be mitigated before the vehicle could have even approached a dangerous situation, thanks to the early detection. Interestingly, the usage of a safety factor is more important here, due to the complex dynamics – difference between $\Delta\bar{F}^*_{z,\text{pro}}$ and $\Delta\tilde{F}^*_{z,T}$ is less than 25%.

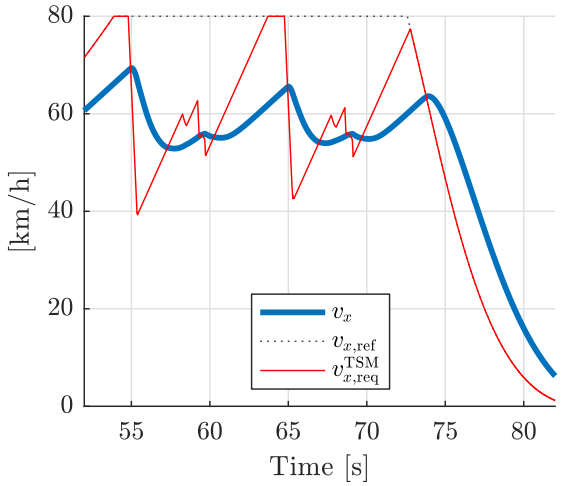

(a) Speed

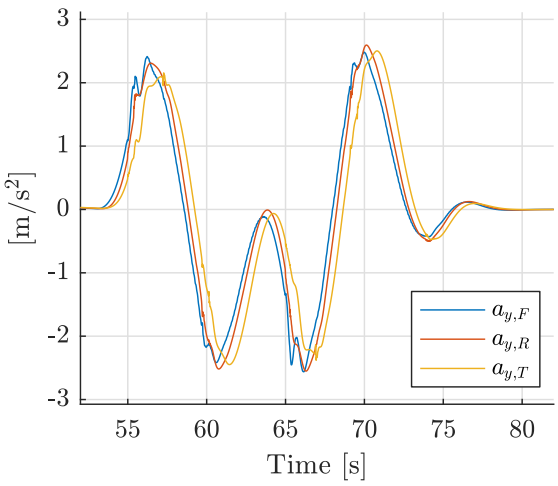

(b) Lateral acceleration

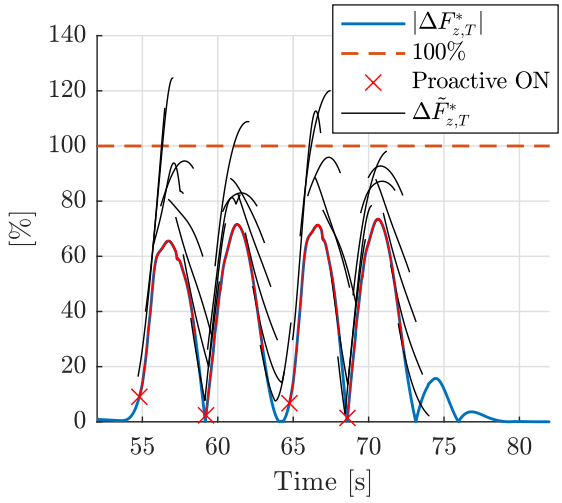

(c) Lateral LTR

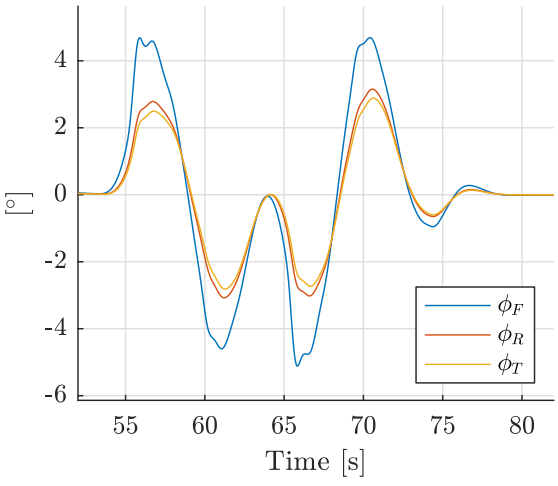

(d) Roll angle

Figure A-12: Proactive Roll Stability Control during an intense double lane change manoeuvre, $\Delta\bar{F}^*_{z,\text{pro}} = 80\%$, $c_{s,2} = 1.25$

Evasion manoeuvre at high speed

Although the previously mentioned characteristics apply here, as well, setting the safety factor is of high importance: $\Delta\tilde{F}^*_{z,T} \approx \Delta\bar{F}^*_{z,\text{pro}}$ applies, even with $c_{s,2} = 1.25$. The largest contributor to the inaccurate prediction at suddenly changing roll angles is likely the $\ddot{\phi} = 0$ neglection in (4-5). The sudden evasion was preceded by slight slaloms, to "teach" the roll prediction model. This was done based on the fact that in real-life, until the truck reaches 80 km/h, it is likely to have done turns already, where the roll motion model could be fitted. Without a converged roll prediction model, rollover mitigation cannot succeed in this test case.

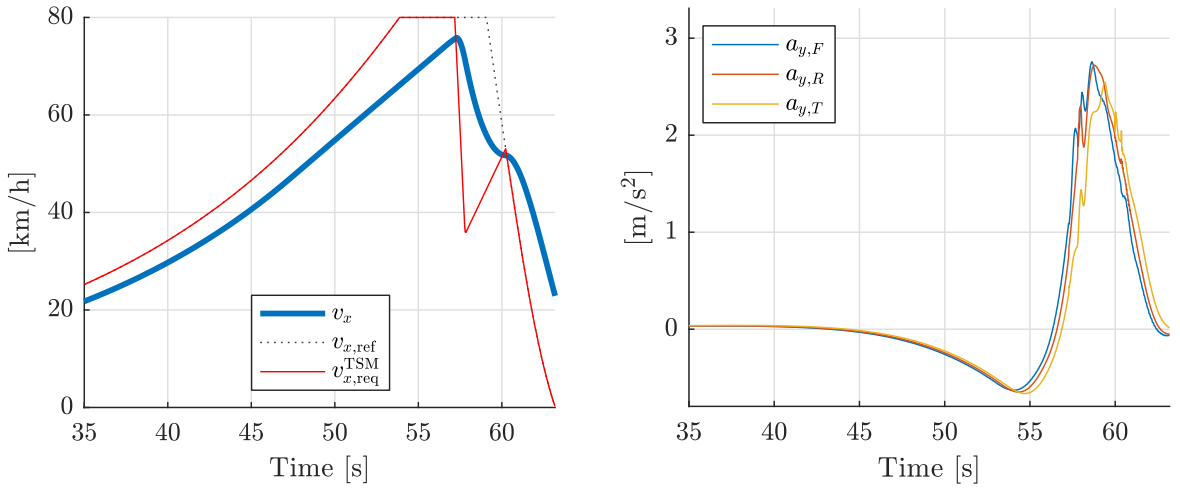

(a) Speed

(b) Lateral acceleration

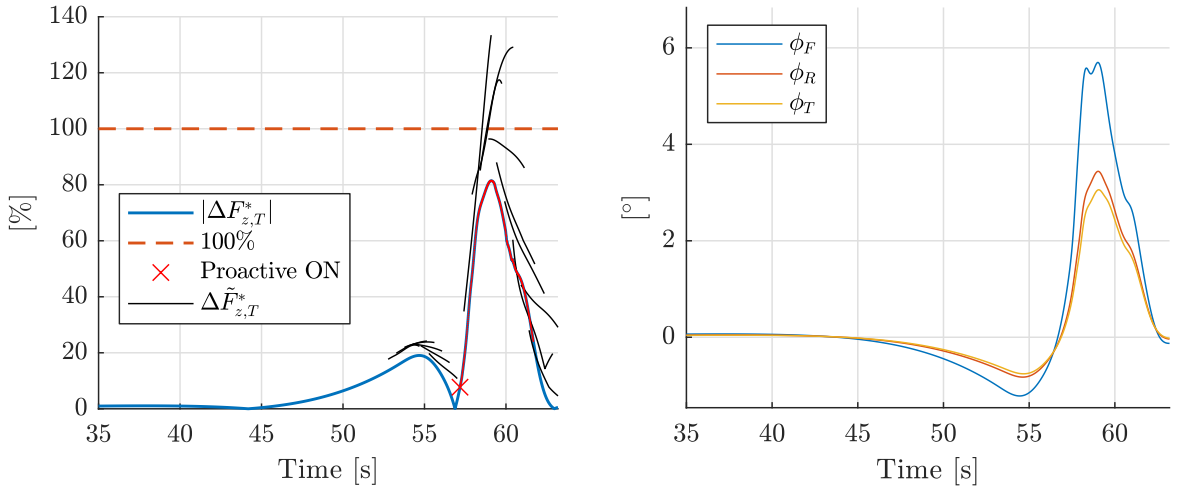

(c) Lateral LTR

(d) Roll angle

Figure A-13: Proactive Roll Stability Control during an evasion manoeuvre at high speed, $\Delta\bar{F}^*_{z,\text{pro}} = 80\%$, $c_{s,2} = 1.25$

Hook manoeuvre, comparison with a hard acceleration constraint

One might make the claim that roll motion predictions are unnecessary, if the trajectory generation and tracking algorithms guarantee that none of the vehicle units in closed-loop will exceed a pre-defined, hard lateral acceleration limit, $\bar{a}_y^{\text{hard}}$. While this can be indeed true, the constraint $\bar{a}_y^{\text{hard}}$ has to be very conservative to account for evasion manoeuvres and cases which involve excited roll motion. A comparison between such an approach and the proposed proactive design is made by Figure A-14. Here, the simulation corresponds to that depicted by Figure 5-15.

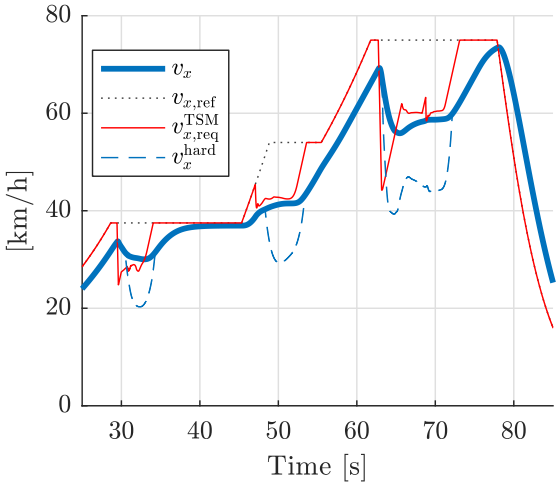

Figure A-14: Evolution of speed using the proactive RSC, in comparison with the speed levels that would result from a hard lateral acceleration constraint $\bar{a}_y^{\text{hard}} = 2$ m/s^2

A speed level was calculated in real time, which would ensure that $a_{y,R}(k) < 2$ m/s^2 , $\forall k \in \mathbb{Z}^+$. This was done according to the current yaw rate of the tractor, based on (2-23):

$$v_x^{\text{hard}}(k) = \frac{\bar{a}_y^{\text{hard}}}{|\dot{\psi}_1(k)|} \tag{A-1}$$

where v_x^{hard} is the maximal speed at time step k, ensuring that $a_{y,R}(k) < 2$ m/s^2 . While (A-1) is a simplified model of a complex case, it gives an approximate figure of how much more limiting such an approach would be. If a mission route involves lots of sharp corners, using a roll motion prediction-based speed limitation instead of a hard lateral acceleration constraint might result in a significantly faster mission execution time.

A-4 Additional results of reactive Roll Stability Control simulations

Double lane change

As Figure A-15 shows, the reactive RSC was able to prevent a rollover in a highly dynamic manoeuvre. Due to the faster changes in the steering action (and the larger delay in the tyre

dynamics), the detection algorithm based on (6-1) recognizes the rollover danger even earlier than in the hook manoeuvre illustrated by Figure 6-3.

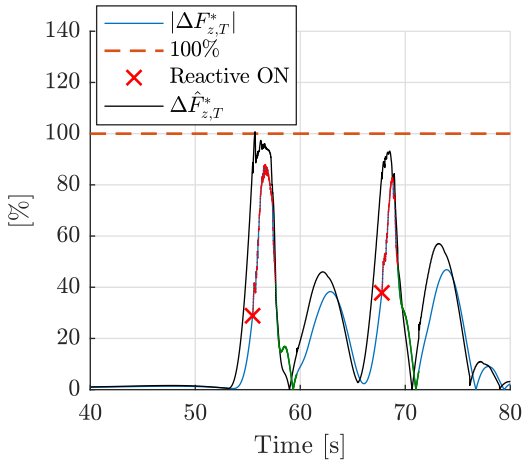

(a) Lateral LTR – red line: RSC active, green line: Post-intervention

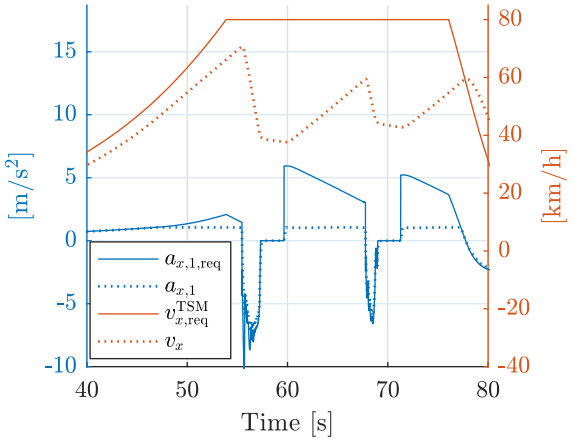

(b) Speed and longitudinal acceleration

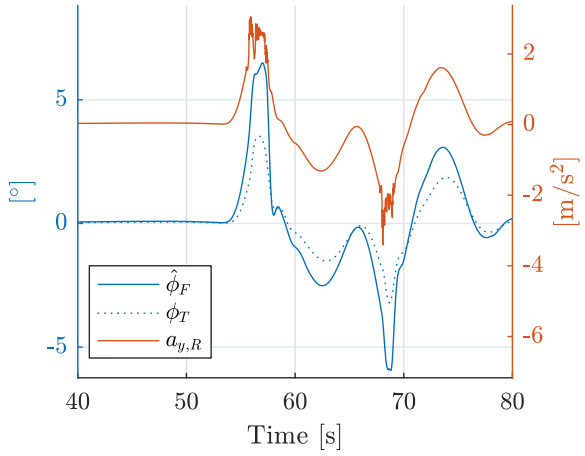

(c) Lateral acceleration and roll angle

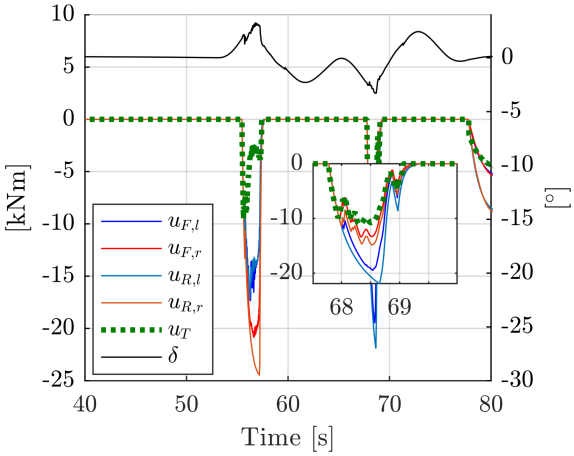

(d) Actuator usage, brakes and steer

Figure A-15: Reactive Roll Stability Control during an intense double lane change manoeuvre, $\Delta \bar{F}^*_{z,\text{re}} = 80\%$, $c_{s,2} = 1.1$

Evasion manoeuvre at high speed

Figure A-16 shows a test case which is perhaps the most important scenario for the reactive RSC, as this could represent a case where the truck has to deviate from a straight reference trajectory, for example to carry out obstacle avoidance. The steering is very dynamic: Without the kinematic relation (6-1) in the detection algorithm, there would be no time to prevent rollover. The motivation behind choosing a safety factor $c_{s,2}$ is validated: the lateral Load Transfer Ratio of the trailer reaches up to 94%, being very close to the edge of rolling over. At this point, opening the steer was indeed needed.

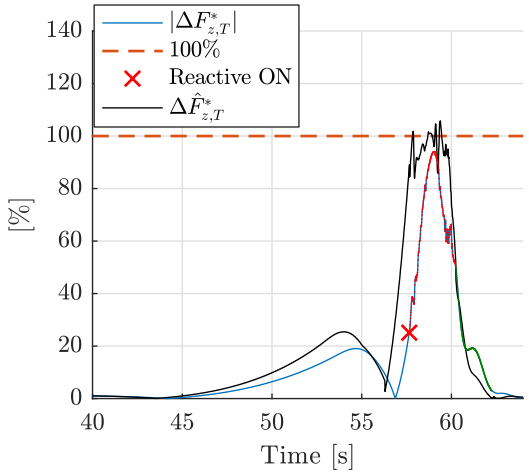

(a) Lateral LTR – red line: RSC active, green line: Post-intervention

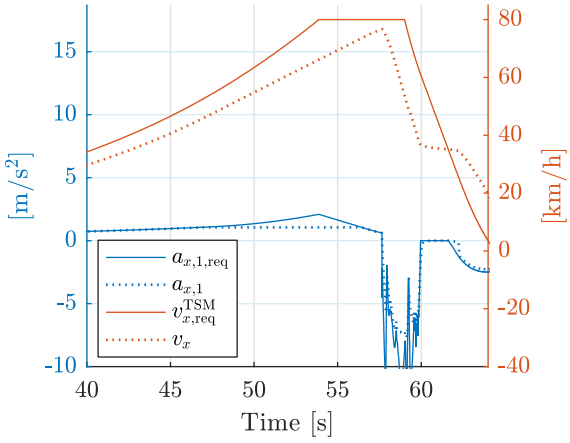

(b) Speed and longitudinal acceleration

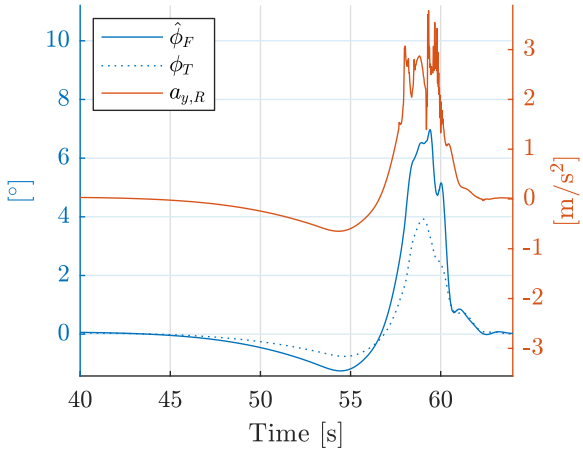

(c) Lateral acceleration and roll angle

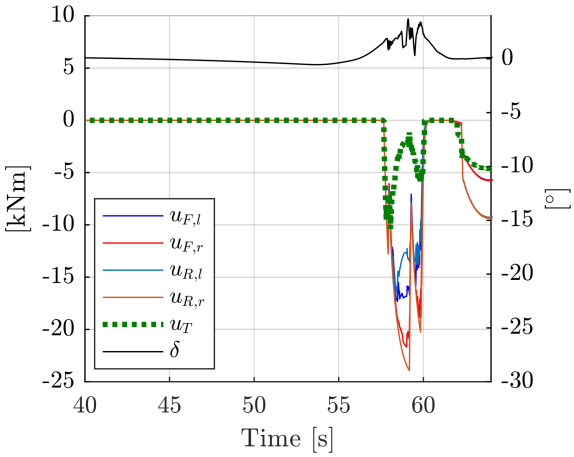

(d) Actuator usage, brakes and steer

Figure A-16: Reactive Roll Stability Control during an evasion manoeuvre at high speed, $\Delta \bar{F}^*_{z,\text{re}} = 80\%$, $c_{s,2} = 1.1$

A-5 Reproduced simulation of the real-life test case

During this simulation, the recorded reference trajectory was used, corresponding to the case represented by Figure 7-4. The brakes were switched off, accordingly. Differences are explained by the following:

- Lack of sensor noise and noise induced by road imperfections and engine,
- the difference between the cab roll angle estimate $\hat{\phi}_F$ and ϕ_T – in the real truck, the cab suspension has been removed, therefore the cab roll angle resembles that of the chassis,
- the engine drag was larger in real-life than in simulations.

Nevertheless, the overall simulated behaviour matches with the recordings.

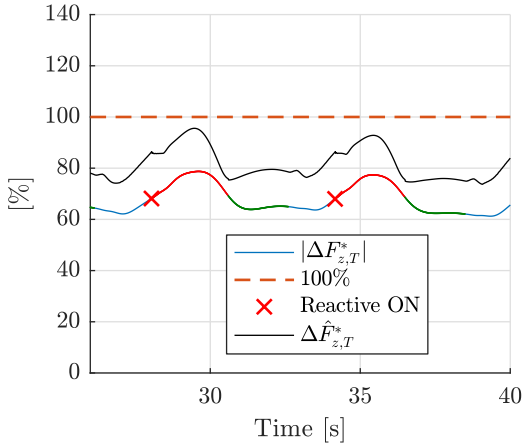

(a) Lateral LTR – red line: RSC active, green line: Post-intervention

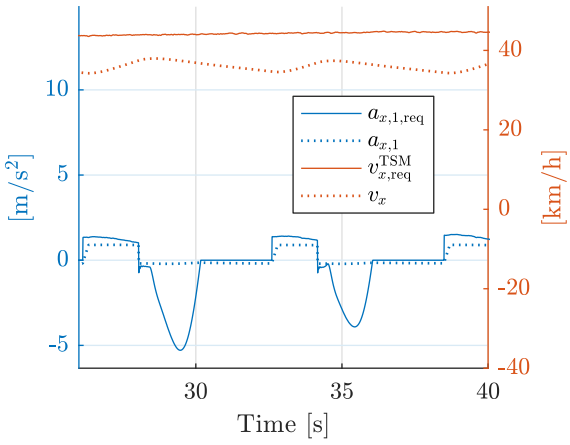

(b) Speed and longitudinal acceleration

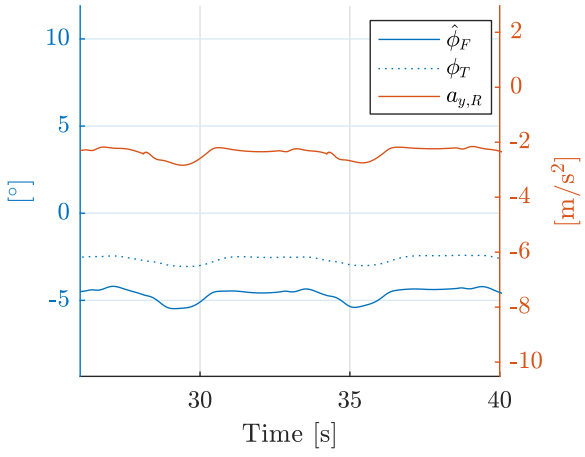

(c) Lateral acceleration and roll angle

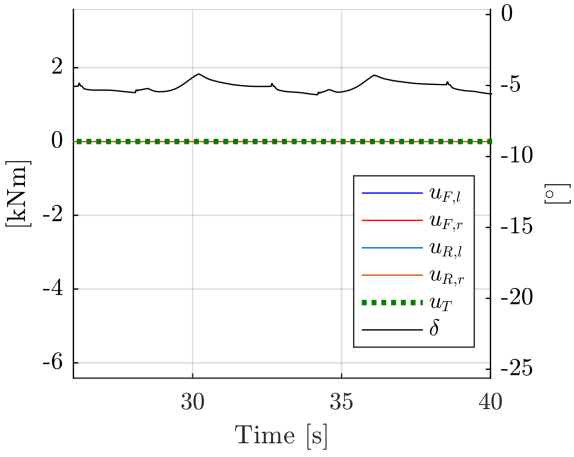

(d) Actuator usage, brakes and steer

Figure A-17: Reproduced simulation of the real-life test case depicted by Figure 7-4; braking actuation has been switched off accordingly – $\Delta \bar{F}^*_{z,\text{re}} = 85\%$, $c_{s,2} = 1.1$

Bibliography

[1] A. Report and S. Board, "Rollover of a Truck-Tractor and Cargo Tank Semitrailer Carrying Liquefied Petroleum Gas and Subsequent Fire, Highway Accident Report," tech. rep., National Transportation Safety Board, Indianapolis, Indiana, 2009.

[2] "Heavy combination vehicle stability and dynamics - An introduction programme for drivers of heavy motor vehicles," tech. rep., Land Transport NZ, Ikiiki Whenua Aotearoa, New Zealand, 2007.

[3] J. Aurell and T. Wadman, "Vehicle combinations based on the modular concept," Tech. Rep. 1, Volvo Trucks, Committee 54: Vehicles and Transports, 2007.

[4] R. Rajamani, *Vehicle Dynamics and Control*. Mechanical Engineering Series, Boston, MA: Springer US, 2012.

[5] B. Shyrokau, "Vehicle Dynamics A - Lecture Slides 4 (Delft University of Technology)," 2014.

[6] A. Sinigaglia, *Actuators Coordination of Heavy Vehicles using Model Predictive Control Allocation*. Msc thesis, Università degli Studi di Padova, 2015.

[7] A. S. Tomar, *Estimation of Steady State Rollover Threshold for High Capacity Transport Vehicles using RCV Calculation Method*. Msc thesis, Chalmers University of Technology, 2015.

[8] C. Winkler, "Rollover of heavy commercial vehicles," *UMTRI Research Review*, vol. 31, no. 4, 1999.

[9] B. Schofield, *Model Based Vehicle Dynamics Control for Active Safety*. Phd thesis, Lund University, 2008.

[10] M. Bertoncello and D. Wee, *Ten ways autonomous driving could redefine the automotive world*. https://www.mckinsey.com/industries/automotive-and-assembly/our-insights/ten-ways-autonomous-driving-could-redefine-the-automotive-world: Retrieved 28 May 2019.

[11] "SAE J3016, Taxonomy and Definitions for Terms Related to On-Road Automated Motor Vehicles," tech. rep., SAE International, Warrendale, PA, 2014.

[12] A. J. McKnight and G. T. Bahouth, "Analysis of large truck rollover crashes," *Traffic injury prevention*, vol. 10, no. 5, pp. 421–426, 2009.

[13] B. Jacobson, *Vehicle Dynamics - Compendium for Course MMF062.* Department of Applied Mechanics, Chalmers University of Technology, 2015.

[14] D. Trombitas, *Roll stability control of autonomous truck combinations.* Literature survey, Delft University of Technology, 2018.

[15] D. John and M. Sampson, *Active roll control of articulated vehicles.* Phd thesis, University of Cambridge, 2000.

[16] H. B. Pacejka, *Tyre and Vehicle Dynamics.* Elsevier, second ed., 2006.

[17] H. Dugoff, P. S. Fancher, and L. Segel, *Tire performance characteristics affecting vehicle response to steering and braking control inputs.* Final report, National Bureau of Standards, 1969.

[18] L. Chen, M. Bian, Y. Luo, and K. Li, "Real-time identification of the tyre-road friction coefficient using an unscented Kalman filter and mean-square-error-weighted fusion," *Proceedings of the Institution of Mechanical Engineers, Part D: Journal of Automobile Engineering*, vol. 230, no. 6, pp. 788–802, 2016.

[19] J. Svendenius and M. Gäfvert, "A semi-empirical dynamic tire model for combined-slip forces," *Vehicle System Dynamics*, vol. 44, no. 2, pp. 189–208, 2006.

[20] J. Y. Wong, *Theory of Ground Vehicles.* John Wiley and Sons, second ed., 2008.

[21] E. Sabelström and X. Sun, *Centre of Gravity Height Estimation for Heavy Vehicles.* Msc thesis, Chalmers University of Technology, 2011.

[22] N. J. V. Duijkeren, *Real-time receding horizon trajectory generation for long heavy vehicle combinations on highways.* Msc thesis, Delft University of Technology, 2014.

[23] M. F. J. Luijten and V. C. Group, *Lateral Dynamic Behaviour of Articulated Commercial Vehicles.* Msc thesis, Eindhoven University ofTechnology, 2010.

[24] P. Nilsson, *Traffic Situation Management for Driving Automation of Articulated Heavy Road Transports From driver behaviour towards highway autopilot.* Phd thesis, Chalmers University of Technology, 2017.

[25] M. Samuel, M. Hussein, and M. B. Mohamad, "A Review of some Pure-Pursuit based Path Tracking Techniques for Control of Autonomous Vehicle," *International Journal of Computer Applications*, vol. 135, no. 1, pp. 35–38, 2016.

[26] P. Sundström and K. Tagesson, *On Real Time Adaptive and Dynamically Constrained Control Allocation for Stability Control of Heavy Vehicles.* Msc thesis, Chalmers University of Technology, 2008.

[27] H. J. Ferreau, C. Kirches, and A. Potschka, *qpOASES*. projects.coin-or.org/qpOASES: Retrieved 6 June 2019.

[28] P. W. Blow, J. H. Woodrooffe, and P. F. Sweatman, "Vehicle Stability and Control Research for U.S. Comprehensive Truck Size and Weight (TS&W) Study," *SAE transactions*, pp. 617–623, 1998.

[29] M. Ei-Gindy, N. Mrad, and X. Tong, "Sensitivity of rearward amplication control of a truck/full trailer to tyre cornering stiffness variations," *Proceedings of the Institution of Mechanical Engineers, Part D: Journal of Automobile Engineering*, vol. 215, no. 5, pp. 579–588, 2001.

[30] D. D. Furleigh, M. J. Vanderploeg, and C. Y. Oh, "Multiple Steered Axles for Reducing the Rollover Risks of Heavy Articulated Trucks," tech. rep., SAE International, 1988.

[31] P. Liu, S. Rakheja, and A. K. W. Ahmed, "Detection of Dynamic Roll Instability of Heavy Vehicles for Open-Loop Rollover Control," tech. rep., SAE International, 1997.

[32] E. J. Stone and D. Cebon, "An experimental semi-active anti-roll system," in *Proceedings of the Institution of Mechanical Engineers, Part D: Journal of Automobile Engineering*, vol. 222, pp. 2415–2433, 2008.

[33] R. Rajamani and D. N. Piyabongkarn, "New paradigms for the integration of yaw stability and rollover prevention functions in vehicle stability control," *IEEE Transactions on Intelligent Transportation Systems*, vol. 14, no. 1, pp. 249–261, 2013.

[34] R. Rajamani, G. Phanomchoeng, D. Piyabongkarn, and J. Y. Lew, "Algorithms for Real-Time Estimation of Individual Wheel Tire-Road Friction Coefficient," vol. 17, no. 6, pp. 1183–1195, 2012.

[35] S. Haykin, *Adaptive Filter Theory*. Prentice Hall, 2002.

[36] M. Verhaegen and V. Verdult, *Filtering and System Identification*. Cambridge University Press, 2007.

[37] R. Tafner, M. Reichhartinger, and M. Horn, "Robust vehicle roll dynamics identification based on roll rate measurements," *IFAC Proceedings Volumes*, vol. 45, no. 30, pp. 72–78, 2012.

[38] M. Ataei, A. Khajepour, and S. Jeon, "A general rollover index for tripped and untripped rollovers on flat and sloped roads," *Proceedings of the Institution of Mechanical Engineers, Part D: Journal of Automobile Engineering*, vol. 233, no. 2, pp. 304–316, 2019.

Glossary

List of Acronyms

TU Delft	Delft University of Technology
SAE	Society of Automotive Engineers
SRT	Steady-State Rollover Threshold
CoG	Centre of Gravity
DoF	Degrees of Freedom
RWA	Rearward Amplification
RSC	Roll Stability Control
LTR	Load Transfer Ratio
ARC	Active Roll Control
CA	Control Allocation
ABS	Anti-Lock Braking System
TCS	Traction Control System
FD	Functionality Domain
FA	Functionality Area
FU	Functionality Unit
RLS	Recursive Least Squares
SLS	Sequential Least Squares
WLS	Weighted Least Squares
ESC	Electronic Stability Control

MPC	Model Predictive Control
RRT	Rapidly-Expanding Random Trees
AV	Autonomous Vehicle
TSM	Traffic Situation Management
VMM	Vehicle Motion Management
TG	Target Generator
ROI	Rollover Index
SISO	Single-Input Single-Output

List of Symbols

$\Delta\phi_w$	Warp angle of the trailer
δ^{ff}	Feed-forward steering command
δ_o	Steering angle of the outer wheel
λ	Weighting parameter
λ_a	Acceleration filtering factor
λ_i	An eigenvalue of $\hat{A}_d$
ω_n	Undamped natural frequency
ϕ_{bank}	Road bank angle
ρ	Curvature
σ_x	Longitudinal slip
σ_y	Lateral slip
Θ	Parameter estimate matrix
$\varphi(k)$	Data (or regression) vector
Υ	Transformation from spatial to temporal parametrization
ξ	Damping factor
α	Slip angle
β	Body side-slip angle
δ	Steering angle
δ_i	Steering angle of the inner wheel
$\dot{\psi}$	Yaw rate
γ	Articulation angle
γ_c	Camber angle
λ_{id}	Exponential forgetting factor
μ	Friction coefficient
ω	Angular velocity

ϕ	Total roll angle
ϕ_s	Roll angle of the sprung mass
ϕ_t	Roll angle due to tyre compliance
σ	Total slip
$\bar{M}_i$	Torque capability of tyre i
ΔF_z^*	Load Transfer Ratio
$\check{s}$	Complex parameter of Laplace-domain functions
A_c, B_c	Continuous-time system matrices
A_d, B_d	Discrete-time system matrices
A_G	Steady-state gain
a_y	Lateral acceleration
$a_{y,R}^{\text{kin}}$	Lateral acceleration of the rear tractor axle, resulting from the kinematic bicycle model
C_{id}	Tuning matrix
$c_{s,1/2}$	Safety factors corresponding to tractor and trailer units
$e_{\dot{\psi}}$	Yaw rate error
e_{id}	Identification error
f_{cl}	Closed-loop system description
G_a	Transfer function from lateral acceleration reference to lateral acceleration
I	Identity matrix
K	Update gain vector
l_{wb}	Wheel base
$n_{1/2,i}$	Numerator coefficients, corresponding to a particular $\omega_{n,i}$ bandwidth
q	Time-shift operator
$R(\delta)$	Rotation matrix
R_R^{inst}	Radius from the centre of instantaneous rotation to the rear axle
s	Natural parameter
s_0	Path length at the starting point of the trajectory
s_H	Spatial horizon length
s_l	Path length
t_H	Temporal time horizon length
u_d	Input set-point
u_e	Engine torque
v_y	Lateral velocity
X_i	Dimensionless constant feature of vehicle unit i
x_R, y_R	Position of the rear axle
y_r	Plant output vector
a	Distance between unit CoG and front axle
B	Control efficiency matrix
b	Distance between unit CoG and rear axle

b_ϕ	Suspension roll damping coefficient
C_α	Lateral (or cornering) stiffness
C_M	Aligning stiffness
C_x	Longitudinal (or braking) stiffness
$d_{1/2/3,i}$	Denominator coefficients, corresponding to a particular $\omega_{n,i}$ bandwidth
f	System dynamics
F_x	Force in the direction of the x-axis
F_y	Force in the direction of the y-axis
F_z	Force in the direction of the z-axis
F_{friction}	Tyre force resulting from friction
g	Gravitational constant
h	Actuator dynamics
h_1	Distance between fifth wheel and tractor rear axle
h_{cg}	CoG height
h_{rc}	Height of suspension roll centre from ground
I_{xx}	Roll moment of inertia about the CoG
k	Time step
k_ϕ	Suspension roll stiffness
l_t	Vehicle track width
m	Total mass of the vehicle unit
M_z	Moment about the z-axis
n_H	Number of time steps in the temporal prediction horizon
q_1	Length of an average moment arm
R	Suspension roll centre
$r(k)$	One point of the reference trajectory at time instance k
R_e	Effective rolling radius of the wheel
s_1	Distance of the neutral steer point from the CoG
T_s	Sampling time
t_W	Data acquisition window
u	System input
v	Virtual input
v_x	Longitudinal velocity
w_i	Weighting factor of actuator i
W_u	System input weighting matrix
W_v	Virtual input weighting matrix
x	State vector
$y(k)$	Measurement vector
$_1$	Tractor unit
$_2$	Trailer unit
$_{\text{ach}}$	Achieved value

pro	Value associated with proactive Roll Stability Control
ref	Reference value
req	Required value
re	Value associated with reactive Roll Stability Control
F	Tractor front axle
l	Left side
R	Tractor rear axle
r	Right side
T	Semitrailer axle (group)
*	Normalized value
TSM	Signal produced by Functionality Domain-Traffic Situation Management
VMM	Signal produced by Functionality Domain-Vehicle Motion Management
$\bar{\square}$	Maximal value
$\hat{\square}$	Estimated value
$\tilde{\square}$	Predicted value
$\underline{\square}$	Minimal value